Impact of the mechanical properties of lymphoma cells on phagocytosis efficiency by macrophages

by

Diana Giron-Ceron

Bachelor of Science, Universidad del Valle, 2017

Thesis Submitted in Partial Fulfillment of the
Requirements for the Degree of
Master of Science

in the
Department of Molecular Biology and Biochemistry
Faculty of Science

SIMON FRASER UNIVERSITY
Fall 2023

Declaration of Committee

Name:	**Diana Giron-Ceron**
Degree:	**Master of Science (Molecular Biology and Biochemistry)**
Title:	**Impact of the mechanical properties of lymphoma cells on phagocytosis efficiency by macrophages**
Committee:	**Chair:** **Mani Larijani** Professor, Molecular Biology and Biochemistry
	Valentin Jaumouillé Supervisor Assistant Professor, Molecular Biology and Biochemistry
	Jonathan Choy Committee Member Professor, Molecular Biology and Biochemistry
	Ly Vu Committee Member Assistant Professor, Pharmaceutical Sciences University of British Columbia
	Sharon Gorski Committee Member Professor, Molecular Biology and Biochemistry
	Lorena Braid Examiner Assistant Professor, Molecular Biology and Biochemistry

Abstract

Macrophages, typically the most abundant immune cell in the tumor microenvironment, eliminate unwanted particles through phagocytosis, yet rarely internalize cancer cells. Antibody-based therapies are being developed to promote the elimination of tumoral cells via phagocytosis. Phagocytosis of lymphoma cells upon CD47-blockade requires the mechanosensitive integrin Mac-1; however, malignant cells often display reduced cellular stiffness. As aggressive lymphomas frequently exhibit loss-of-function mutations in the RhoA pathway, we hypothesize that these mutations reduce the stiffness of lymphoma cells, preventing their phagocytosis. Here, we show that mutations in the RhoA pathway of Burkitt lymphoma cells modify their actin cortex density and stiffness. Whereas RhoA mutations do not alter the expression of CD47 or Mac-1 ligands, they modulate the phagocytosis of lymphoma cells by macrophages in correlation with their stiffness. Overall, our findings suggest that loss-of-function mutations in the RhoA pathway reduce the stiffness of lymphoma cells and facilitate their escape from phagocytosis.

Keywords: Burkitt lymphoma; macrophages; phagocytosis; Mac-1 integrin; actin cortex; RhoA pathway

Acknowledgements

I am fortunate to have many people in my life and career to thank for their company, kindness, friendship, and mentoring. Without their support, this thesis could not have been possible. First, I want to thank the institution that made me fall in love with research and encouraged me to continue this pathway. To all the members of the Centro Internacional de Entrenamiento e Investigaciones Médicas (CIDEIM - Colombia), thank you for showing me the remarkable aspects of research when scientists are in the right place. Particularly, I want to thank my mentor, Dr. Olga Fernández, for teaching me the crucial skills for completing this project. Your unconditional support, guidance, and advice throughout these years helped me to move forward with my career and look up to the type of researcher that I want to become. To Lady Rios Serna, Coordinator of the Immunology Laboratory of Universidad ICESI - Colombia, who went above and beyond by guiding me to properly analyze the flow cytometry data of my project.

I have no words to thank Dr. Carl Lowenberger from the Biological Sciences Department at Simon Fraser University. Many generations of researchers have learned from Dr. Lowenberger how to be integral scientists, and I am very honored to be one of them. Muchas gracias Dr. Carl, for your unconditional support to my family, for supporting my career, and for opening the doors of your laboratory to have me learn from you and your students, who are my friends now. To the members of the Lowenberger Laboratory, Dr. Claudia Umaña, Dr. Nicolás Salcedo, Dr. Andrea Arévalo, Shireen Noor, and Keenan Elliott, thank you for the time we spend together enjoying science, work, and life. You made me feel at home.

I also enjoyed unforgettable moments with the Molecular Biology and Biochemistry Graduate Caucus students, Kevin Luong, Aleksa Nenadic, Shaianne Stein, Stephanie Sonea and Iqra Yaseen. Thanks for your kindness, friendship, and support. I enjoyed working with you, planning events for the Department, and learning lots of Canadian slang (which I had to search for while doing the Caucus minutes). Without knowing it, you were present when I needed it the most, and I am grateful for meeting you all during my master's.

To my beloved husband Miguel, thank you for your unconditional support and love, for believing in me, for pushing me to become my best version, and for standing up

together overcoming difficult times that made us grow as a family. To my parents, Nubia and Jairo, my siblings Angela and Jair, my niece Sofi, and nephews Samuel and Julian; despite the distance, I keep remembering that “el tiempo pasa y estaremos juntos nuevamente”.

I am also very thankful to Sophia Goksoyr, Harjap Grewal, and Hannah Buteau for their professionalism, continuous support, and indispensable role with students at Simon Fraser University. Thanks to your actions, I am moving forward with my life, and I am very grateful for your kindness during this time.

Lastly, I want to thank Dr. Cartagena and Kun Do from the National Institute of Biomedical Imaging and Bioengineering – section Mechanobiology, for performing the Atomic Force Microscopy experiments essential for this project. From my current laboratory, Ana Pavlenkova, and Taranjot Kaur for their friendship and support. The Molecular Biology and Biochemistry Department for the scholarships provided to fund the time during my masters, and the members of my committee, Dr. Jonathan Choy, Dr. Ly Vu, and Dr. Sharon Gorski, for their insightful feedback and for motivating me to continue learning through their research questions in each presentation of my project.

Table of Contents

List of Figures

List of Acronyms

AFM	Atomic Force Microscopy
Angio-TAMs	Proangiogenic tumor-associated macrophages
Arp2/3 complex	Actin Related Protein 2/3 complex
BCR	B-cell receptor
BL	Burkitt lymphoma
BMDM	Bone marrow derived macrophages
CD47	Leukocyte surface antigen CD47
CR	Complement receptor
DC	Dendritic cells
DLBCL	Diffuse large B cell lymphoma
EBV	Epstein-Barr virus
ERM	Ezrin-radixin-moesin
F-actin	Filamentous actin
FACS	Fluorescence-activated cell sorting
FcR	Fc receptors
FcγR	Fc-gamma receptors
GC	Germinal centers
GEF	Guanine nucleotide exchange factors
HIV	Human Immunodeficiency Virus
IFN-TAMs	Interferon primed tumor-associated macrophages
Ig	Immunoglobulin
Inflam-TAMs	Inflammatory cytokine enrich-TAMs
ITAM	Immunoreceptor tyrosine-based activation motif
LA-1	Leukadherin-1
LA-TAMs	Lipid-associated tumor-associated macrophages
LPS	Lipopolysaccharide
Mac-1	Macrophage-1 antigen (or integrin αMβ2)
MC38	Mouse colon cell line
MDSC	Myeloid-derived-suppressor cells

MHC-I	Major histocompatibility complex type I molecules
MHC-II	Major histocompatibility complex class II
MKL1	Megakaryocytic leukemia 1 (also known as MRTFA)
MβCD	Methyl-β-cyclodextrin
NHL	Non-Hodgkin lymphoma
NK	Natural Killer cells
PI	Phagocytic index
Prolif-TAMs	Proliferating tumor-associated macrophages
Reg-TAMs	Immune regulatory tumor-associated macrophages
RhoA	Transforming protein RhoA (small GTPase)
ROCK	Rho kinase
RTM-TAMs	Resident-tissue macrophage-like tumor-associated macrophages
SBTS	Sleeping Beauty Transposon System
SFU	Simon Fraser University
SHM	Immunoglobulin somatic hypermutation
SIRPα	Signal regulatory protein alpha
Syk	Spleen tyrosine kinase
T-reg	Immunosuppressive regulatory T cells
TAM	Tumor-associated macrophages
TAN	Tumor-associated neutrophils
TGFβ	Transforming Growing Factor β
TLRs	Toll-like receptors
VEGF	Vascular endothelial growth factor

Chapter 1. Introduction

1.1. Lymphoma definition: non-Hodgkin lymphoma

Lymphomas are neoplastic disorders arising from lymphocytes, an adaptive immune cell present in the lymphatic system[1]. There are more than 80 types of lymphomas classified into the following major categories: B cell, T cell, Natural Killer cell neoplasms, and Hodgkin lymphoma[2]. The classification is determined by the morphological, genetic, and immunophenotypic characterization of malignant cells[2,3]. Therefore, identification of distinctive genetic alterations, cell lineage of origin, clonality, and cell maturation stage is paramount to treat this cancer type.

Lymphomas are typically divided into Hodgkin and Non-Hodgkin lymphoma based on the presence or absence of Reed-Sternberg cells, a large and multinucleated cell derived from B lymphocytes and that originates likely from the germinal or post germinal center. Reed-Sternberg cells are considered the histological hallmark of Hodgkin lymphoma[4]. Non-Hodgkin lymphoma (NHL) includes a diverse class of B-cell and T-cell malignancies; however, mature B cell neoplasms represent greater than 80% of non-Hodgkin lymphomas[5]. NHL is the most prevalent hematological malignancy worldwide. In contrast to Hodgkin lymphoma, it lacks Reed-Sternberg cells, and on histopathological analysis is positive for CD15, a glycan that mediates chemotaxis and inflammatory extravasation, and CD30, a marker expressed on activated B cells that upon binding leads to the activation of proinflammatory pathways and regulates apoptosis [4–6]. There are three major forms of aggressive B cell lymphomas, the most common is Diffuse large B cell lymphoma (DLBCL, ~30% of cases), followed by Burkitt lymphoma (2% of cases), and high-grade B cell lymphoma[2]. According to 2021 statistics, around 12,000 new cases of non-Hodgkin lymphoma were expected in Canada, representing the 5th most common cancer type in the country. Besides, lymphoma accounts for 13% of malignancies in children aged 0 to 14 and 18% among those diagnosed at ages between 15 and 29 years[7].

1.1.1. Burkitt lymphoma

Burkitt lymphoma (BL) is a B cell non-Hodgkin lymphoma characterized by rapid cell proliferation and aggressive clinical progression[8]. Lymphomas manifest with painless

cervical masses with or without “B symptoms” (fever, night sweats, and weight loss). Burkitt lymphoma mainly affects children (3-6 / 100,000) and can present as extranodal compromise (outside the neck and mediastinum) or acute leukemia [9,10]. In Canada, BL represents up to 40% of all childhood lymphomas, and it has a bimodal peak of incidence in children between 5 and 10 years old and adults between the ages of 30 and 50 years[11]. Burkitt lymphoma presentation can be sporadic or associated with viral and parasitic infections like the Human Immunodeficiency Virus (HIV), Chikungunya virus, Epstein-Barr virus (EBV), and *Plasmodium falciparum* (malaria)[12–14]. Interestingly, BL was the first lymphoma linked to a viral infection, and the first cancer associated with a chromosomal translocation (translocation 8:14) which occurs when the heavy chain locus on chromosome 14 and the c-MYC oncogene on chromosome 8 re-attach after breakage, causing the expression of strong B cell enhancers that leads to an overexpression of the MYC oncogene[15–17]. Burkitt lymphoma accounts for approximately 1% to 5% of all non-Hodgkin lymphomas and has a higher prevalence in males compared to females (3-4:1)[10]. This differential prevalence is associated with the exposure to environmental carcinogens, immunological and hormonal factors, body size and tumor biology[18].

1.1.2. Epidemiological and clinical features of Burkitt lymphoma variants

BL has three subtypes characterized by different epidemiology, risk factors, and clinical presentations: endemic, sporadic, and immunodeficiency-related[19]. Endemic BL is the cause of 50% of all childhood cancer in Africa (incidence of approx. 3-6 cases per 100,000 children per year)[8] and typically affects the jaw, facial bones, abdomen, or kidneys[20]. This variant has rapid B cell proliferation and can quickly produce large tumors that are fatal without treatment. Endemic Burkitt lymphoma is associated with geographical areas with a high prevalence of *Plasmodium falciparum* and EBV infection, like equatorial Africa and Papua New Guinea[21]. The coinfection is considered a polymicrobial stimulus for malignancy because *P. falciparum* could increase susceptibility to EBV infection and exacerbate the immune response against the virus[20]. For instance, *P. falciparum* parasites may interact with B cells latently infected with EBV and promote their clonal expansion or differentiation into plasma cells contributing to viral proliferation and higher viral load[22,23]. According to *ex vivo* research models, *P.*

falciparum induces B cell proliferation and production of antibodies through unknown mechanisms[21]

The immunodeficiency-related subtype is frequently diagnosed in those with HIV and EBV coinfections and is the less studied subtype. This variant may also develop in patients with congenital immunodeficiency and allograft recipients[8]. It represents up to 40% of reported lymphoma cases in people living with HIV, especially among those with elevated CD4 counts (> 200 cells/uL). The most frequent tumor sites are lymph nodes, bone marrow (causing cytopenia), and the central nervous system. Extranodal sites are observed more frequently in HIV-associated cases. It is typically diagnosed in older patients (over 40 usually), and its presentation is similar to sporadic BL, although significant variability among cases is reported[8,15].

HIV proteins like Tat, gp120, p17 matrix protein, and CD40-L have been implicated in Burkitt lymphoma pathogenesis[24]. For instance, the Tat protein can lead to aberrant production of single-stranded DNA cytosine deaminase[25]. When exposed to B cells, this protein activates the nuclease encoding *RAG1* gene, promoting DNA damage and nuclear translocation of the *MYC* gene. Also, the gp120, p17, and CD40-L proteins can have direct roles in lymphomagenesis. Gp120 promotes B cell activation in the germinal center and upregulates single-stranded DNA cytosine deaminase promoting immunoglobulin (Ig) subclass switch[26,27]. On the other hand, the CD40-L protein promotes somatic hypermutation in B cell germinal centers, and the mutation Ser75Ter in the p17 protein increases the growth and proliferation of B cells[28]. It has been suggested that patients with low CD4 T cells in HIV-associated Burkitt lymphoma have a better prognosis. The crosstalk between CD4 T cells and B cells promotes B cell activation and survival. Thus, low numbers of CD4 T cells can reduce germinal center activity (lower somatic hypermutation) and decrease the genomic diversity of Burkitt lymphoma cells[29].

HIV-associated Burkitt lymphoma has a worldwide geographic distribution, and cytological analysis shows an EBV prevalence of 40% in people living with HIV [30]. This variant affects populations across all ages. In Canada, the mean incidence was 148.33 per million HIV-positive individuals every year (2000 - 2010) [14]. The treatment outcome of patients with HIV-associated BL has improved vastly in the last few years. The introduction of highly active antiretroviral therapy has led to improved survival.

Combination of highly active antiretroviral therapy with systemic chemotherapy ± monoclonal antibodies (anti-CD20) has shown remission rates of 48% to 92%, and an overall survival rate of 80% according to phase II pilot clinical trials[31].

The sporadic Burkitt lymphoma subtype predominates in Western Europe, North America, and East Asia, being more common in the pediatric population[15]. Compared to the endemic variant, sporadic Burkitt lymphoma occurs at a 10-fold lower incidence, and coinfection with EBV is lower (10% to 30%)[32]; the incidence proportion of sporadic BL is 0.01 per 100,000 individuals[21]. The peak incidence is around 11 years old and represents approximately 30% to 40% of all pediatric lymphomas in North America. Adult onset sporadic BL is rare (<1%), and its diagnosis is more frequent in the third decade of life and in men than in women (3.5:1 ratio)[9]. The primary tumor site is within the abdomen in 60% to 80% of cases[33], particularly the small intestine (bowel) or mesenteric and retroperitoneal lymph nodes. The histological analysis from affected intestines contains abundant Peyer's patches, which are oval or rectangular clusters of subepithelial lymphoid follicles[12,15]. Outside of the abdomen, the most common tumor sites include the head and neck. Extranodal or disseminated disease leads to systemic symptoms such as bone pain and anemia. Hematologic changes indicate bone marrow infiltration and occur in 30% of sporadic Burkitt lymphoma cases at diagnosis[34].

All variants of Burkitt lymphoma have rapid cellular proliferation and approximately 70% of patients are diagnosed at advanced stages (III or IV)[33]. However, children diagnosed at advanced stages have better long-term survival ranging from 80% to 90%. Furthermore, early stage (I and II) detection improves survival rate to more than 90%[35]. Finally, despite improvements in survival using chemotherapy in combination with monoclonal antibody therapies (like Rituximab), around 20% of patients experience relapse or refractory disease and are non-responsive to treatment; therefore, novel approaches that combine chemotherapy, immunotherapy and treatment of the concomitant infection are urgently needed for BL variants[36].

1.1.3. Molecular classification of Burkitt lymphoma, germinal center-cell of origin

The germinal center (GC) is a histological structure within peripheral lymphoid organs where B cells multiply, develop, and are selected. The B cells selected in the GC

display high-affinity antibodies and can become secreting plasma cells or memory B cells[37]. The GC is formed by the dark and light zones, two compartments named after their histological appearance (**Figure 1.1**)[38]. The dark zone contains rapidly proliferating B cells that undergo a programmed process of mutation referred to as immunoglobulin somatic hypermutation (SHM)[39]. In this process, the B cell receptor (BCR), composed of two identical heavy-chain and two identical light-chain polypeptides bound covalently by disulfide bridges, accumulate point mutations in their V-region to modify their affinity for antigens[40]. After several cycles of rapid proliferation and SHM, smaller and nondividing B cells move to the light zone and undergo positive selection according to their BCR affinity. The light zone contains follicular dendritic and helper T cells that capture antigens and present them to B cells. B cells with low affinity for antigens or unstimulated by T cells activate an apoptotic signaling cascade and are engulfed by tingible body macrophages. In contrast, B cells with high affinity for antigens receive pro-survival signals, differentiate into long-lived plasma cells or memory B cells, and exit the germinal center [39,41,42].

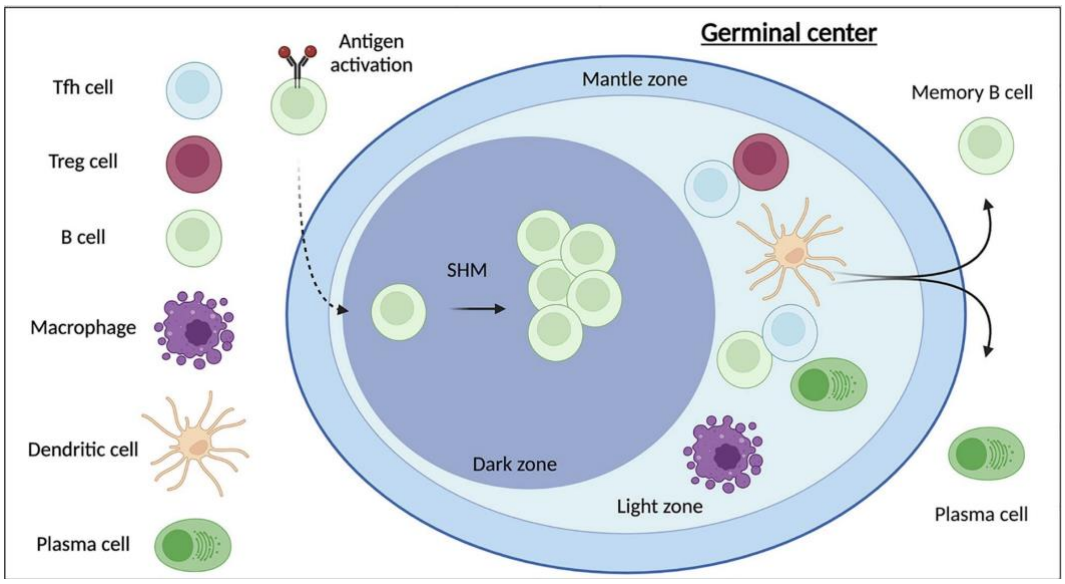

Figure 1.1. Organization of the germinal center in secondary lymphoid nodes. The germinal center is composed of three zones: mantle, dark, and light. Peripherally activated B cells enter the germinal center through the dark zone, where they undergo somatic hypermutation (SMH) of their immune receptor. After crossing to the light zone, they interact with resident follicular/regulatory T helper cells and dendritic cells. Adapted from Mayberry et al. 2022[38], under CC BY license (https://doi.org/10.3389%2Ffimmu.2022.864949).

The SHM that occurs in the germinal center's dark zone does not select for favorable or unfavorable mutations. The resulting mutations are evaluated in the light

zone or outside of the germinal center; these regulatory processes employ cell-to-cell interactions and soluble signals to activate/repress transcriptional programs that determine the survival of the lymphocyte[39]. Thus, abnormalities in these checkpoint mechanisms may contribute to malignant B cell transformation. For instance, chromosomal translocations of an Ig loci to an oncogene during SHM can generate uninhibited expression of the oncogene[41]. Dysregulation of oncogenes and Ig loci mutations are hallmarks of B cell lymphomas that can occur at different stages of B cell development. Most B cell NHL, including Burkitt lymphoma, follicular lymphoma, and DLBCL, originate from germinal center B cells stuck at different stages of maturation. B cell lymphomas are classified according to the histological sites in the lymphoid node where they originated and the histological resemblance of malignant B cells to a differentiation stage in the GC[41,43]. Based on transcriptomic and morphological analyses of malignant B cells, Burkitt lymphoma derives from the dark zone B cells. Follicular lymphoma and DLBCL have a more diverse composition and resemble B cells stuck at GC differentiation, post-germinal center transit, and plasma cell differentiation[39,43].

1.1.4. Mechanisms of B cell lymphoma pathogenesis

There are three major forms of aggressive B cell lymphomas: DLBCL, Burkitt lymphoma, and high-grade B cell lymphoma. The transcriptional modulators required for successful germinal center maturation are intercorrelated. Therefore, mutations and factors affecting these regulatory transcriptional networks promote genetic alterations and contribute directly to lymphomagenesis[39]. Whole-genome and exome analyses of non-Hodgkin lymphoma tissue show genetic amplifications, deletion, translocations, and point mutations contributing to malignant transformation. Other common genetic alterations in NHL are chromosomal translocations and aberrant SHM. A hallmark of lymphoma is the translocation of one Ig loci and a proto-oncogene, as described previously. The translocations are classified into three categories based on their breakpoint mechanism [39,41]: breakpoints derived from mistakes in the recombination-activating gene-mediated V(D)J recombination process, translocations mediated by errors in the activation-induced cytidine deaminase-dependent process, and the activation-induced-cytidine-deaminase-mediated SHM mechanism that generates immunoglobulin-MYC translocations[39,44].

Aberrant immunoglobulin somatic hypermutations target non-immunoglobulin loci and promote malignant transformation[44]. The characteristic oncogenic events of Burkitt lymphoma include mutated IgV sequences, aberrant expression of MYC, and activation of the phosphatidylinositol 3 kinase signaling pathway. The *MYC* oncogene codes for the MYC transcription factor, which participates in cell cycle regulation, proliferation, hematopoiesis, and apoptosis[45]. This oncogene is rapidly transcribed downstream of several membrane receptor complexes, including the T cell receptor, the Transforming Growing Factor β (TGFβ) receptor, the ERK/MAPK kinase pathway, and others[46]. Chromosomal rearrangements, activation of enhancers, retroviral integration, and mutations in signaling pathways can promote *MYC* instability[45]. Interestingly, the translocation of the *MYC* gene has a higher prevalence in DLBCL (5% to 10%) than in Burkitt lymphoma[47]. The E2A transcription factor (encoded by *TCF3*) is also critical for lymphocyte development and can contribute to tumorigenesis. Loss of *TCF3* favours the dysregulation of *MYC* and the proliferation of hematopoietic cells [48–50]. However, when overexpressed, *TCF3* supports the survival of B cells through “tonic” BCR signaling and activation of the PI3K pathway. This pathway is required for cell survival and is a hallmark of malignancy in BL[39,51]. Finally, loss of function mutations in the RhoA pathway are prevalent in Burkitt’s lymphoma and DLBCL tumors. The RhoA protein is the main downstream effector of Gα13 signaling, a G-protein coupled receptor whose gene (*GNA13*) is commonly mutated in Burkitt lymphoma. Punctual mutations in RhoA have been described in 8.5% of pediatric Burkitt lymphoma[52], and around 40% of cases present mutations in genes associated with the RhoA pathway. Mutations affecting the RhoA pathway through inactivation of Gα13 regulators are commonly reported in DLBCL (up to 30%), particularly in germinal center B-cell-like DLBCL [53,54]. Yet, the contributions of altered signaling in the RhoA pathway over malignant growth have not been widely explored and remain relevant topics for research.

1.2. The tumor microenvironment

Tumors are not exclusively neoplastic cells, instead, they are a complex and dynamic environment containing cellular and non-cellular components. The tumor microenvironment is defined as the collection of malignant cells, non-cancerous cells (fibroblasts, adipocytes, immune, and endothelial cells), extracellular matrix components (collagen, elastin, glycosaminoglycans, glycoproteins, and proteoglycans), and the

endocrine or paracrine secretions from any of these cellular components (cytokines, chemokines, growth factors, hormones, etc.)[55]. As a metabolically active tissue, the tumor microenvironment contributes to all stages of cancer development via contact-dependent interactions among cells, secretion of active vesicles, and paracrine signaling[56]. Particularly, this environment promotes and maintains cancer hallmarks such as increased proliferative rate, escape from cell cycle control, immune evasion, replicative immortality, chronic inflammation, angiogenesis, genome instability, dysregulated cellular metabolism, and tissue invasion[57–59]. The specific composition of cells in the tumor microenvironment can change according to the primary cancer site and the patient's inherent characteristics (**Figure 1.2**) [56,60]. Overall, the continuous crosstalk between neoplastic cells and the tumor microenvironment drives the survival and dissemination of cancer[61].

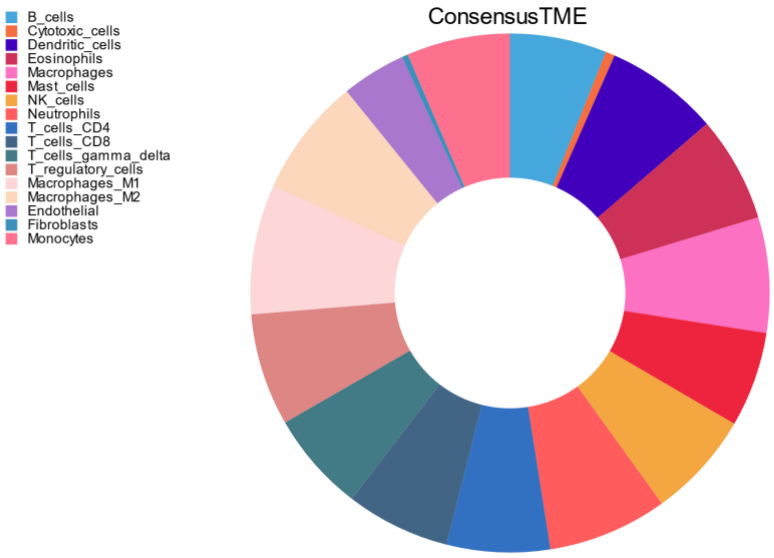

Figure 1.2. Cellular composition of diffuse large B cell lymphoma tumors. Derived from single cell transcriptomics analysis of tumor datasets contained in The Cancer Genome Atlas Database (n = 58 primary tumors). Processed using TIMEDB interactive visualization[60]

1.2.1. The role of the tumor microenvironment in cancer progression

The stromal and noncellular components of the tumor microenvironment are not passive bystanders in tumorigenesis. Instead, they participate in metabolic regulation,

proliferation, and immune evasion. The extracellular matrix provides structural support to the tumor and is mainly produced by stromal cells. Its exact composition and the turnover of its components are closely regulated through different stages of tumor progression and depend on the primary tumor type, its stromal cell composition, and the physical properties of the tissue. Most tumors have a stiff and dense extracellular matrix due to the increased deposition of collagen[62], preventing infiltration by cytotoxic and antigen-presenting cells. A major cell determinant in malignant progression are cancer-associated fibroblasts, the primary source of extracellular matrix components in the tumor[63]. Cancer-associated fibroblasts, unlike their normal counterparts, are metabolically active, mobile, and sensitive to proinflammatory (IL-1, IL-6, TNFα) and mechanical stimuli. These fibroblasts are pleiotropic, with several specialized subtypes described, and have increased expression of smooth muscle actin, vimentin, platelet-derived growth factor receptor α/β, and fibroblast-specific protein 1[56,63,64]. They contribute to the immunosuppressive environment by secreting TGF-β and CXCL12, activating myeloid-derived immunosuppressive cells (IL-6, IL-1β, vascular endothelial growth factor [VEGF], CSF-1, CCL2), and creating a mechanical barrier of extracellular components that impedes immune infiltration[56]. Cancer-associated fibroblasts regulate the concentration of fibrotic proteins in the extracellular matrix and remodel it using metalloproteinases. Therefore, they favour the migration of malignant cells and the development of new blood vessels[65]. Besides, these tumoral fibroblasts constantly secrete pro-survival mediators (TGF-β and hepatocyte growth factor) and produce angiogenic factors (CXCL12, VEGF, FGF2)[66,67]. Finally, they facilitate the immortalization of neoplastic cells via the production of PAI-1 to block caspase-3-mediated cell apoptosis[63,67].

Adipocytes in the tumor microenvironment are metabolically active and participate in cancer progression. The adipose tissue maintains tissular hypoxia and inflammation by secreting damage-associated molecular patterns, creating an ideal niche for mutations and malignant transformation[66,68]. Adipocytes are also thought to participate in angiogenesis, tumor growth, and extracellular matrix remodeling. The adipocytes of breast and ovarian tumors support the survival of cancerous tissue by producing estrogen and other lipidic hormones. The adipokine leptin, a regulator of anabolism and catabolism balance, can be employed as a growth factor in cancer. In contrast, the anti-inflammatory molecule adiponectin is typically suppressed in cancer.

Besides, cancer-associated adipocytes serve as a reservoir of lipid biomolecules to sustain the increased proliferative rate of tumoral cells[68].

A sufficient blood supply is mandatory for cancer cells survival once a tumor reaches a diameter of 2 mm. Before that, tumors derive all necessary nutrients through passive diffusion. Therefore, after this threshold, the tumor reprograms the surrounding tissue to make new vessels and sustain its growth. Angiogenesis, the development of new vasculature, is actively promoted by malignant cells, cancer-associated fibroblasts, infiltrating immune cells, and endothelial cells[69]. Tumors have overt pro-angiogenic signaling (driven by elevated VEGF and low oxygen pressure) that leads to disorganized and defective growth of the vascular endothelium. Tumoral vessels are structurally and functionally poor and perpetuate the chronic inflammatory and hypoxic state of the malignant tissue[56,66]. Benign endothelial cells are structural components of blood vessels and divide only occasionally. On tumors, the endothelium has increased glycolytic metabolism, active proliferation, poor intracellular junctions, and increased motility[69,70]. This endothelium also participates in immune evasion and metastasis. For instance, it prevents immune cell infiltration by decreasing the expression of adhesion molecules (ICAM-1, selectins)[56]. In metastatic dissemination, malignant cells penetrate capillaries through a dynamic and tightly regulated process. The porous and leaky nature of the vessel walls, loss of basement membrane architecture, and scarcity of pericytes covering the endothelium facilitate this migration[56].

The tumor microenvironment is rich in soluble factors like cytokines, exosomes, and signaling nucleic acids. Cytokines and other paracrine mediators are secreted by immune, malignant, and stromal cells in the tumor microenvironment and mediate responses through specific receptors in their targets. Exosomes are extracellular vesicles derived from endosome compartments through the invagination of the membrane. As they are cytoplasmatic in origin, they can contain adhesion molecules, enzymes, signaling factors, or nucleic acids. In cancer, exosomes from malignant cells promote the growth (through microRNA) of other cancer cells. Besides, they mediate communication between malignant and non-malignant cells (particularly cancer-associated fibroblasts) and can signal distant tissues through hematologic dissemination[71]. MicroRNA and long non-coding RNA play relevant roles in tumor progression. Micro RNAs are short (< 15 nucleotides) regulatory molecules that coordinate messenger RNA transcription; in cancer, they modulate pro-tumoral

enzymatic and signaling pathways. One of the better-known cancer-related micro–RNA is mir-21, a molecule that is overexpressed in several cancer types (colorectal, pancreas, glioma, breast, and others) to downregulate the tumor suppressor function of genes such as *PDCD4*, *TPM1*, *MARCK5*, and *PTEN*[72]. Long non-coding RNA have more than 200 nucleotides, are not transcribed, and have central roles in most cellular processes. They participate in signaling pathways, act as decoys to prevent binding of transcription factors to their target DNA, guide proteins towards their targets, and serve as building scaffolds for peptidic complexes[73]. In cancer, long non-coding RNA may have either pro-tumoral or inhibitory properties and are closely related to the functional networks of tumor suppressor genes and oncogenes. Furthermore, many other non-coding RNA (MEG3, NEAT1, lincRNA-p21) seem to regulate the expression of adhesion molecules and epithelial-mesenchymal transition prior to metastasis.

1.2.2. Immune cell composition and their function in the tumor microenvironment

The cellular diversity in the tumor microenvironment varies by cancer type, tissue affected, and disease stage. Single-cell RNA sequencing and mass cytometry analyses from various cancer types reveal high cellular complexity in the tumor site. Innate and adaptive immune cells are key components of the cancer microenvironment that promote or inhibit tumor growth[74]. Infiltrating innate immune cells such as macrophages, neutrophils, natural killers, dendritic cells, and myeloid-derived suppressor cells secrete cytokines (IL-17, IL-6, IL23, TNF) and chemokines (CXCL9 and CXCL10) that recruit other immune cells and facilitate antigen-specific adaptive responses[75]. While innate immune cells fail to control tumor progression by themselves, adaptative immunity, particularly cytotoxic tumor-infiltrating lymphocytes, has potent anti-tumor mechanisms. These lymphocytes recognize tumoral antigens presented by innate immune cells in major histocompatibility complex type I molecules (MHC-I) and activate the targeted killing of malignant cells. However, many of these functions are reprogrammed by malignant cells and the tumor microenvironment to inhibit immunosurveillance and favor tumor growth[76,77].

Tumor-associated neutrophils (TAN) elicit tumor-supportive functions that promote growth, angiogenesis, and metastasis. For example, TAN remodel the extracellular matrix by releasing transforming growth factor-beta (TGF-β) to induce

epidermal mesenchymal transition in lung cancer tissue [77]. Also, TAN secrete oncostatin-M and matrix metalloproteinase 9 that increase the expression of vascular endothelial growth factor (VEGF) to promote angiogenesis, malignant cell intravasation, and metastasis[75,76]. Neutrophils influence lymphocyte T and natural killer cells' cytotoxic effector functions through the production of neutrophil extracellular traps[78]. These traps are tridimensional meshes of chromatin, antimicrobial enzymes (myeloperoxidase, neutrophil elastase), and antimicrobial peptides that are typically found in the primary tumor site during metastasis, or in the bloodstream during localized breast, lung, and colorectal cancer. The extracellular traps also create a physical barrier that prevents interactions between cytotoxic CD8+ T cells and their tumoral targets. Thus, the absence of positive stimuli combined with the abundant suppressor stimuli in the tumor microenvironment (PD-1, LAG3, and Tim3) contribute to lymphocyte exhaustion[79–81]. Finally, neutrophils can have direct tumor suppressor functions mediated by Fcγ receptor expression. For instance, an *ex vivo* model of B cell lymphoma in the presence of anti-CD52 and anti-CD20 monoclonal antibodies revealed that neutrophils can eliminate cancer cells via antibody-dependent cell cytotoxicity[77].

Natural killer cells contribute to immunosurveillance by recognizing and destroying cells with known damage or stress signals in their membrane. Natural killer cells (NK) are $CD56^{+}$, $CD3^{-}$ innate lymphoid cells that circulate in the blood to maintain tissue homeostasis. They recognize membrane-bound signals through germline encoded inhibitory and stimulatory receptors. Hence, they complement the cytotoxic function of lymphocytes, which require antigen presentation in the context of major histocompatibility complexes. The balance between signals received in NK activating and inhibitory receptors determines if an effector function is triggered[82]. When activated, NK have two major mechanisms for target destruction, they can secrete pre-formed granzymes and perforins or express death ligands (FasL, and TRAIL)[82,83]. The degree of infiltration by NK in the tumor microenvironment is variable and dependent on tumor localization, histological type, and local chemotactic signals[84]. In the early stages of a tumor, NK effectively control malignant growth through their immunosensing activity, but established tumors develop mechanisms that hamper their function. For instance, immunoediting (mutations that improve immune escape or increase fitness) and changes in surface receptors prevent the recognition of cancer cells by leukocytes. Also, the immunosuppressive environment of the tumor (cellular and soluble factors) impedes

NK cell activity by reducing the number of stimulatory signals present on cancer cell membranes[83,84].

Dendritic cells (DC) are professional antigen-presenting cells that stimulate adaptive immunity against tumoral antigens. These myeloid lineage cells have different functional subsets, but their primary role is activating T cell effector functions against specific peptide antigens. DC engulf, process, and present these antigens in major histocompatibility complex molecules to T lymphocytes. To activate naive T cells, they migrate to secondary lymphoid organs, express co-stimulatory molecules, secrete chemotactic signals, and release proinflammatory cytokines[85]. The most important subtype in cancer is classical type 1 DC, this subtype is capable of cross-presentation (present extracellular antigens with MHC-I molecules) and induction of CD8+ T cells cytotoxicity against tumors[77]. However, the tolerogenic environment of tumors can impair anti-tumor adaptive immunity by inactivating DC. Stimuli such as IL-10, TGF-β, and VEGF block DC maturation[85,86]. Immature DC lack the necessary costimulatory factors to activate cytotoxic T cells; instead, this poor stimulus promotes a tolerogenic T-cell phenotype. Tumors may also exclude DC through a chemotactic gradient, which confers resistance to therapies that increase the activity of cytotoxic lymphocytes[87].

Myeloid-derived-suppressor cells (MDSC) are pro-tumoral cells derived from polymorphonuclear or monocytic progenitors. MDSC have a Th2 immune response profile and are commonly found in sites with chronic inflammatory processes where myeloproliferative signals are abundant (rich in GM-CSF, M-CSF, IL-6, and IL-1β) [77]. They differ from their normal myeloid counterparts in their tolerogenic effector profile (targeting T cells), increased lipid metabolism, enhanced glycolysis, and unique transcriptomic profile[88,89]. MDSC actively produce reactive oxygen species and nitric oxide to block cytotoxic responses from CD8+ T cells and NK; furthermore, they avidly internalize and degrade arginine, a limiting amino acid for lymphocyte activation. MDSC synthesize and secrete IL-10 and TGF-β, enhancing the immunosuppressive signal of the tumor microenvironment and reprogramming other cells towards a tolerogenic phenotype[90]. MDSC also promote angiogenesis through remodeling of the extracellular matrix and secretion of VEGF[77].

Lymphocytes, especially cytotoxic DC8+ T cells, can recognize and destroy malignant cells and effectively control tumor growth at all stages. CD8+ T cells recognize

tumor-specific antigens in major histocompatibility complex class I molecules and require co-stimulatory signals for activation (ligands and cytokines). CD4+ T cells provide the necessary stimuli to potentiate the response of other leukocytes, including antigen-presenting cells, and facilitate the activation of cytotoxic lymphocytes[74]. However, the overall effect of T cells in the tumor microenvironment relies on the balance between suppressive and stimulatory signals. T regulatory cells (CD4+, FOXP3+) are a subset of T-cells that mediates tolerogenic responses by impeding the function of all other lymphocytes. The development of a tumor-sustaining microenvironment (IL-10, IL-4, IL-13, and TGF-β) around malignant cells contributes to the elevated presence of immunosuppressive regulatory T cells (T-reg) populations on tumors[91]. As mentioned previously, cancer cells undergo immunoediting and change their surface antigens to decrease their recognition by many immune cells, including lymphocytes. Also, neoplastic cells increase the number of inhibitory signals for CD8+ T cells, preventing their activation in the presence of suitable antigens. These inhibitory signals for CD8+ T cells are the target of immune checkpoint therapies, where monoclonal antibodies against these signals (anti-CTLA4, anti-PD1, anti-PDL1) increase anti-tumoral cytotoxicity[74,91].

The role of B cells in non-hematological cancer is debated and may range from pro-tumoral to tumor-controlling. B lymphocytes develop and mature in the bone marrow and have antigen-specific receptors in their membrane. Once activated, B cells optimize the affinity of their B cell receptor (BCR) and transform into actively antibody-secreting plasma cells or memory cells. B cells are incredibly diverse and have a broad range of functional phenotypes, with up to 13 classes described in the tumor microenvironment[92]. The repertoire of cancer-associated antigens recognized by antibodies includes tumor suppressor proteins, aberrant peptides, and self-proteins. Via antibodies, B lymphocytes promote phagocytosis of malignant cells and antibody-dependent cellular toxicity. Furthermore, they contribute to chemotaxis and immune cell activation by producing IFN-γ, TNF, IL-2, GM-CSF, and IL-6. Interestingly, B cells have displayed pro-tumoral effects too. A subset of B cells that actively secretes IL-10 (sometimes TGF-β and IL-35 too) has been described in several cancers as a possible inducer of immune tolerance. Besides, in the context of cancer, most antibodies target self-antigens and generate unspecific and ineffective immune responses that maintain the chronic inflammation of the tumor[92,93].

1.2.3. Macrophages, the most abundant immune cell in the tumor microenvironment

Tumor-associated macrophages (TAM) are typically the most abundant innate immune cells in the tumor microenvironment[94,95]. Macrophages are professional phagocytes that participate in tissue homeostasis, inflammatory responses, and immune defense against pathogens. Macrophages engulf, digest, and present peptide antigens through the major histocompatibility complex class II to activate cells of the adaptive immune system and promote antigen-specific responses[96]. After encountering an appropriate stimulus (antigens, pathogen-associated molecular patterns, or damage-associated molecular patterns), macrophages release soluble cytokines that activate and promote the recruitment of other immune cells. Still, these steps can be hijacked in pathological processes to promote inflammation. The tumor microenvironment avidly recruits macrophages to the tumor site during all stages of cancer[96,97]. However, their metabolism and function are reprogrammed to promote malignant growth and sustain inflammation[98]. Therefore, TAM are heterogenous and can exhibit anti-inflammatory and proinflammatory effector profiles. Reprogrammed TAM display impaired phagocytic capacity and cannot destroy malignant cells or present their antigens to promote adaptive cytotoxic immune responses[99,100].

TAMs have diverse pro-tumoral and anti-tumoral properties. In tumor-bearing cancer patients, an increase of $Ly6C^{+}$ monocytes derived from bone marrow myeloid progenitors is observed because of sustained stimuli by low-level cancer-derived growth factors, cytokines, and damage-associated molecular patterns. These bone marrow derived monocytes are then recruited to primary and metastatic sites by a gradient of M-CSF1, IL-1β, VEGF, and CCL2; after reaching the tumor, they differentiate into TAMs[101]. Conversely, tumor resident macrophages encounter proinflammatory signals since the early stages of cancer that can subvert their phenotype. Their role in the tumor site varies depending on the organ. For instance, lung and pancreatic cancer TAM contribute to tumor progression by favoring fibrosis[102,103]. However, in breast cancer mouse models, TAM seems to be initially beneficial but with a decreasing effect on malignant cells throughout the disease[101].

In cancer, macrophages adapt their function according to the stimuli and cellular composition of the tumor microenvironment. Thus, there is a significant diversity of

TAMs with complex metabolic signatures between different cancer types and within the same tumor[101]. For instance, proinflammatory MHC-II TAMs are characterized by the expression of CD80, CD86, inducible nitric oxidase synthase, and CD68. These TAMs have lower oxidative and glycolytic metabolism compared to reparative MHC-II TAMs. Interestingly, the use of lactate as a carbon source by reparative MHC-II TAMs increases L-arginine metabolism and enhances their capacity to suppress T cells[104]. Single-cell RNA-sequencing technology has revealed the diversity of TAM gene expression[101,105]. According to their transcriptomic profile, TAMs are grouped in seven major subsets across multiple cancer types: inflammatory cytokine enriched-TAMs (Inflam-TAMs), immune regulatory-TAMs (Reg-TAMs), proangiogenic-TAMs (Angio-TAMs), lipid-associated-TAMs (LA-TAMs), resident-tissue macrophage-like TAMs (RTM-TAMs), proliferating-TAMs (Prolif-TAMs), and interferon primed-TAMs (IFN-TAMs).

Inflam-TAMs are characterized by high expression of inflammatory cytokines like IL1-β, CXCL1/2/3/8, CCL3, and CCL3L1, which depend on the activity of NFKB1, NFE2L2, and REL transcription factors. Inflam-TAMs recruit and regulate monocytes, lymphocytes, and granulocytes in a proinflammatory tumor microenvironment through the production of CXCL1, CXCL2, and CXCL3 (recognized by CXCR receptors) or the secretion of CCL3L1 and CCL3 (recognized by CCR1, CCR3, and CCR5)[105]. Reg-TAMs express ARG1, MRC1, and CX3CR1 and have immunosuppressive and angiogenic functions at inflammation sites. They promote macrophage survival in the tumor site and contribute to tumor growth and metastasis[105,106]. Angio-TAMs, characterized by the expression of VEGFA, SPP1, VCAN, FCN1, and THBS1, are commonly found in hypoxic regions of the tumor microenvironment. This subtype favors tumor metastasis via the VEGF growth factor, which facilitates cell intravasation and chemotherapy resistance[105,107]. LA-TAMs express lipid-related genes like *APOC1*, *APOE*, *ACP5* and *FABP5*. They have an increased lipid metabolism (synthesis and catabolism) associated with inflammation and tolerance-related functions. Also, *ex vivo* mice models (MC38) of melanoma have shown that TAMs absorb tumor-derived lipids promoting Arg1 expression to suppress anti-tumoral immunity[108]. RTM-TAMs promote the induction of epithelial-mesenchymal transition and the recruitment of T-reg to the tumor site. The identification of RTM-TAMs in lung cancer mice and human tumors suggests that they also participate in other unknown regulatory processes[105,109]. Also, prolif-TAMs express proliferation markers (MKI67), cell cycle and cell division genes (*CDK1* and *CDC45*,

respectively), and the high mobility group box 1 protein, an intracellular protein that enhances chemoresistance and inflammation in the tumor site[110]. Finally, IFN-TAMs highly express IFN-regulated genes, including *CXCL10*, *PDL1*, *ISG15*, and M1-like markers (MHCII and CD86). Therefore, this tumor-associated macrophage subset resembles proinflammatory M1-like macrophages. Moreover, IFN-TAMs have been identified in many tumor types and have shown primarily pro-tumoral functions by mediating the recruitment of T-reg. Overall, while transcriptomic analyses have shown the diversity of TAMs at the single-cell level, there is no standardized nomenclature and annotation of TAMs and their molecular signatures[105].

1.2.4. The tumor microenvironment in B cell lymphomas

The tumor microenvironments of B cell lymphomas showcase a diverse proportion of malignant to stromal cells. On one edge of the spectrum, Hodgkin lymphoma has an extensive network of support cells with scarce neoplastic B cells. On the other end, rapidly proliferating lymphomas, like the Burkitt lymphoma, have an almost exclusionary population of malignant cells. Interestingly, lymphomas located in secondary lymphoid organs have a tumor microenvironment similar to the normal tissue[111]. Likely, these malignancies hijack the established secondary lymphoid architecture which already supports the survival of lymphocytes. The soluble components of the microenvironment are dependent on the site of origin and the specific lymphoma subtype[111]. Alternatively, the tumor microenvironment of lymphomas can be classified according to their degree of immune cell infiltration and the presence of a proinflammatory transcriptional program; these phenotypes are thought to correlate with responsiveness to immune checkpoint blockade[112].

In Burkitt lymphoma, anti-inflammatory macrophages have been described as the prominent tumor microenvironment immune cell component, creating the characteristic “starry sky” appearance in the histological analysis of tumor tissue[113]. However, the phagocytic activity of TAMs against living malignant cells is almost null as they mainly internalize apoptotic cells and debris. TAMs express molecules that contribute to anti-inflammatory responses and immune evasion. For instance, they express PD-1 ligands that bind to the inhibitory PD-1 receptor on cytotoxic $CD8^+$ T cells. Furthermore, *in vitro* experiments using Raji cells showed that malignant cells secrete IL-1 and IL-13, inducing expression of PD-L1 on TAMs (mediated by the STAT3 and STAT6

transcription factors)[114]. Additionally, TAMs express the signal regulatory protein alpha (SIRPα) on their cell surface, which binds to the overexpressed CD47 ligand of malignant cells and inhibits their phagocytic activity. Therefore, the use of blocking antibodies to increase the uptake of malignant cells by blocking “do not eat me” ligands, represents a promising therapeutic strategy for non-Hodgkin B cell lymphomas[115–117].

1.3. Burkitt lymphoma therapies

The first line of treatment for lymphoma is chemotherapy and the specific regime depends on disease severity, molecular characterization, previous therapies, and prognostic score results. Radiotherapy has limited relevance and is provided only for localized or refractory circumscribed lesions. Even in aggressive lymphomas, treatment has curative intent and five-year survival remains high (>70%) for most subtypes[6,118]. In aggressive non-Hodgkin lymphoma, a typical regime named CHOP consists of three active anti-proliferative compounds (cyclophosphamide, doxorubicin, and vincristine) with an immunosuppressive corticosteroid (prednisolone). For B cell lymphomas, particularly diffuse large B cell lymphoma, regimes containing antibodies against the surface marker CD20 (Rituximab) have drastically improved survival[119,120]. Statistics from the United States of America show aggregated survival for all non-Hodgkin lymphoma cases of 74.3% at 5 years. However, patients of male sex, black ethnicity, and advanced cancer stages continue to present reduced survival[121].

The treatment of Burkitt lymphoma poses a formidable challenge owing to its aggressive and advancing nature, coupled with the heightened risk of central nervous system dissemination. Addressing this malignancy requires a comprehensive approach to effectively combat its rapid progression. In general, five-year survival is above 80% in randomized trials and 70% in real-world conditions[122]. Conditions such as elevated lactate dehydrogenase (indicative of tumor lysis syndrome), central nervous system compromise, history of relapse, and disseminated disease are associated with poorer outcomes[119,123]. Intensive and short-course chemotherapy with drug delivery into the spinal canal is the first option for most patients. Commonly used combinations contain multiple DNA chelating agents and immunosuppressive drugs: CODOX-M-IVAC (cyclophosphamide, vincristine, doxorubicin, methotrexate with etoposide, and cytarabine), or hyper CVAD (cyclophosphamide, vincristine, doxorubicin, dexamethasone, methotrexate, and cytarabine)[118]. Recently, the addition of Rituximab to

most regimes has shown better event-free survival and overall survival, even for advanced cases with bone marrow or central nervous system compromise. However, there is no large randomized controlled clinical trial comparing Rituximab-based regimes and classic intensive chemotherapy; furthermore, refractory cases continue to respond poorly to all available combinations[119,123].

Novel immunotherapeutic drugs based on monoclonal antibodies, such as Rituximab (anti-CD20) and anti-CD47, can improve patient outcomes in lymphoma. CD20 is a transmembrane surface molecule abundantly expressed in B-cell lymphomas. Rituximab was developed over two decades ago (around 1994) and is a chimeric antibody (mouse variable domain and human constant domain) that binds to CD20 and ultimately induces lysis of malignant B cells. Possible mechanisms include complement-mediated cytotoxicity and antibody-dependent cellular cytotoxicity mediated by FcγR, with recent evidence from animal models highlighting the importance of phagocytosis in B cell removal[124–126]. Moreover, Rituximab has indirect effects on malignant cells, promoting apoptosis, sensitizing cancer cells to chemotherapy, and inducing structural changes in the cells[127]. Currently, it is widely used as a first-line therapy for many non-Hodgkin lymphoma subtypes, including Burkitt lymphoma and DLBCL. As some patients are resistant to therapy, ongoing research is elucidating the resistance mechanisms and exploring what subgroups are more likely to benefit from regimes including Rituximab[128,129]. Although other anti-CD20 monoclonal antibodies have been developed and tested for NHL, they have not shown improved clinical outcomes compared to Rituximab for DLBCL[130]. CD47 is an immunoglobulin family protein expressed on the surface of many cells and acts as a “don’t eat me” signal that prevents phagocytosis. It is abundantly expressed in cancerous cells, particularly in blood malignancies, and contributes to immune evasion by binding to the inhibitory receptor SIRP-α (expressed mostly on specialized phagocytic cells)[131]. Inhibition of this axis through monoclonal antibodies (anti-CD47) has shown preclinical evidence of increased phagocytic uptake of cancer cells and tumor size reduction in several cancers. Additionally, anti-CD47 monoclonal antibodies induce phagocytosis through several mechanisms. For instance, after the CD47 blockade, there is an induction of phosphatidylserine exposure, promoting the recognition of apoptotic cancer cells. Furthermore, this blockade also induces antibody-dependent cell cytotoxicity, leading to subsequent phagocytosis[131]. Finally, numerous early clinical trials with anti-CD47 single

or combination regimens are ongoing and the completed ones highlight tolerability of this approach [131,132].

1.4. Phagocytosis, the versatile defense mechanism of macrophages

Phagocytosis is a defense mechanism used by professional phagocytes from the innate immune system, like dendritic cells, granulocytes (neutrophils and eosinophils), and macrophages. This process involves the recognition and ingestion of a variety of particles of different sizes (≥ 0.5-μm), including microorganisms, foreign substances, apoptotic and malignant cells. After internalization, phagocytes present antigens to cells from the adaptive immune response (lymphocytes) to generate a specific reaction that may include proinflammatory cytokines, chemotaxis, and the generation of long-lasting memory cells. Moreover, the clearance of various particles, different from microorganisms, shows the relevant role of phagocytosis in tissue homeostasis and remodeling[133].

1.4.1. Phagocytosis mediated by Fc-γ receptors.

To initiate internalization, receptors in the phagocytic cell interact with ligands on the target (**Figure 1.3**). Opsonic receptors like Fc receptors (FcR) and complement receptors (CR) recognize host-derived proteins (opsonins) such as antibodies, fibronectin, complement proteins, and mannose-binding lectin bound to antigens and initiate phagocytosis. Also, several non-opsonic receptors, such as Dectin-1, Dectin-2, and CD33, have specific tissue and target-dependent roles that facilitate engulfment. Moreover, pathogen-associated molecular patterns can be recognized by Toll-like receptors (TLRs) that cooperate with phagocytic receptors to increase the internalization efficiency of the target[134]. The effectiveness of receptor and ligand binding depends on their affinity and the density of ligands in the target's membrane.

Receptor-ligand interactions trigger signaling pathways that facilitate internalization and activation of macrophages. For instance, during Fcγ receptor-mediated phagocytosis, FcγRI glycoproteins bind the Fc portion of IgG-opsonized particles[134]. Mouse-derived macrophages express pro-phagocytic FcγRI, FcγRIII, and FcγRIV, while FcγRIIB is inhibitory. As the Fcγ chain of these receptors is a dimer, each

activating monomer has an immunoreceptor tyrosine-based activation motif (ITAM), which contains two tyrosine residues required for downstream signaling. Upon receptor clustering, the ITAM motif is phosphorylated by Src family kinases. ITAM phosphorylation promotes the binding of the spleen tyrosine kinase (Syk), an enzyme with two Src homology 2 domains. Syk also phosphorylates downstream intermediates such as the adaptor molecule “linker for activation of T cells”, phosphatidylinositol-3-kinase, and phospholipase Cγ to initiate intracellular pathways that contribute to phagocytosis and transcriptional activation[135]. Phosphorylation of phosphatidylinositol-3-kinase regulates the activation of contractile proteins like myosin and the GTPase Rac, which in turn promote actin remodeling and activation of molecules like the c-Jun N-terminal Kinase and the nuclear factor NF-κB that induces proinflammatory gene expression. Furthermore, phosphorylated phospholipase Cγ produces inositol triphosphate and diacylglycerol to activate the protein kinase C. Finally, protein kinase C activates ERK and p38, extracellular signal-regulated kinases, to promote proinflammatory immune responses. Furthermore, the downstream effects of this cascade activate the guanine nucleotide exchange factor (GEF) Vav which in turn activates GTPases of the Rho and Rac family to promote actin polymerization and the cytoskeleton structural changes crucial for phagocytosis[134,136].

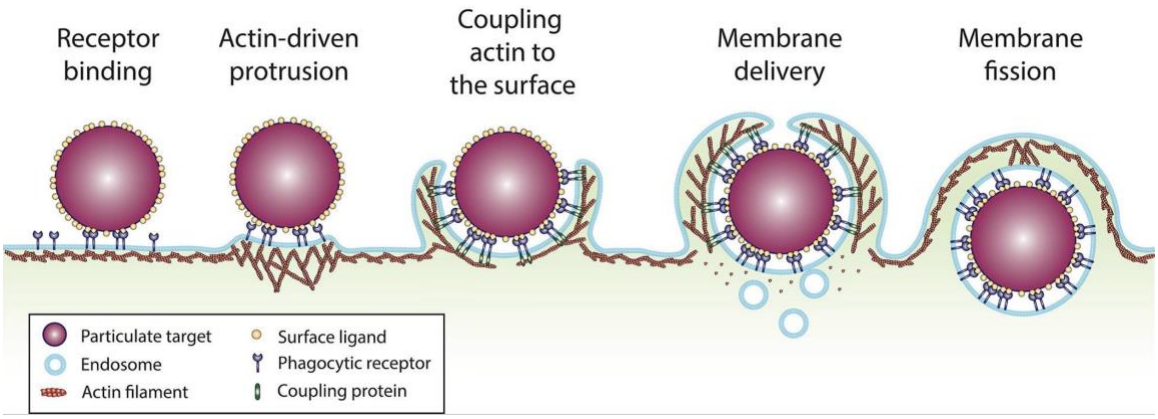

Figure 1.3. Schematic representation of the major steps in phagocytosis. Phagocytosis is a receptor dependent process that requires specific binding between receptor in the phagocytic cell and ligands on the target. After the initial contact, the actin cortex is remodeled to facilitate activation of membrane receptors and increase the surface of contact with the target, creating the phagocytic cup. Finally, the depolymerization of actin at the base of the phagocytic cup allows transit of the newly created phagolysosome into the cytoplasm. Adapted from Jaumouillé and Waterman 2020 (https://doi.org/10.3389/fimmu.2020.01097), under license CC BY.

1.4.2. Phagocytosis mediated by complement receptors.

Complement receptors (CR) also mediate phagocytosis. There are three groups of receptors: CR1 and CR2, formed by short consensus repeat elements; CR3 and CR4, which are integrins from the β2 family; and CRIg, that belongs to the immunoglobulin Ig-superfamily. CR3, also known as αMβ2, CD11b/CD18, and Mac-1 integrin, is the most efficient phagocytic complement receptor in macrophages and mediates the internalization of cancer cells during CD47 blockade[137] (**Figure 1.4**). The Mac-1 integrin is a heterodimeric receptor formed by the subunits α and β. These subunits have an ectodomain, a transmembrane helix, and cytoplasmic tails. The α-subunit ectodomain has a Mg^{2+}-binding-ion-dependant adhesive site and the Adjacent to MIDAS site, which binds to Ca^{2+} or Mn^{2+} and inhibits or activates Mac-1 by promoting conformational changes in its structure[138]. These conformational changes involve the separation of the cytoplasmic tail. Resting integrins display an inactive state characterized by a "bent" conformation with a closed ligand-binding site and contracted membrane proximal regions. Upon integrin activation, the β-subunit detaches from the α-chain separating the membrane proximal regions and opening the ligand binding site[138,139]. The switch from a bent to an extended-open conformation requires the binding of the protein talin to the cytosolic domain of the β chains. Talin connects the integrin with the cytoskeleton through an actin-binding site in its rod domain. This binding generates a force-transmission link between integrins and the cytoskeleton promoting the conformational change of the integrin to an extended conformation with increased affinity for ligands. Vinculin is a protein that binds and reinforces the bridge created by talin between the cell cortex and the integrin. The force transmitted across talin exposes a binding site for vinculin, and attachment of vinculin is also promoted by the phosphorylation of paxillin, another adaptor protein that binds to the β subunit of integrins[140,141]. Finally, effective Mac-1 mediated internalization also requires intracellular factors involved in cytoskeleton regulation, including RhoA, the Arp 2/3 complex, and mDia1[140].

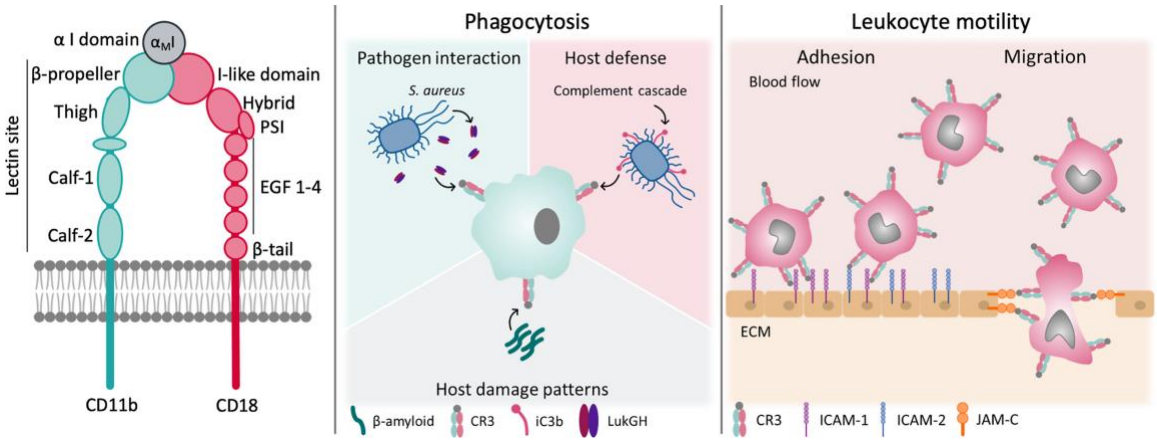

Figure 1.4. Structure of the Mac-1 integrin and its role in phagocytosis and leukocyte motility.

The Mac-1 integrin is formed by the CD11b and CD18 subunits. The extra cytoplasmatic domain binds to various targets to promote their internalization. On the other hand, the intra cytoplasmatic domains bind to the actin cytoskeleton to increase tension, pulling forces and internalization efficiency. The Mac-1 integrin mediates the phagocytosis of pathogens through its direct interaction or the activation of the complement cascade. Additionally, it is involved in homeostatic processes through the recognition of host damage patterns. Finally, the Mac-1 integrin is required for leukocyte motility by binding to the ligands ICAM-1 and ICAM-2 present in the endothelium. Adapted from Lamer et al. 2023 (https://doi.org/10.3389/fimmu.2021.662164)[142] under license under license CC BY.

1.5. The mechanical properties of mammalian cells

The actin cortex is a cytoskeleton structure located underneath the cell membrane in many eukaryotic cells. This cortical cytoskeleton is primarily formed by a disorganized and tightly packed mesh of filamentous actin (F-actin); its thickness and structural organization change according to the cell type and location along the cell membrane[143–145]. This actin cortex determines the tension and form of cells and participates in cell migration, division, and polarization; it also controls specialization in supracellular tissue organization. To regulate the shape of a cell, the actin cortex connects to membrane proteins (ICAM 1-3, CD44, CD43) through linkers like the ezrin-radixin-moesin (ERM) complex or myosin-1 motors. Furthermore, the cortex architecture is the major determinant of the tension along the cell surface[146]. The cortical tension is the force exerted on a piece of the cell cortex by its surrounding network. This property can be measured experimentally and serves as a proxy of cell surface tension. Atomic force microscopy is a widely used technique that applies force to a membrane using a cantilever and infers its surface tension based on the deformability of the membrane[147]. The actin cytoskeleton architecture varies along a spectrum between linearly organized filaments crosslinked by myosin II motors (anisotropic bundle) or randomly distributed

filaments (isotropic mesh); the actin cortex presents mostly disorganized fibers. Two major actin-binding proteins regulate this conformation, formins, and the Arp2/3 complex. Once activated by Rho-GTPases, formins (mDia1, Daam1) catalyze a process called actin nucleation, a preliminary step of filament formation where three actin monomers are bound together[148] **(Figure 1.5)**. Arp2/3 can also catalyze nucleation, but it extends from existing filaments to produce new branches at a 70° angle[145,149].

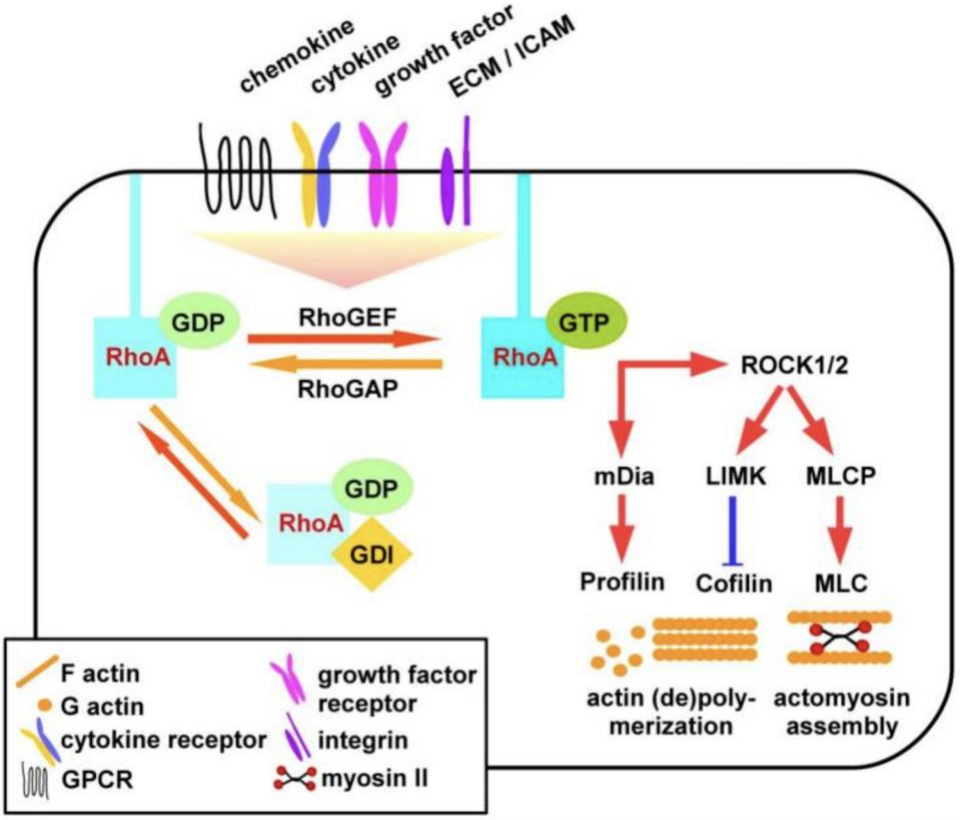

Figure 1.5. RhoA signalling pathway.
Exogenous ligands bind to receptors present on the cell surface and trigger the activation of RhoA GEF. Intracellular events can also promote RhoA GEF activation to engage membrane-bound RhoA, which, in turn, mediates the exchange of GDP by GTP necessary for RhoA activation. The guanine nucleotide dissociation inhibitor (GID) translocates the RhoA protein from the membrane and keeps it in an inactive state. Activation of RhoA regulates cytoskeletal rearrangements. For instance, active RhoA via ROCK/LIMK negatively regulates cofilin, a protein required for F-actin turnover. Additionally, ROCK inhibits MLCP and activates the myosin light chain (MLC) to promote actomyosin assembly for cell motility. Finally, activated RhoA promotes mDia activity that also leads to the activation of profilin, a protein involved in actin remodeling. Adapted from Bros et al. 2019 (https://doi.org/10.3390%2Fcells8070733)[150] under license under license CC BY.

The actin cortex is highly dynamic; its architecture and contractile potential are tightly regulated to maintain the surface tension of the cell. The balance between the branching activity of Arp2/3 and the extension of filaments by mDia defines the local architecture of the actin cytoskeleton. Nucleation-promoting factors and Rho family GTPases regulate the function of these enzymes and impact the cell cortex architecture. For instance, SPIN90 favours mDia nucleation to create long linear filaments, while the Wave regulatory complex interacts with Arp2/3 to increase branching and create an interweaved mesh of actin. Branched filaments are usually shorter as their elongation is quickly adverted by the capping of F-actin barbed ends. The myosin II crosslinkers contribute to the cortical tension because they define the contractile potential of the network. The abundance and activity of myosin motors are regulated by the Rho GTPase signaling pathway. This family of cytoplasmatic enzymes are active when GTP is bound and inactive while bound to GDP. RhoA, one of the most studied members of this family, is thought to be the master regulator of the cell cortex organization. It activates the Rho kinase (ROCK) to phosphorylate and promote the function of myosin II crosslinkers. RhoA also induces formin (mDia) activity to inhibit the severing of actin filaments by cofilin[143,146]. Besides, among the downstream effectors of RhoA is the SLK, which can activate the Ezrin–Radixin–Moesin (ERM) complex[151]. RhoA is a downstream effector of many membrane receptors including cytokine receptors, integrins, and chemokines. As ROCK also mediates cell proliferation, the activity of RhoA is precisely controlled by three proteins. Guanine nucleotide exchange factors (GEF) mediate activation by catalyzing the exchange of GDP to GTP. In contrast, GTPase activating proteins counteract GEF's effect on RhoA by dephosphorylating GTP to GDP. Finally, guanine nucleotide dissociation inhibitors sequester a portion of cytosolic RhoA to avoid overactivation of the pathway[152].

Malignant cells may display abnormal mechanical properties that favor progression and metastasis. In general, the extracellular matrix of a tumor is denser than its normal counterpart and creates a stiffer environment[153]. However, softer and more deformable cells would have increased metastatic potential as they can easily migrate and adapt to bypass all physiological barriers between the primary and distant tumor sites (like the extracellular matrix and endothelial barrier). In recent years, the capacity to analyze the mechanobiological properties of tissues and individual cells has mostly confirmed this hypothesis. Primary studies comparing malignant cells against their

normal counterparts have concluded that neoplastic cells are more deformable, and this property seems to correlate with the grade of the tumor[153–155]. There are no direct comparisons for lymphoma cells against suitable reference cells, only a study reporting that Raji cells have increased deformability compared to normal red blood cells[156]. The overall source of altered biomechanical properties in cancer is not clear. The stiff extracellular matrix of the tumor microenvironment can promote increased deformability in cells through *in vivo* interactions with membrane receptors and activation of transcription factors like YAP and TAZ[154]. Also, changes in the actin cytoskeleton seem to correlate with differences in composition between benign and malignant cells. However, the dynamically changing structure of the cytoskeleton makes it hard to appraise using current available technologies[153,154].

1.5.1. Cytoskeleton reorganization for phagocytosis

During phagocytosis, the cytoskeleton facilitates interactions between receptors and ligands, expands the contact surface, and allows passage of endocytic vesicles to the cytoplasm. Many phagocytic receptors, like Fcγ-R and Dectin-1, are not activated by direct binding to their ligands and instead require lateral clustering along the cell surface[157]. This spatial agglomeration of membrane receptors over their target is facilitated by temporal alteration of the membrane and actin cortex. In a resting state, professional phagocytes constantly reorganize their cell cortex to produce small protrusions that increase their sensing area. Hence, they increase the likelihood of interacting with possible prey compared to unspecialized cells[158]. Also, before phagocytosis begins, receptors have constrained mobility because surrounding large proteins linked to the cytoskeleton impede their free diffusion. After the initial engagement of phagocytic ligands, the cell cortex reorganizes and increases the movement capacity of receptors, which are now free to migrate, interact with ligands, and activate intracellular signals. Key mediators in this initial phase are actin debranching (coronins) and severing proteins (cofilin/gelsolin). Toll-like receptors and chemokine receptors generate localized signals (Syk and Phospholipases activation) that increase the affinity of phagocytic receptors for their ligands and modify the cell cortex morphology to increase ligand-receptor engagement. Once the receptors have tight interactions with their target, the cell extends its membrane (pseudopodia) to expand the surface of contact with the target. This process requires active nucleation of

actin filaments (favored by Arp2/3 activity), which is activated downstream of signals originated in phagocytic receptors (including Mac-1 and FcγR)[133]. Finally, the budding phagosome must traverse to the interior of the cell for further processing. The cortical actin layer beneath the phagocytic cup is depolymerized to allow this transit. Several factors precipitate this process, including the timely depletion of nucleation-promoting agents and the local decrease in phosphorylated lipids that stimulate actin-severing proteins[158].

1.6. Thesis rational and aims

Tumoral cells display increased deformability to migrate during metastasis. Based on the recent understanding of how biomechanical forces mediate the internalization of targets during phagocytosis, we hypothesize that the increased deformability of malignant cells helps them evade phagocytosis. To explore this topic, a suitable model to quantify the internalization of malignant cells by macrophages was developed. We conducted an extensive review of the literature and evaluated the available *in vitro* systems to test our hypotheses. We found important limitations in the accuracy and interpretation of the most widely used microscopy-based assay. Therefore, we established an *in vitro* microscopy model of phagocytosis that improves the quantification accuracy of cancer cell internalization.

To explore the role of the biomechanical properties of malignant cells in macrophage-mediated phagocytosis, we focused on Burkitt lymphoma, a highly aggressive cancer that uses phagocytosis-enhancing antibodies as first-line therapy. However, not all patients respond to pro-phagocytic drugs, and a better understanding of the mechanisms behind the evasion of phagocytosis could improve patient treatment. We modulated the mechanical properties of Raji cells, an *in vitro* human derived Burkitt lymphoma cell line, using mutagenesis and pharmacological approaches, and analyzed the impact of each condition on the internalization efficiency using our newly developed model. Specifically, we investigated the role of RhoA and F-actin polymerization on the biomechanical properties of malignant cells and their phagocytosis efficiency by macrophages.

Chapter 2. Standardization of the *in vitro* model conditions to study the phagocytosis of lymphoma cells

2.1. Introduction

Macrophages are specialized phagocytic white blood cells involved in tissue homeostasis, inflammatory responses, and host defense against microorganisms. As professional phagocytes, macrophages engulf, digest, and present particulate material to cells of the adaptative immune system to promote a specific response. In cancer, macrophages are the predominant myeloid population in the tumor site and are present across all disease stages. However, their metabolism and function are actively reprogrammed by the tumor microenvironment. Therefore, the tumor-associated macrophage population exhibits a heterogeneous phenotype with anti-inflammatory and proinflammatory profiles. Overall, the reprogramming of macrophages decreases their phagocytic capacity and favors tumor progression.

Approaches to enhance the phagocytic capacity of macrophages against cancer cells, like monoclonal antibodies targeting surface receptors in tumoral cells, have improved the prognosis of patients with lymphoproliferative malignancies. For instance, Rituximab was the first monoclonal antibody approved for clinical use in non-Hodgkin lymphomas (NHL), like Burkitt lymphoma. This immunoglobulin G recognizes the surface transmembrane protein CD20, expressed at different stages of B cell differentiation (pre-B cell to plasmablast). Once the binding occurs, B cell internalization is promoted by FcR-mediated phagocytosis. Rituximab has been used as monotherapy, or in combination with chemotherapy to improve the prognosis of B cell NHL. However, relapses and treatment failures have motivated the development of novel approaches to increase the phagocytosis of malignant cells. In many cancers, the self-marker CD47 is a highly expressed membrane protein that interacts with the macrophage signal regulatory protein α (SIRP-α) to block phagocytosis. Therefore, anti-CD47 blocking monoclonal antibodies inhibit this immune checkpoint, potentiating phagocytic responses in macrophages and antigen presentation to CD8+ T cells (**Figure 2.1**). The mechanisms involved in the phagocytosis of cancer cells are largely unknown. FcγR are necessary for the anti-tumoral function of the anti-CD20 monoclonal antibody

Rituximab[124,126]. Also, Chen *et al.* showed that αMβ2 integrin (Mac-1) is required for the engulfment of malignant B cells in the presence of CD47 blockade, whereas FcR are not required[137]. This study revealed an interaction between αMβ2 and SLAMF7 in macrophages. However, it's unclear what ligands of αMβ2 in the cancer cells participate during engulfment.

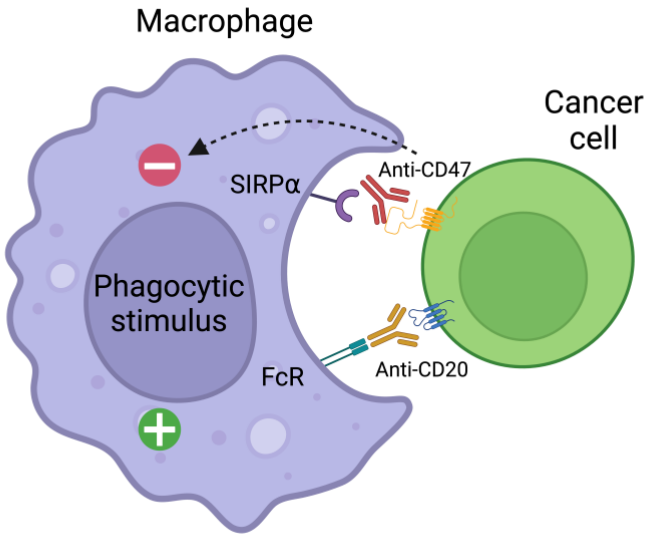

Figure 2.1. Monoclonal antibodies that promote tumoral phagocytosis.
Anti-CD47 blockade impedes interaction between the CD47 "don't eat me" signal on cancer cells with its inhibitory receptor on macrophages, SIRP-α. Monoclonal anti-CD20 antibodies recognize CD20 molecules on B cells. The Fc portion of this antibody interacts with the Fc Receptor on macrophages for antibody-mediated phagocytosis and cellular cytotoxicity. Created with BioRender.com

Based on the recently discovered role of mechanosensing in phagocytosis[140], we believe that the mechanical properties of malignant cells contribute to immune evasion. However, we need an accurate model to quantify internalization and evaluate this hypothesis. So far, the overlap of fluorescent signals from phagocytic and cancer cells in microscopy is used as a proxy for phagocytosis. Yet, the opposition of macrophages and target cells in a two-dimensional plane does not suffice to verify its internalization and could produce inaccurate quantifications. After reviewing the available *in vitro* models of cancer phagocytosis, we decided to develop and standardize a novel assay that allows accurate quantification of internalized cells.

2.2. Methods

2.2.1. *In vitro* model of phagocytosis

To develop the phagocytosis assay of cancer cells, *in vitro* experiments were performed by adhering 50,000 J774A.1 macrophages (DSMZ, ACC 170) to glass coverslips (12 mm, #1.5) in a 24 well plate (Sarstedt, 83.3922.500), followed by 24 hours of incubation at 37℃, 5% CO_2 in 500 µL of DMEM (Gibco) supplemented with 10% heat-inactivated Fetal Bovine Serum (FBS, Wisent, 090-150) per well. After incubation, macrophages were stimulated with 100 ng/mL of interferon gamma (IFN-γ) for 24 hours at 37℃, 5% CO2.

Raji cells (DSMZ, ACC 319), a human B cell line derived from Burkitt lymphoma, were used as our phagocytic target. To evaluate their internalization by macrophages, cells were stained with Calcein Green AM (Invitrogen™, C34852) and Pluronic F-127 (Invitrogen™, P3000MP) in 1 mL of DMEM media without phenol red (Gibco) for 1 hour at 37℃, 5% CO_2. After incubation, cells were washed twice with 1x PBS (Gibco) and centrifuged at 90 *g* for 10 minutes. Cells were diluted in DMEM without phenol red to adjust the concentration to 200,000 cells per 100 µL of media. Macrophage's media was replaced with 500 µL of fresh DMEM without phenol red, anti-CD47 or anti-CD20, or in combination with blocking antibodies (anti-ICAM1, anti-ICAM2, anti-CD18, anti-CD11b, or anti-CD11a) at a 10 µg/mL final concentration and diluted in 20 µL of 1x PBS. Plates were incubated for 15 minutes at 37℃, 5% CO_2. Phagocytosis assays were performed by adding 200,000 Raji cells per well and incubated for 2 hours at 37℃, 5% CO_2. After incubation, cells were washed once, and fixed with paraformaldehyde 4% (Electron Microscopy Sciences, 15714) diluted in 1x PBS for 15 minutes at 37℃, 5% CO_2.

To accurately quantify the internalization of Raji cells by macrophages, an inside-out staining for B cells was developed. After washes, the coverslips were incubated with Hoechst (4 µg/mL) (Invitrogen™, H21486), anti-CD20 (BioXCell, SIM008) and anti-CD11b clone M1/70 (BioXCell, BE0007) primary antibodies in 1x PBS with Bovine Serum Albumin (BSA) 2% for 30 minutes at room temperature and protected from light. After three washes, coverslips were incubated for 30 min under the same conditions with Alexa Fluor-647-conjugated anti-mouse IgG (Jackson ImmunoResearch, 715-605-151) and Cy™3-conjugated anti-rat IgG secondary antibodies (1:400) (Jackson

ImmunoResearch, 715-165-151). Coverslips were washed four times with 1x PBS, transferred to microscope slides with 5 µL of Fluoromount-G™ mounting medium (Invitrogen™, 00-4958-02), and stored at room temperature for 24 hours prior to imaging.

Phagocytic model, cell adherence, and inside-out staining

To standardize the phagocytosis assay of cancer cells, *in vitro* experiments were performed. Initially, bone marrow derived macrophages (BMDM) were extracted from either male or female C57BL/6 mice (6 – 12 weeks of age) provided by the Choy Lab at Simon Fraser University (SFU). The femur and tibia were flushed with 1x PBS, and cells were centrifuged at 500 *g* for 10 minutes. Erythrocytes were lysed using 1 mL of 1x Red Blood Cell lysis buffer (Invitrogen™, 00-4333-57) and incubated for 1 minute at room temperature. The progenitors were centrifugated and diluted in 3 mL of DMEM (Gibco, 11995-065) supplemented with 10% FBS. 400,000 cells/mL were seeded and propagated in Petri dishes for three days using 10 mL of DMEM supplemented with 10% FBS and 10 ug/mL of M-CSF (Peprotech, 315-02) at 37℃, 5% CO_2. After incubation, 5 mL of media were replaced by fresh DMEM supplemented with 10% FBS and 10 ug/mL of M-CSF. Macrophages were incubated for four days at 37℃, 5% CO_2. Once the progenitors differentiated, BMDM were detached from the Petri dishes plates using Trypsin-EDTA (0,25%) phenol red (Gibco™, 25200056) and 50,000 macrophages per well were seeded in a 24 well plate (Sarstedt, 83.3922.500) with glass coverslips (12mm, #1.0). Cells were incubated for 24 hours at 37℃, 5% CO_2. Macrophages were activated using CCL3 (Peprotech, 250-09) and CCL5 chemokines (Peprotech, 250-07) for 24 hours at 37℃, 5% CO_2. Phagocytosis assays were performed by adding 200,000 B cells (Raji) in combination with anti-CD47 or anti-CD20, and blocking antibodies as required per condition.

The evaluation of B cell internalization using BMDM required the preparation of progenitor cells every week. Thus, we decided to standardize J774A.1 macrophages as our *in vitro* model of phagocytosis and optimize the frequency of experiments and the viability of cells. Glass coverslips were transferred to a 24 well plate (Sarstedt, 83.3922.500). Various concentrations of macrophages were evaluated for cell adherence during the standardization process (30 x 10^3, 35 x 10^3, 40 x 10^3, 45 x 10^3 and

50 x 10^3 macrophages) and incubated for 24 hours at 37℃, 5% CO_2 in 500 µL of DMEM supplemented with 10% FBS.

Activation of macrophages

BMDM were stimulated with 10 ng/mL of CCL3 and 100 ng/mL of CCL5 chemokines during the standardization process. J774A.1 macrophages were activated with 100 ng/mL of IFN-γ (Peprotech, H3116) for 24 hours at 37℃, 5% CO_2 before the phagocytosis assay. 100 UI of Lipopolysaccharide (LPS) (Sigma-Aldrich, L4005-100MG) was also used to evaluate macrophage activation. The effect of IFN-γ and LPS was assessed alone and in combination with anti-CD20 and anti-CD47 antibodies.

Inside-out staining of living Raji cells

To accurately quantify the internalization of living lymphoma cells by macrophages, various viability dyes were tested. Raji cells were dyed with 1 µM of CellTrace™ Far Red Cell Proliferation Kit (Invitrogen, C34572), 1 mM of CellTrace™ Calcein Green, AM (Invitrogen, 65-0853-81), CellTrace™ Calcein Red-Orange, AM (Invitrogen, C34851), 1 mM of Calcein Deep Red™, AM ester (Fisher Scientific, 50-225-0024), 1.5 mM of Propidium Iodide (Invitrogen, P3566), and 2 µM of Cell Proliferation Dye eFluor™ 450 (eBioscience™, 65-0842-85). 2 x 10^6 Raji cells were centrifuged at 500 *g* for 5 minutes, at room temperature. Cells were resuspended in 1 mL of DMEM and staining reagents were added according to the experimental conditions. Cells were incubated for 1 hour at 37℃, 5% CO_2. Cells treated with the CellTrace™ Far Red Cell Proliferation Kit were incubated only for 20 minutes. After incubation, cells were washed twice with 1x PBS, and 400,000 Raji cells were adhered to 12 mm glass coverslips (12mm, #1.0) previously coated with Poly-L-Lysine (Gibco) at 0.5 mg/mL in 1x PBS for 20 minutes, at room temperature. Coverslips were washed once, and fixed with paraformaldehyde 4% diluted in 1x PBS for 15 minutes at 37℃, 5% CO_2.

An inside-out staining for B cells was standardized to differentiate cells internalized by macrophages from those non-internalized. After two hours of macrophages and Raji cells co-incubation, coverslips were fixed and incubated for 30 minutes at room temperature with primary and secondary antibody combinations to label the cell membrane. Coverslips were washed three times with 1x PBS after each

incubation and stored at room temperature (protected from light) for 24 hours before imaging.

The standardized inside-out staining requires the incubation of coverslips with Hoechst (4 µg/mL), anti-CD20, and anti-CD11b clone M1/70 (BioXCell, BE0007) primary antibodies in 1x PBS with BSA 2% for 30 minutes at room temperature. After three washes, cells were incubated with Alexa Fluor-647-conjugated anti-human IgG (Jackson ImmunoResearch, 709-605-149) and Cy™3-conjugated anti-rat IgG (Jackson ImmunoResearch, 712-165-153) secondary antibodies in 1x PBS with BSA 2% for 30 min (1:400) also at room temperature. Anti-CD20 antibodies allow the recognition of non-internalized B cells, while anti-CD11b clone M1/70 binds to the macrophage membrane. Coverslips were washed four times and transferred to microscope slides with 5 µL of Fluoromount-G™ mounting medium. Coverslips were stored at room temperature (protected from light) for 24 hours prior to imaging.

Leukadherin concentrations

We evaluated the effect of Leukadherin-1 (LA-1, a Mac-1 integrin agonist) (Sigma-Aldrich, SML0886-5mg) on phagocytosis assays of Raji cells by macrophages. Briefly, cells were co-incubated for two hours at 37℃ and 5% CO_2 in 500 µL of DMEM depleted of phenol red (Gibco). Leukadherin (2.5, 5, 7.5, and 10 µM) and anti-CD20 or anti-CD47 antibodies (10 µg/mL) were added as required. After incubation, coverslips were washed three times with 1x PBS and transferred to microscope slides with 5 µL of Fluoromount-G™ mounting medium. Coverslips were stored at room temperature (protected from light) for 24 hours and prior to imaging.

2.2.2. Confocal microscopy imaging

The phagocytosis assay (Raji B cells by J774A.1 macrophages) was analyzed using images obtained on a Yokogawa CSU-W1 spinning disk confocal head mounted on Nikon Eclipse Ti2 microscope. The NIS Elements (Nikon) software was used to adjust the microscope functions. Phagocytosis assays were imaged on glass coverslips with an x40 1.3 NA oil objective. Illumination was provided by solid-state lasers 405 nm (for Hoechst dye, nuclei visualization), 488 nm (for EGFP excitation, Calcein green AM), 561 nm (for mCherry and Alexa Fluor-647-conjugated anti-mouse IgG, B cell membrane), and 655 nm (for Cy™3-cojugated anti-rat IgG, macrophage membrane).

Emission was collected via multi-bandpass dichromic and single-bandpass emission filters (455/50 nm for blue, 525/360 nm for green, 605/52 nm for red, and 705/72 for far red). Ten images per channel and condition were captured in rapid succession for multicolor images with Perfect Focus. Images were analyzed and quantified using ImageJ version 1.54f[159]. For 3D imaging, confocal stacks were assembled with NIS Elements (Nikon).

2.2.3. Cell lines and antibodies

J774A.1 macrophages were cultured in DMEM (Gibco) medium supplemented with 10% heat-inactivated FBS at 37℃ in a 5% CO2 incubator. To evaluate the internalization of cancer cells, we used Raji cells (B cell lymphoma, provided by the Morin Lab at SFU) as phagocytic targets. This cell line was cultured in RPMI 1640 medium (Gibco) supplemented with 10% heat-inactivated FBS at 37℃ in a 5% CO2 incubator. To evaluate the effect of cytokines in the activation of macrophages, BMDM were extracted from either male or female C57BL/6 mice (6 – 12 weeks of age) provided by the Choy Lab at SFU. Femur and tibia were flushed with 1x PBS, erythrocytes were lysed with 1x Red Blood Cell lysis buffer, and 400,000 cells/mL were seeded and propagated in Petri dishes for 5 days using DMEM supplemented with heat-inactivated FBS and 10 ug/mL of M-CSF.

For flow cytometry and ligand blockade the following antibodies were used at 10 µg/mL: monoclonal anti-CD11b clone M1/70 (BioXCell, BE0007), anti-CD18 clone GAME-46 (BD Biosciences, 55-52-80), anti-F4/80 (BioXCell, BE0206), anti-ICAM1 (BioXCell, BE0020-2), anti-ICAM2 (Invitrogen, BMS109), anti-CD47 (BioXCell, BE0019-1), anti-CD20, Alexa Fluor® 647-conjugated anti-human IgG (Jackson ImmunoResearch, 709-605-149), Cy™3-cojugated anti-mouse IgG (Jackson ImmunoResearch, 715-165-151), human IgG1 isotype control (BioXCell, BP0297), and IgGA2 isotype control (BioXCell, BE0085). For the inside-out staining, anti-CD20 and Alexa Fluor® 647-conjugated anti-human IgG (1:400) were used as primary and secondary antibodies to label the membrane of B cells. The membrane of macrophages was labeled with anti-CD11b clone M1/70 and Cy™3-cojugated anti-rat IgG antibodies (1:400).

2.2.4. Statistical analysis and reproducibility

Two pilot experiments were performed and quantified to define the number of replicates required to achieve a precise phagocytic index (PI). Initially, five images per condition were taken and quantified. However, to minimize variability, ten images per condition were taken by spinning disk confocal microscopy.

The number of macrophages, internalized-intact B cells, internalized-fragmented B cells, non-internalized B cells in contact and not in contact with macrophages were manually quantified using ImageJ version 1.74f. The phagocytic index was calculated for each image dividing the number of internalized B cells (intact and fragmented) by the number of macrophages per image. Statistical analyses were performed using GraphPad Prism 9.5.1 for MacOS. Error bars represent standard errors of the mean. Three independent replicates were performed per experiment. A non-parametric two-tailed Mann-Whitney test was used for statistical comparison between conditions.

2.3. Results

2.3.1. Target of phagocytosis

We used Raji cells, a human B cell line derived from Burkitt lymphoma, as the phagocytic target. To allow tracking of their internalization by macrophages, we evaluated various dyes during the standardization process including Calcein Green, Calcein Red-Orange, Calcein Deep Red, Propidium Iodide, CellTrace™, and proliferation dye (at different concentrations). Among them, Calcein Green and Red-Orange homogenously stained Raji cells and showed the best fluorescence intensity **(Appendix A1)**. Also, Calcein green's fluorescence spectrum is compatible with the emission from the reporter employed for B cell transfection (pSBtet-GFP). Therefore, Calcein Green was selected to stain, identify, and quantify living lymphoma cells in our *in vitro* model of phagocytosis.

We noticed that some lymphoma cells overlay the macrophages but are not internalized. To avoid the erroneous counting of these overlapping cells as phagocytosed, we developed an inside-out staining. A combination of primary and secondary antibodies at different concentrations was evaluated to find the optimal

fluorescence emission for macrophage and B cell identification **(Appendix A2)**. Briefly, after fixation, cells were incubated with anti-CD20 (primary antibody), and anti-human IgG Alexa Fluor-647 (secondary antibody). Anti-CD20 antibodies bind to CD20 ligand on the membrane of B cells and let us visualize non-internalized cells; in contrast, phagocytosed cells lack any fluorescent signal. Additionally, we labeled the membrane of macrophages with anti-CD11b clone M1/70 antibodies to facilitate the identification of Raji cells colocalized above the macrophage but not necessarily internalized **(Figure 2.2)**. Thus, with the inside-out staining we can easily identify and quantify only internalized cells that lack anti-CD20 fluorescence.

2.3.2. Selection of phagocytic cell line

We performed *in vitro* experiments with BMDM and the mice cell line J774A.1 as potential phagocytic cells in our assay. Initially, progenitor cells were obtained from C57BL/6 mice femurs and differentiated into macrophages. As the internalization of cancer cells by non-stimulated macrophages is low (approximately 4-11%), BMDM were activated using CCL3 and CCL5 chemokines, which have been identified in the tumor microenvironment of lymphomas as known activators of Mac-1. Our phagocytosis assays were performed by adding 200,000 Raji cells and CD47 or CD20 blocking antibodies[160,161]. No significant differences in the proportion of macrophages that internalized cancer cells (phagocytic index) were observed compared to the control in the presence of anti-CD47 (with CCL5 $p = 0.2544$; with CCL3 $p = 0.3039$) or anti-CD20 antibodies (with CCL5 $p = 0.9527$; with CCL3 $p > 0.9999$) **(Appendix A3)**. We concluded that CCL5 and CCL3 were not effective stimuli for our phagocytic cells in this context.

Our initial approach to the phagocytosis assay using BMDM was labour intensive, requiring the preparation of progenitor cells every week. Thus, we tested J774A.1 macrophages as an alternative *in vitro* phagocytic cell to optimize the frequency of experiments and improve their viability. We evaluated different concentrations (30 x 10^3, 35 x 10^3, 40 x 10^3, 45 x 10^3, and 50 x 10^3) to determine the optimal one for quantification of B cell internalization. The best distribution of cells in the coverslip was found by adhering 50 x 10^3 macrophages per well. Moreover, this concentration prevented cell detachment after the necessary washing steps of the phagocytosis assays. At lower concentrations, cells displayed decreased adherence. For instance, no

differences were observed between 10 x 10^3 and 35 x 10^3macrophages per well **(Appendix A4)**; however, the cell concentration was lower due to mechanical perturbation of the media. Although the cell distribution of conditions with 40 x 10^3, 40 x 10^3, and 45 x 10^3 were similar, cells clumped on the coverslips affecting macrophage adherence and quantification of internalized B cells **(Appendix A4)**. Based on these results, we selected J774A.1 macrophages as phagocytic cells at a concentration of 50 x 10^3 cells per well.

2.3.3. Evaluation of stimuli for phagocytosis

The CCL5 and CCL3 chemokines did not affect B cell internalization, which could be associated with the expression levels of these chemokines receptors (CCRs) in the J774.A1 mouse cell line. Moreover, the role of these cytokines in the proinflammatory immune response is mainly related to cell recruitment and chemotaxis. Therefore, the adherence of macrophages to the coverslips prevents the involvement of additional cells to potentiate the antitumoral response and phagocytosis[162]. We also tested LPS and IFN-γ as stimuli for J774A.1 macrophages. We added 50 x 10^3 cells in combination with anti-CD47 or anti-CD20 antibodies. We selected these compounds (LPS and IFN-γ) based on their widespread use in macrophage models of phagocytosis and promoters of proinflammatory phenotype[163,164]. Phagocytosis of lymphoma cells by macrophages stimulated with LPS and IFN- γ showed a significant difference in the internalization of Raji cells compared to unstimulated macrophages (LPS: 0.19, IFN- γ: 0.09, control: 0.05, $p < 0.0001$). The PI with LPS was higher compared to IFN- γ (LPS: 0.19; IFN-γ: 0.09, control: 0.05, $p < 0.0001$). No significant differences in the PI were observed among the two stimuli in combination with CD47 blockade (LPS: 0.30, IFN-γ: 0.29, $p = 0.6460$) or anti-CD20 antibodies (LPS: 0.36, IFN-γ: 0.36, $p = 0.9444$) **(Figure 2.3)**. Therefore, the effect of LPS on internalization seems to be less dependent on monoclonal antibodies and may also involve phagocytosis mechanisms that do not necessarily include Mac-1 or FcR. Moreover, the internalization of B cells by macrophages using IFN-γ or LPS was significantly higher with the addition of anti-CD20 (PI with LPS: 0.36, with IFN-γ: 0.36, and CD20 alone: 0.22; $p < 0.0001$) or anti-CD47 antibodies (PI with LPS: 0.30, with IFN-γ: 0.29, and CD47 alone: 0.17; $p < 0.0001$). These results highlight the role of proinflammatory signals on macrophage activation and their phagocytic capacity. Unlike LPS, IFN-γ is a cytokine released by activated T cells in the tumor microenvironment

that endorses immune surveillance[164] by promoting the activation of IFN-γ responding macrophages; therefore, we selected IFN-γ as the stimulus for our phagocytosis model. Finally, additional cytokines could be tested in future experiments to stimulate macrophages; for instance, IL-10 and IL-1β are molecules that play a role in the physiopathology of non-Hodgkin lymphomas by promoting B cell growth activity and macrophage activation *in vitro*[165,166].

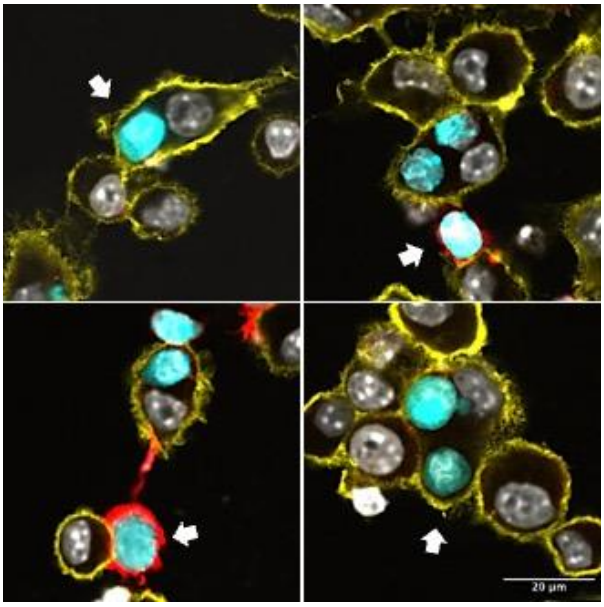

Figure 2.2. Inside-out staining of Raji cells and J774A.1 macrophages.
Non-internalized Raji cells were stained with Calcein green (cyan). The CD20 membrane ligand of non-internalized Raji cells was targeted using anti-CD20 antibodies (red = anti-CD20). Once lymphoma cells are phagocytosed by macrophages (yellow = anti-CD11b clone M1/70), the red fluorescence disappears (40x).

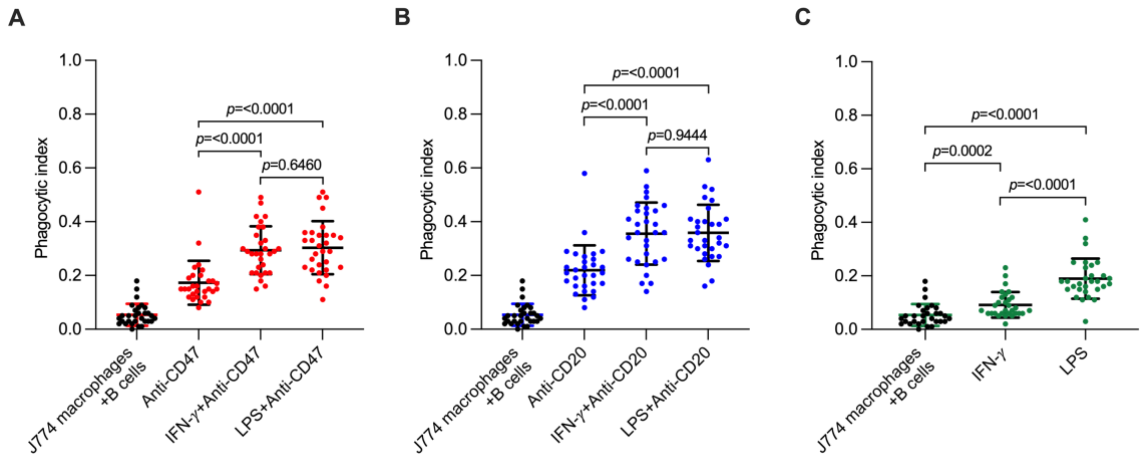

Figure 2.3. Stimulation of J774.A1 macrophages with IFN-γ and LPS.
Internalization of Raji cells after 2 hours of incubation with J774.A1 macrophages and **(A)** anti-CD47, **(B)** anti-CD20, **(C)** or without antibodies. Macrophages were stimulated for 24 hours before the assay (n = 30 fields of view, three experimental replicates). Bars represent means and SD. Mann-Whitney test was used for comparisons.

2.3.4. Quality assurance of the phagocytic model

Next, we corroborated the role of integrins in the internalization of Raji cells using the *in vitro* phagocytosis model **(Figure 2.4).** The Mac-1 integrin is abundantly expressed on the surface of monocytes/macrophages to interact with its ligands ICAM-1 and ICAM-2 as part of its function in cell adhesion, migration, proliferation, and phagocytosis. Interestingly, activated macrophages at sites with high level inflammation show higher levels of the Mac-1 integrin[167]. In the context of hematopoietic cancers, Mac-1 (a heterodimer composed of CD11b and CD18) facilitates the internalization of malignant cells during the CD47 blockade[137]. A significant decrease in internalized Raji cells was found when blocking any of the two subunits in the presence of anti-CD47 (CD11b = 0.15 – $p < 0.0001$; CD18 = 0.16 – $p < 0.0001$; control = 0.34) and anti-CD20 antibodies (CD11b = 0.15 – $p < 0.0001$; CD18 = 0.18 – $p < 0.0001$; control = 0.18) **(Figure 2.5)**. With this analysis, we confirmed the role of the Mac-1 integrin in our standardized model of phagocytosis and that its functionality depends on both subunits.

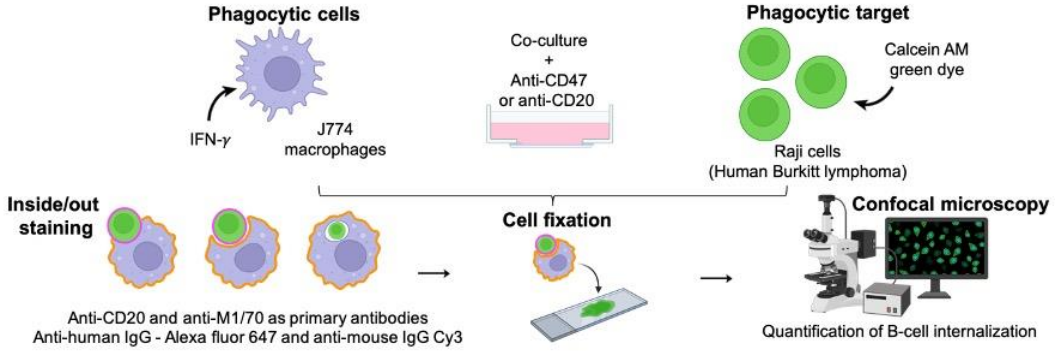

Figure 2.4. Standardized in vitro model conditions to study the phagocytosis of lymphoma cells.

J774A.1 macrophages (50,000 cells/500 µL) were adhered on 12 mm coverslips in a 24 well plate. After incubation for 24 hours at 37℃, 5% CO2, macrophages were stimulated with 100 ng/mL of IFN-γ. Then, anti-CD47 or anti-CD20 antibodies were added to each condition (10 µg/mL) 30 minutes before the addition of cancer cells. Raji cells were stained with Calcein green for 1 hour at 37℃, 5% CO2. Cells were incubated for 2 hours and fixed with paraformaldehyde 4%. Anti-CD20 was used as primary antibody to label non-internalized Raji cells and IgG anti-human Alexa fluor 647 was used as secondary antibody. Anti-CD11b clone M1/70 was used to label the membrane of macrophages and IgG anti-mouse Cy3 was used as secondary antibody. Cells were mounted using Fluoromount-G and visualized after 24 hours in the confocal microscope at 40x. Created with BioRender.com.

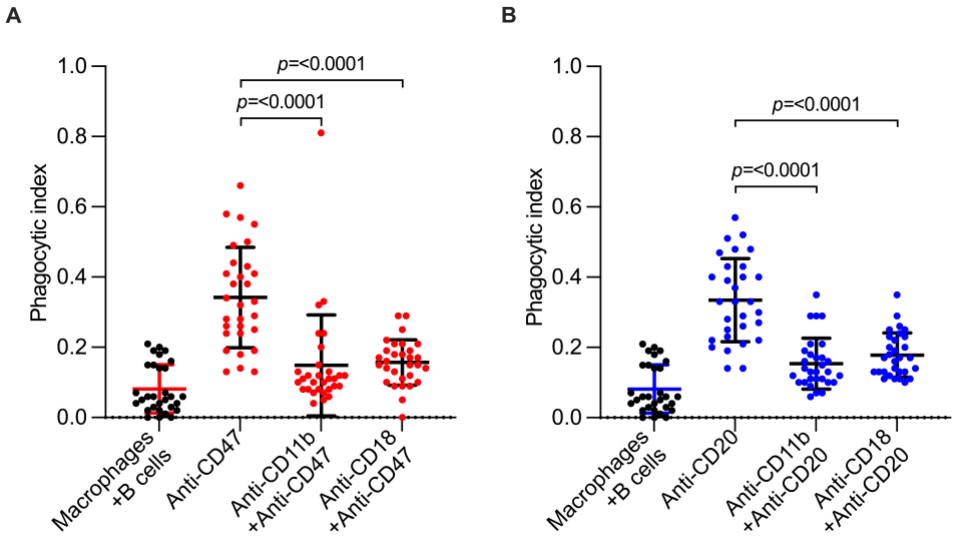

Figure 2.5. Mac-1 integrin is required for internalization of living lymphoma cells by macrophages during anti-CD47 blockade and Rituximab.

Internalization of Raji cells after 2 hours of incubation with J774A.1 macrophages and **(A)** anti-CD47 or **(B)** anti-CD20 antibodies (n = 30 fields of view, three experimental replicates). Bars represent means and SD. Mann-Whitney test was used for comparisons.

Mac-1 is known to interact with several ligands for cell adhesion and internalization; although the ligands mediating tumoral cell internalization are not established[137]. The blockade of Mac-1 major ligands (ICAM-1 and ICAM-2), showed that ICAM-2 is necessary for Mac-1 mediated phagocytosis of lymphoma cells during CD47 blockade. In contrast, ICAM-1 and ICAM-2 ligands were necessary for Raji cell internalization in the presence of anti-CD20 antibodies **(Figure 2.6)**. To explore the role of other members of the β2 family of integrins on the phagocytosis of lymphoma cells, we evaluated the phagocytic rate of Raji cells after blocking the CD11a subunit of the αLβ2 integrin. We found a significantly decreased uptake of malignant cells after this blockade and in the presence of anti-CD47 (PI = 0.15 vs 0.26, p = < 0.0001) or anti-CD20 antibodies (PI = 0.16 vs 0.27, p < 0.0001) (**Figure 2.7**). However, blocking the CD11b subunit produces a stronger decrease in phagocytosis compared to CD11a with both antibodies, anti-CD47 (Normalized PI of 0.44 vs 0.58, p = 0.0037) and anti-CD20 (Normalized PI of 0.47 vs 0.61, p = 0.0132) **(Figure 2.7)**. These results suggest that other members of the β2 integrin family could mediate the internalization of lymphoma cells, providing insights into the role of structural membrane surface proteins for future studies. For instance, we could knock out the alfa subunit of other integrins from the β2 family of integrins (αX, αL, αD) to independently evaluate their role in the phagocytosis of cancer cells[168]. This approach will determine their relevance in B cell internalization. However, as expected and previously described in the literature, the Mac-1 integrin is more relevant for the internalization capacity of macrophages[167].

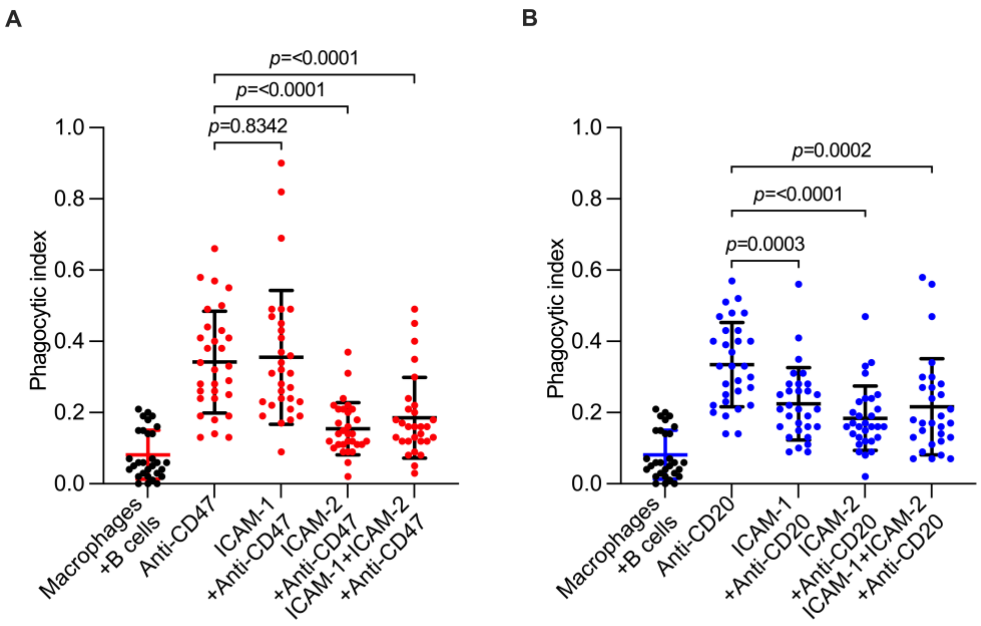

Figure 2.6. ICAM-2 is required for phagocytosis as a ligand of Mac-1 integrin during CD47 blockade and Rituximab.

In the presence of **(A)** the CD47 blockade, only ICAM-2 is necessary for phagocytosis as a ligand of the Mac-1 integrin, while **(B)** ICAM-1 and ICAM-2 are required during Rituximab mediated phagocytosis (n = 30 fields of view, three experimental replicates). Bars represent means and SD. Mann-Whitney test was used for comparisons.

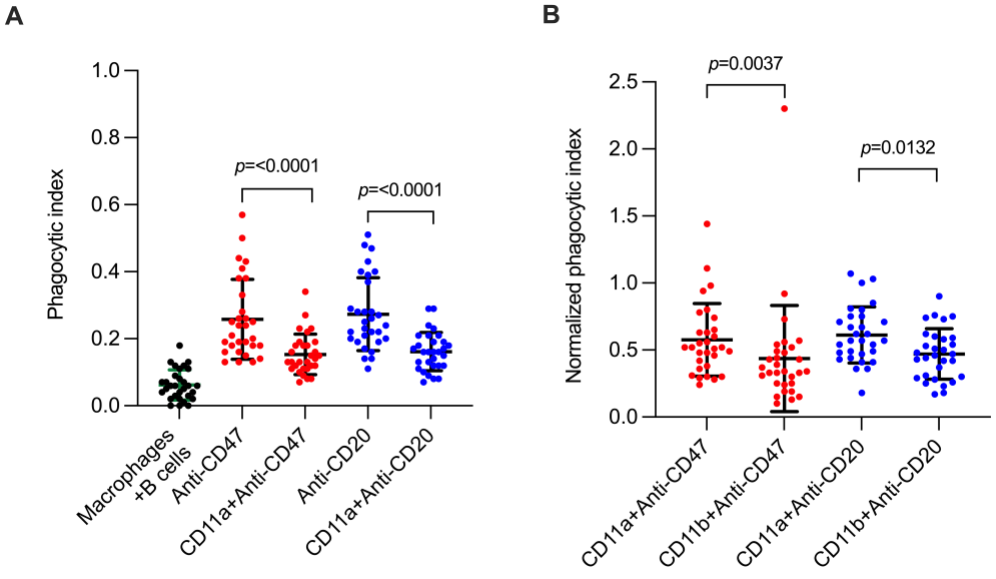

Figure 2.7. LFA-1 integrin (CD11a/CD18) is also involved in the internalization of lymphoma cells during CD47 blockade and Rituximab.

Blockade of the CD11a subunit of the αLβ2 integrin decreased internalization of Raji cells after 2 hours of incubation with J774A.1 macrophages in the presence of **(A)** anti-CD47 or anti-CD20 antibodies. **(B)** Comparison of B cell internalization by macrophages after blocking the CD11a

and CD11b subunits (n = 30 fields of view, three experimental replicates). Bars represent means and SD. Mann-Whitney test was used for comparisons.

We further evaluated the role of the Mac-1 integrin in the internalization of lymphoma cells by using its agonist Leukadherin (LA-1). To find the ideal *in vitro* concentration that enhances Mac-1 mediated phagocytosis, we picked two LA-1 concentrations recommended in the scientific literature. The optimal concentrations of 2.5 and 5 μM were used in combination with anti-CD47 or anti-CD20 antibodies. The use of Leukadherin 5 μM and anti-CD47 did not increased the phagocytosis of malignant B cells (PI of 0.30 vs 0.36, p = 0.0303); however, in the presence of anti-CD20 antibodies a significantly higher phagocytosis efficiency of lymphoma cells was observed (PI of 0.44 vs 0.35, p = 0.0004). Furthermore, while the use of 2.5 μM in the presence of Rituximab also showed an increased B cell uptake (p = 0.0002), no differences were observed using this concentration in combination with the CD47 blockade (p = 0.1881) **(Figure 2.8)**. Our data confirms that Mac-1 activation via the LA-1 agonist contributes to higher internalization efficiency during the Rituximab mediated phagocytosis.

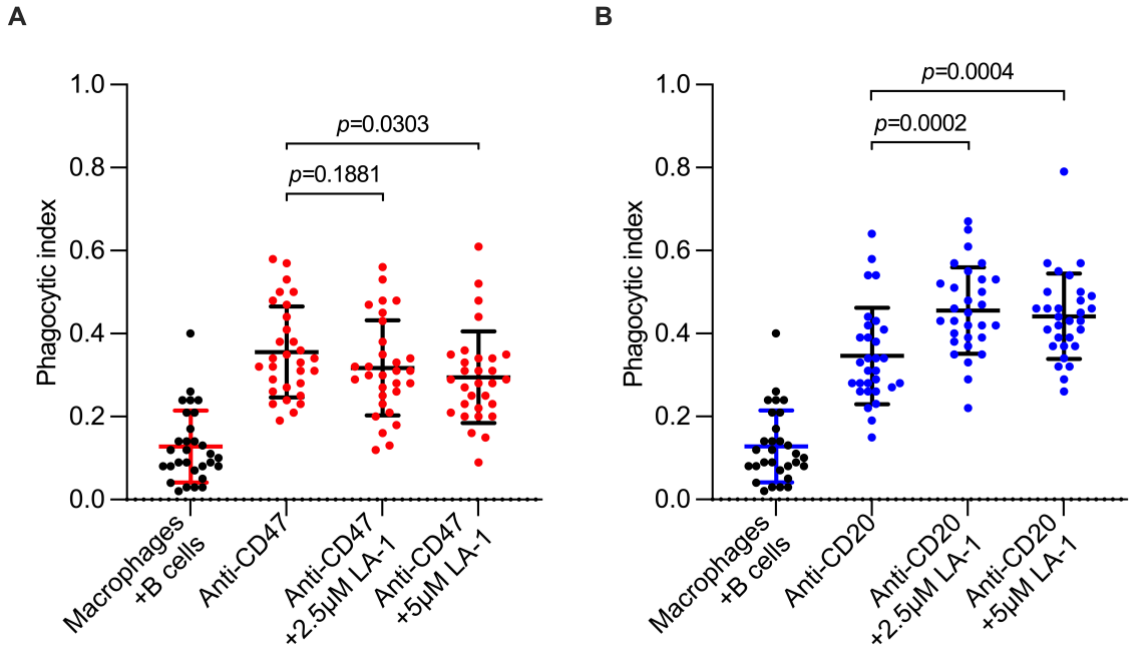

Figure 2.8. Leukadherin (LA-1) impacts Mac-1 dependent phagocytosis during CD47 blockade and in the presence of Rituximab.
Internalization of Raji cells after 2 hours of incubation with J774A.1 macrophages in the presence of **(A)** anti-CD47 or **(B)** anti-CD20 antibodies and Leukadherin at 2.5 and 5 μM (n = 30 fields of

view, three experimental replicates). Bars represent means and SD. Mann-Whitney test was used for comparisons.

2.4. Discussion

Macrophages are abundant professional phagocytic cells in the tumor microenvironment, particularly in B cell lymphoma. Phagocytosis checkpoints (like CD47) are membrane molecules displayed by many cell types to prevent internalization by professional phagocytes. Recently, it was established that anti-CD47 monoclonal antibodies can increase the uptake of malignant cells by macrophages, showcasing the promising future of pro-phagocytic therapies for cancer[169,170]. Particularly, molecules targeting CD47 are actively being evaluated in pre-approval clinical trials (phase III) for hematological malignancies[171]. Many of these potential pro-phagocytic drugs need preliminary efficacy evaluation using *in vitro* or *ex vivo* models. To contribute to a deeper understanding of phagocytosis during cancer, we have developed a robust macrophage phagocytosis assay for malignant targets that improves upon available options by accurately discriminating internalized cells from those juxtaposed in the two-dimensional microscopy field. The model we developed has the added benefit of labeling living cells, as we wanted to subtract the internalization of apoptotic bodies from the actual anti-tumoral activity. Finally, this model uses commercially available cell lines and is adaptable to many conditions, targets, and macrophages, making it a versatile option for early evaluation of therapeutics in cancer research laboratories with trained personnel.

We decided to optimize the baseline function of macrophages using enhancers of phagocytosis. Initially, CCL3 and CCL5, two chemokines involved in recruitment and function of lymphoma TAM , were used as stimuli[172]. Despite their possible association with TAM function and their role in the tumor microenvironment in B cell lymphomas, they were poor inducers of phagocytosis. Thus, we employed two commonly used immune activators, LPS and IFN-γ. Both compounds activate macrophages towards a classic phenotype that is associated with proinflammatory signaling and anti-tumoral potential[173]. However, in contrast to IFN-γ, LPS is a bacterial derivate not commonly present in the tumor microenvironment of blood malignancies; although LPS contributes to increased priming of macrophages, we used IFN-γ to stimulate the subset of IFN-TAM, making our experiments closer to the *in vivo* conditions. Nevertheless, the concentration of IFN-γ present in the tumor microenvironment has not been determined,

therefore, we used the IFN-γ concentration previously described for *in vitro* assays. Furthermore, LPS enhanced phagocytosis in the absence of antibody-based therapies. As LPS activates macrophages through diverging downstream signaling cascades of its primary receptor, TLR4, it can promote internalization through pathways beyond Mac-1 or FcR mediated phagocytosis[174].

To corroborate that our model was ideal to test Mac-1 mediated phagocytosis, we verified the functionality of this integrin using an agonist and blocking its subunits. As described previously by Chen et al., blocking the subunits of Mac-1 (CD11b and CD18) drastically decreased the phagocytosis efficiency promoted by anti-CD47 antibodies [137]. Furthermore, in the presence of recommended concentrations of the Mac-1 agonist LA-1 [175,176], we found an increased efficiency of phagocytosis. Interestingly, the threshold for enhancing phagocytosis was lower in CD47 blockade than in CD20, which is likely related to the key role of the integrin during CD47 blockade [137]. In contrast, the Mac-1 integrin is likely playing a supportive role to the FcR in Rituximab-mediated internalization[126,177].

Microscopy-based assays are the most employed method to investigate phagocytosis of cancer cells, but there are viable alternatives. The most common model labels the membrane of target and effector cells with fluorophores and infers internalization based on the closeness or juxtaposition of both signals on the microscopy plane[178–180]. In our protocol, we facilitate the differentiation between contiguous and internalized cells by adding a secondary dye that labels exclusively extracellular targets. Thus, we avoid mistakenly counting cells that only colocalize with the phagocyte. Furthermore, the addition of a viability dye to the target improves our capacity to differentiate phagocytosis of living malignant cells from efferocytosis (internalization of apoptotic bodies). Alternatively, other authors use flow cytometry to measure phagocytosis in a suspension [181,182]. These methods improve the throughput of evaluation, permitting simultaneous analysis of different conditions and targets, making them ideal for the analysis of patient-derived samples. Viability dyes are also commonly used in flow cytometry and allow accurate estimation of living cell phagocytosis. However, flow cytometry assays may increase variability between experiments and require additional preparation compared with microscopic evaluation.

Based on our phagocytosis experiments, and comparing the phagocytic index of assays in which only 5 fields of view were analyzed, at least 10 images per condition must be quantified to minimize the inter-experiment variability of the phagocytic index. Manually counting this large volume of data is labor-intensive and unfeasible. Our group is currently evaluating a machine learning based approach to analyze the images that can reduce the load on operators while maintaining accuracy. As a proof of concept, the adaption of an algorithm to automatically count the number of macrophages based on particle dimension and fluorescence signal reduced the time required to analyze a single condition from 6 to 3h. This phagocytosis model is suitable for the initial evaluation of compounds and biological conditions; however, it does not reproduce the complex tumor microenvironment where malignant cells and phagocytes interact *in vivo*[111]. Using animal, xenograft, and organoid models could better mimic human conditions and allow the interaction of malignant and immune cells with components of the tumor microenvironment and the extracellular matrix. Nevertheless, the specific effect on phagocytosis would be harder to measure, and will require advance techniques, like tissue cytometry, to evaluate B cell internalization. Moreover, the use of these models requires additional laboratory infrastructure and specialize/trained personnel, which could limit its implementation. We evaluated the suitability of the assay to study Mac-1 mediated phagocytosis, so further characterization should focus on FcγR. Also, additional soluble stimuli present in the tumor microenvironment of B cell lymphomas, like IL-10 and IL-1β, can be evaluated and standardized depending on the research objectives.

In summary, we present a robust microscopy-based protocol to analyze and quantify phagocytosis. Although it can easily be adapted to other targets, our initial report uses human Burkitt lymphoma derived cells. This model improves upon available alternatives by allowing more accurate quantification of phagocytosis efficiency using novel fluorescence labeling approaches. Specifically, we believe that this model can support further evaluation of the role of phagocytosis as an anti-tumoral immune mechanism and help optimize resources by assessing potential therapeutics *in vitro*. Finally, our phagocytosis assay could be employed to analyze samples from patients or healthy volunteers by obtaining and testing the capacity of primary macrophages (phagocytic target) to internalize cancer cells. The application of this model using primary cells could unveil differences and variability among patients, shedding light on

their antitumor immune response (phagocytic capacity of immune cells) and the impact of tumor composition on cancer progression.

Chapter 3. Implications of RhoA activity in lymphoma cells on their phagocytosis by macrophages

3.1. Introduction

The treatment of Burkitt lymphoma remains difficult under certain circumstances. Despite recent advances in diagnostics and therapeutics, around 20% of patients do not respond to first-line therapy. Moreover, patients with late cancer stages and metastasis have a poor prognosis due to the reduced effectiveness of all available regimes[119]. Rituximab is a monoclonal antibody used in B cell lymphoma to target CD20, a molecule abundantly expressed on the surface of B cells. Its mechanism of action is not completely clear, but it likely involves an increase in antibody-dependent phagocytosis, antibody-dependent cellular cytotoxicity, and complement-dependent cytotoxicity[126]. Furthermore, tumor-associated macrophages seem to be instrumental in the effectiveness of this and other antibody therapies[124]. Currently, Rituximab is widely used as a first-line agent in aggressive B cell malignancies, including Burkitt lymphoma where it has shown significantly improved outcomes[119,183].

The proven effectiveness of Rituximab as a therapeutic agent for B cell malignancies has inspired interest in using phagocytosis-promoting agents as anti-tumoral immunotherapy. CD47 is a “don’t eat me” signal commonly displayed by malignant cells to avoid phagocytosis by macrophages. Preliminary therapeutic trials have shown promising results with anti-CD47 monoclonal antibodies, particularly for hematologic malignancies. However, similar to Rituximab, not all patients respond to therapy and some may even present serious adverse events due to the off-target action of these monoclonal antibodies[169]. Thus, there is a growing need to find strategies that improve the efficacy and minimize unwanted effects of phagocytosis-based therapies for cancer.

Mac-1 mediated phagocytosis is a mechanosensitive process with a positive correlation between engulfment and target stiffness[140]. This association between target cell stiffness and increased phagocytosis may play a role in cancer immune evasion as malignant cells have increased deformability and possibly decreased surface tension. However, how malignant cells modify their biomechanical properties (affecting the

stiffness) and the effect of this altered state on immune activity or evasion remains unclear. The cortical actin cytoskeleton is the major determinant of a cell's surface tension and likely plays a role in the increased deformability of tumoral cells. Here, we explore how modifying the mechanical properties of Burkitt lymphoma cells, a highly aggressive lymphoma, affects their phagocytosis rate by macrophages. We employed an inducible mutagenesis approach to alter RhoA, the key determinant of the actin cortex architecture, evaluated the impact of these modifications on cell stiffness using atomic force microscopy (AFM), and explored the connection between changes in biomechanical properties and phagocytosis using our novel *in vitro* assay.

3.2. Methods

3.2.1. Cloning strategy and plasmid preparation

The pSBtet-Hygro plasmid was purchased from Addgene (60508) and used as the vector backbone structure. This vector was cut using the SfiI restriction enzyme (Thermo Scientific, FD1824). The mEGFP insert (a gift from Michael Davidson) was cloned into the pSBtet-Hygro vector along with the dominant negative mutated RhoA plasmids RhoA-T19N (Addgene, 12967) or RhoA-R5Q (Addgene, 81294) using InFusion Cloning (Takara Bio, 638946). For the constitutively active mutated RhoA construct, the pcDNA3-EGFP-RhoA-Q63L plasmid (Addgene, 12968) was cut using the enzyme EcoRI-HF (New England Biolabs, R31015) and cloned into the pSBtet-Hygro vector. Finally, as controls, the EGFP-RhoA-WT (donated by the Grinstein Lab, University of Toronto) was cloned into the pSBtet-Hygro vector. Furthermore, the Sleeping Beauty Transposon System (SBTS) was used to express the RhoA mutations in a doxycycline-dependent manner. Successful cloning of inserts was evaluated and confirmed by Sanger sequencing using primers flanking the GFP insertion site **(Appendix B1).** Finally, the mCherry, MKL1, and De-Act constructs were already prepared and available in our laboratory.

To evaluate the role of Mac-1 in the internalization of cancer cells with higher and lower stiffness, we modified the mechanical properties of Raji cells by inserting punctual mutations in RhoA, the major regulator of the actin cytoskeleton. Constitutively active (pSBtet-Q63L), dominant negative (pSBtet-T19N), and pSBtet GFP-control constructs were generated using the SBTS. RhoA is a protein that cycles between biologically

active (GTP-bound) and inactive (GDP-bound) states. The constitutively active mutation substitutes glutamine with leucine at residue 63, located in the nucleotide binding site. The mutated RhoA prevents hydrolyzation of the γ-phosphate group of the bound GTP and keeps the protein in an active state. The active RhoA promotes actin polymerization through the effectors mDia, and PI(4)P5K[184,185]. On the contrary, the dominant negative mutant of RhoA has a substitution in position 16 of threonine for asparagine and promotes a tight binding of the mutated RhoA to the guanine nucleotide exchange factors (GEFs) that regulate GTP/GDP exchange in RhoA. This close interaction prevents the GEFs from activating endogenous or mutated RhoA and blocks their downstream signaling[186].

The SBTS was created based on an extinct Salmon transposon (Tc1/mariner family) to provide stable and long-term expression of transfected sequences. The SBTS contains the regions for gene transfer flanked by the transposase target repeats. The transposase is usually provided in a separate plasmid to prevent constant re-insertion of the sequence of interest. We are using an inducible SBTS that contains an inducible and a constitutive cassette **(Figure 3.1)**. The constitutive cassette is under the influence of an independent promoter; it actively expresses a polycistronic mRNA containing a reverse tetracycline-controlled transactivator, a reporter protein (GFP), and a selection marker (Hygromycin resistance). The inducible section contains the gene of interest (mutated RhoA) under the influence of an inducible tetracycline-dependent promoter. When exposed to tetracycline or its derivate doxycycline, the reverse tetracycline-controlled transactivator protein gains the capacity to interact with the inducible promoter, and the gene of interest is transcribed. Thus, we can control the expression of our mutated RhoA protein during the phagocytosis assays without compromising the survival of transfected cells[187,188].

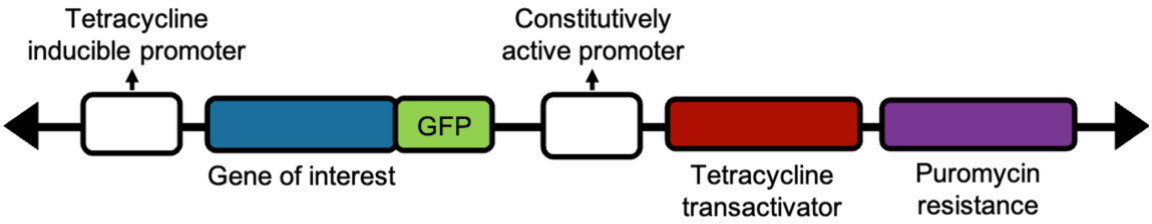

Figure 3.1. Schematic of the Sleeping Beauty Transposon System (SBTS).
The SBTS vector contains two regions under the influence of different promoters. Under a constitutively active promoter, we have a multigene operon with sustained transcription of an antibiotic resistance cassette, and a tetracycline transactivator. In the presence of

tetracycline/doxycycline, the transactivator becomes active and induces transcription of the region under the influence of the inducible promoter. The inducible region contains our gene of interest tagged with a fluorescent peptide. Created with BioRender.com.

Modification of the mechanical properties of lymphoma cells: mutagenesis approach

Raji cells were transfected using Amaxa nucleofector kit V (Lonza). Cells were cultured in RPMI1640 with 10% heat-inactivated FBS (Wisent, 090-150), at 37 ℃ in a 5% CO_2 incubator. 2 x 10^6 Raji cells per condition were centrifuged at 90 *g* for 10 minutes at room temperature. After centrifugation, cells were diluted in 100 µL of nucleofector mix (82 µL of nucleofector solution and 18 µL of supplement solution). To insert the mutations of interest, the SB100 transposon plasmid was added to each condition in combination with pSBtet-GFP, pSBtet-T19N-RhoA, pSBtet-Q63L-RhoA, pSBtet-R5Q-RhoA, pSBtet-GFP-WT-RhoA, m-cherry, MKL1, or De-Act plasmids. The transposon plasmid SB100 and plasmid of interest DNA ratio was 1:20, with a maximum concentration of 2 µg of DNA and 10 µL of volume. After plasmid addition, cells were transferred to Amaxa nucleofector cuvettes and transfected by electroporation using the M13 program. After electroporation, 500 µL of RPMI 1640 with 10% heat-inactivated FBS was added to the cell suspension and transferred to a flask containing 4.5 mL of fresh media. Cells were incubated for three days at 37 ℃ in a 5% CO_2 incubator, and antibiotics for the selection of transfected cells were added to each condition. Transfected cells were selected with antibiotics for three weeks prior to cell sorting, with weekly cell passage and addition of antibiotics.

Antibiotic selection

For the selection of transfected Raji cells after electroporation, the effect of four antibiotics on cell survival was evaluated in the standardization process at the following concentrations: Geneticin (Gibco – 10131035; 125, 250, 500, 1000, 2000 µg/mL), Hygromycin (Invitrogen – 10687010; 75, 150, 300, 600, 1200 µg/mL), Puromycin (Gibco – A1113803; 1, 2, 4, 8, 16 µg/mL), and Blasticidin (Gibco – A1113903; 2.5, 5, 10, 20, 40 µg/mL). Cell survival assays were performed by seeding 50,000 Raji cells in 1 mL of RPMI1640 (Gibco) with 10% heat-inactivated FBS (Wisent, 090-150) in a 24 non tissue culture treated plate (Sarstedt, 83.3922.500). 20 µL of each drug concentrated 25x were added to each well according to the experimental conditions. Cells were incubated for 48 hours at 37 ℃ in a 5% CO_2 incubator. After incubation, 100 µL of cells were passaged to

400 µL of fresh media and a second antibiotic addition was done as previously described. Cells were incubated for 48 hours at 37 ℃ in a 5% CO_2 incubator. Cells from each condition were manually counted using a Neubauer chamber, and the EC50 was defined according to the cell viability determined by Trypan blue.

Doxycycline inducible expression

To evaluate the doxycycline-inducible expression of inserted mutations in transfected Raji cells, two incubation times (24 and 48 hours), two doxycycline solvents (PBS or DMSO), and various concentrations (0.1, 0.2, 0.5, 0.7, and 1 µg/mL) were evaluated in the standardization process. 100,000 wild-type (WT) and transfected Raji cells with pSBtet-GFP plasmids were seeded in 1 mL of RPMI1640 (Gibco) with 10% heat-inactivated FBS (Wisent, 090-150) in a 24 non tissue culture treated well plate (Sarstedt, 83.3922.500) per condition. Doxycycline was prepared with sterile 1x PBS at 1 mg/mL. Serial dilutions were done to achieve the required final concentrations. To measure the GFP expression of transfected Raji cells by flow cytometry, after 24 and 48 hours of incubation at 37 ℃ in a 5% CO_2 incubator, cells were transferred to 5 mL polystyrene Falcon tubes (Falcon, 352058), washed with 1x PBS, and resuspended in 1 mL of sterile 1x PBS with 1 mM of EDTA (Invitrogen, 15575020) (flow cytometry solution).

3.2.2. Fluorescence-activated cell sorting for Raji cells

To isolate a pure population of transfected Raji cells under antibiotic pressure, the culture suspension was sorted by fluorescence-activated cell sorting (FACS) using a BD FACS Aria Fusion. The sorting buffer solution was prepared with 1x PBS, 1 mM of EDTA, and 25 mL HEPES pH 7.0 (Gibco, 15630080). The solution was sterilized with a 0.2 µm filter and 10% heat-inactivated FBS was added to enhance cell viability. 3 x 10^6 transfected Raji cells were centrifuged for 6 minutes at 1000 *g*, room temperature. Cells were resuspended in 1 mL of cold sorting buffer solution, transferred to polystyrene tubes, and maintained at 4℃. To increase cell viability, 500 µL of PBS with 10% heat-inactivated FBS were added to the collection tubes. Cells were sorted with a 100-micron nozzle and at a flow rate of 1.0 for 15 minutes.

Flow cytometry

To evaluate the GFP fluorescence emission of transfected Raji cells and the expression levels of ICAM-1, ICAM-2, CD47, and CD20 membrane ligands, 1 mL of culture was transferred to a 24 well plate (Sarstedt, 83.3922.500) and stimulated with 1 µg/mL of doxycycline for 24 hours at 37 ℃ in a 5% CO_2 incubator. After incubation, cells were transferred to a 1.5 mL vial and centrifuged at 1000 *g* for 5 minutes (room temperature). The cell pellet was resuspended in 500 µL of flow cytometry solution (PBS 1x and BSA 1%. Primary antibodies were added to each vial according to the experimental setup and incubated at room temperature for 30 minutes. Then, cells were centrifugated at 500 *g* for 5 minutes (room temperature) and washed with 1x PBS. The remaining cell pellets were resuspended in 100 µL of secondary antibodies diluted in 1x PBS (1:400), and incubated at room temperature for 30 minutes with 1 mL of flow cytometry solution added to each condition. Samples were kept at 4℃ prior to flow cytometry analysis. The filters and parameters used for the acquisition of events were FITC (300), APC (564), BV421 (440), FSC (70), and SSC (240).

3.2.3. Modification of the mechanical properties of lymphoma cells: pharmacological approach

To modulate the activity of endogenous RhoA, Raji cells were treated with 1 and 5 µg/mL of CT04 RhoA inhibitor (Cytoskeleton, Inc. CT04-A) and CN03 RhoA activator (Cytoskeleton, Inc. CN03-A). The effect of this treatment was evaluated in RPMI 1640 media with and without 10% of heat-inactivated FBS. Raji cells (400,000) were centrifuged at 90 *g* for 5 minutes, at room temperature, and resuspended with 500 µL of media. Then, the RhoA activator or inhibitor was added to each tube. Cell suspensions were incubated for 3 hours at 37 ℃ and 5% CO_2. Simultaneously, we used 24-well plates to prepare 12 mm coverslips (12mm, #1.0) coated with Poly-L-Lysine (Gibco) at 0.5 mg/mL in PBS for 20 minutes at room temperature (Sarstedt, 83.3922.500) and then removed all solutions. Once the cell suspensions finished their three hours of incubation, we added 500 uL of each tube to the wells with the coverslips and incubated for 1 additional hour. Finally, cells were washed three times with 1x PBS, and fixed with cytoskeleton buffer followed by a phalloidin staining.

To reduce the membrane's cholesterol levels during the standardization process, Raji cells were treated with 10 mM of methyl-β-cyclodextrin (MβCD) (Sigma-Aldrich, C4555-1G). Treated Raji cells (400,000) were adhered on 12 mm coverslips coated with Poly-L-Lysine (Gibco) at 0.5 mg/mL. Cells were incubated for 1 hour at 37 ℃ and 5% CO_2. After incubation, the cells were stained using the phalloidin staining to visualize polymerized actin on the cell cortex.

Phalloidin staining

To verify the effect of the RhoA mutations and RhoA activator and inhibitor treatments on the density of filamentous actin at the cortex of Raji cells, a phalloidin staining was performed. Cells were fixed using cytoskeleton buffer (625 µL of 32% paraformaldehyde, 1 mL of sucrose 0.32 M, 500 µL of cytoskeleton buffer, and 2.875 µL of ddH_2O) for 15 minutes at 37 ℃ and 5% CO_2. After three washes with 1x PBS, nonspecific binding was prevented by blocking with BSA 2% in 1x PBS. After three additional washes, cells were incubated with anti-CD47 antibody (10 µg/mL) in BSA 2% for 30 minutes at room temperature (protected from light). After incubation, the coverslips were washed three times with 1x PBS and cells were permeabilized (850 µL of 10X PBS, 445 µL of Triton 10%, 7.225 mL of ddH_2O) for 5 minutes at room temperature, followed by a final set of washes (1x PBS, three times). After permeabilization, unspecific binding was prevented once again and coverslips were incubated for 30 minutes with Alexa Fluor-647-conjugated anti-mouse IgG (1:400), DAPI (3 µM), and Alexa Fluor 568 Phalloidin (Invitrogen, A12280) or Alexa Fluor 488 Phalloidin (Invitrogen, A12379) in 1x PBS with BSA 1% and Tween 0.1%. Finally, the coverslips were washed four times with 1x PBS, transferred to microscope slides with 5 µL of Fluoromount-G™ mounting medium (Invitrogen™, 00-4958-02), and stored at room temperature for 24 hours before imaging.

Confocal microscopy

To evaluate the density of the actin cortex in RhoA mutated Raji cells (treated with RhoA inhibitor or activator and methyl-β-cyclodextrin), cells were visualized on a Yokogawa CSU-W1 spinning disk confocal head mounted on Nikon Eclipse Ti2 microscope. The NIS Elements (Nikon) software was used to control the microscope functions. Phagocytosis assays were imaged on glass coverslips with an 40x 1.3 NA oil objective. Illumination was provided by solid-state lasers 405 nm (for Hoechst dye, nuclei

visualization), 488 nm (for EGFP excitation, Calcein Green AM), 561 nm (for mCherry and Alexa Fluor-647-conjugated anti-mouse IgG, B cell membrane), and 655 nm (for Cy™3-conjugated anti-rat IgG, macrophage membrane). Emission was collected via multi-bandpass dichromic and single-bandpass emission filters (455/50 nm for blue, 525/360 nm for green, 605/52 nm for red, and 705/72 for far red). Ten images in each channel per condition were captured in rapid succession for multicolor imaging and with Perfect Focus. Images were analyzed and quantified using ImageJ[159]. For 3D imaging, confocal stacks were assembled with NIS Elements (Nikon).

Atomic force microscopy

Raji cells were plated on a glass-bottom dish (Willco Wells) pre-coated with 0.01% poly-L-lysine (Life Technologies) and immersed in RPMI media (Gibco) supplemented with 10% FBS (Life Technologies) and 10mM HEPES (Life Technologies). Experiments were performed using a Bruker Bioscope Catalyst AFM system (Bruker) mounted on an inverted Axiovert 200M microscope (Zeiss) equipped with a confocal laser scanning microscope 510 Meta (Zeiss) and a 40X objective lens (0.95 NA, Plan-Apochromat, Zeiss). Raji cells were maintained at physiologically relevant 37 ℃ temperature using a heated stage (Bruker). A soft gold coated silicon nitride AFM probe (HQ:CSC38/tipless/Cr-Au, MikroMasch) was used and the tipless microcantilevers were pre-calibrated using the standard thermal noise fluctuation method. The estimated spring constants for microcantilevers used were 0.03 – 0.09 N/m. After calibration, the AFM probe was placed on top of a cell. Five successive curves with a delay of 10 seconds between curves were performed on each cell. The deflection trigger threshold was set to 2-8 nm yielding applied forces between 60pN to 720pN. The cellular cortical tension was determined by fitting the small deformation region of the force curve and solving for the surface tension using the cortex tension method outlined by Cartagena-Rivera et al.[189]. Briefly, this method defines the force balance between the additional applied tipless cantilever force with the pressure excess inside the spherical cells and the corresponding surface tension. For fitting, deformation depths between 0-400 nm were found to be consistent in yielding good fits (R^2>0.9). Force curves that presented 1) large slopes due to hydrodynamic drag in the region of the curve before initial contact point 2) noisy approach curves due to environmental vibrations, and/or 3) jumps in the curve due to cantilever slippage or moving cells, were discarded from the analysis. All curve analyses were performed using a custom script

written in MATLAB (MathWorks) openly accessible on GitHub (https://github.com/NIBIBmechanobiologylab).

3.2.4. Statistical analysis and reproducibility

The mean fluorescence intensity of the actin cortex was determined by manually drawing a region-of-interest in the 561 nm channel using ImageJ[159]. Quantification of the background was subtracted from each region-of-interest acquired per cell. Statistical analyses were performed using GraphPad Prism 9.5.1 for MacOS. Error bars represented standard errors of the mean. The quantification of internalized cells as well as the total amount of macrophages and B cells was done manually by a single operator to avoid interobserver error. Three independent replicates were performed for each experiment. To compare the data between experimental conditions, the non-parametric two-tailed Mann-Whitney test was used in GraphPad Prism 9.5.1 for MacOS.

3.3. Results

3.3.1. RhoA mutated cell lines

To find the ideal antibiotic and dosage for the selection of transfected lymphoma cells, we performed survival assays of WT Raji cells using different concentrations of Geneticin, Hygromycin, Puromycin, and Blasticidin **(Appendix B2)**. The selection of Raji cells with 300 µg/mL of Hygromycin reduced cell survival by a magnitude of eight compared to the condition without the drug (800,000 cells/mL vs 100,000 cells/mL). Also, adding Hygromycin did not generate pH changes (acidification) compared to Geneticin when used at its optimal concentration for selection (1 mg/mL). Although Puromycin and Blasticidin also displayed a high effect on cell survival at low concentrations, Hygromycin was chosen based on the availability of constructs for plasmid preparation.

Raji cells were transfected by electroporation with the pSBtet-GFP-RhoA, pSBtet-GFP-RhoA-WT, pSBtet-GFP-RhoA-Q63L, pSBtet-GFP-RhoA-T19N, or pSBtet-GFP-RhoA-R5Q plasmids and exposed to Hygromycin for selection of cells that successfully integrated the constructs. Then, to obtain a pure population of transfected cells, we selected GFP expressing cells using FACS. Cells were treated with the C3

exoenzyme of *Clostridium botulinum* to inhibit RhoA and modify the actin cortex levels of B cells. This molecule irreversibly inactivates RhoA by ADP-ribosylating asparagine 41 [190,191]. To increase the actin cortex levels, cells were treated with the *Escherichia coli* cytotoxic necrotizing factor-1; this molecule maintains RhoA in a constitutively active state by preventing the activity of Rho GTPases (change of glutamine-63 into glutamate)[192]. Besides, to reduce Raji cell stiffness, cells were treated with methyl-beta-cyclodextrin (MβCD), a pharmacological excipient that increases cell permeability, reduces cholesterol levels in the cell membrane and depolymerizes the actin cytoskeleton[193]. Also, to account for the effect of FBS in the actin cortex levels at different incubation times, untreated Raji cells were included under the same experimental conditions. **(Appendix B3)**. To evaluate the modification of the actin cortex in RhoA mutated and chemically modified Raji cells, the actin cortex was stained using phalloidin, a phallotoxin that binds specifically to F-actin subunits preventing its depolymerization[194]. Our results showed that dominant negative mutations and inhibition of RhoA using the C3 exoenzyme significantly decreased the F-actin levels of Raji cells compared to the control ($p < 0.0001$) **(Figures 3.2-B and 3.2-C)**. Also, constitutively active RhoA mutated cells significantly increased F-actin levels in the cells ($p < 0.0001$) **(Figure 3.2-A)**; however, no significant changes were observed in RhoA activation with *E. coli* cytotoxic necrotizing factor-1 ($p = 0.3753$) **(Figure 3.2-C)**. These results suggest that the RhoA pathway controls the levels of actin polymerization in the cell. Furthermore, inhibition and activation of RhoA using constitutively active and dominant negative mutations effectively modifies F-actin levels in Raji cells, confirming its reliability to study the impact of the mechanical properties of B cells **(Figure 3.2-D)**.

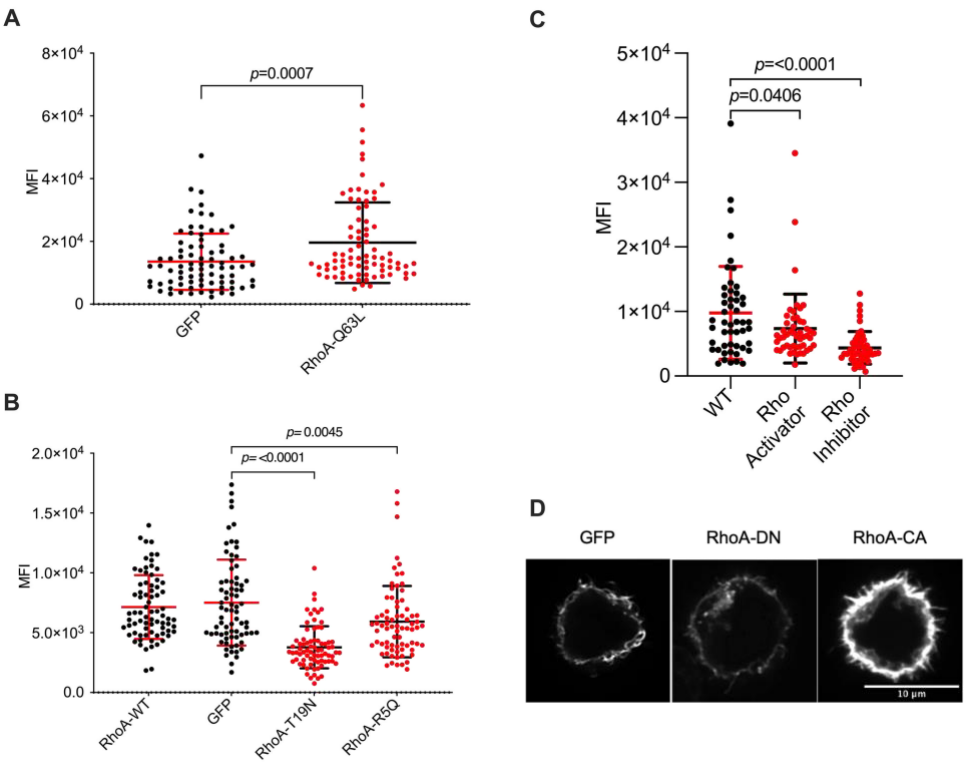

Figure 3.2. RhoA activity regulates the density of the actin cortex in Burkitt lymphoma cells.

Quantification of the actin cortex brightness (Mean Fluorescence Intensity – MFI) of **(A)** constitutively active and **(B)** dominant negative mutated Raji cells using ImageJ. RhoA-CA denotes the constitutively active mutation, while T19N and R5Q are dominant negative mutations **(C)** Raji cells were treated with the RhoA inhibitor (C3 exoenzyme of *C. botulinum*) and activator (*E. coli* cytotoxic necrotizing factor-1) for 4 hours (n = 3 experimental replicates). Polymerized actin cortex filaments were stained with Phalloidin. Bars represent means and SD. Mann Whitney test was used for comparison. **(D)** Actin cortex brightness of GFP control cells, RhoA dominant negative and constitutively active mutated cells.

To evaluate the internalization of transfected Raji cells by J774 macrophages, the standardized *in vitro* model of phagocytosis was used. Raji cells were exposed to doxycycline for 24 hours to induce the expression of constitutively active and dominant negative mutations. Remarkably, the phagocytosis of constitutively active RhoA expressing Raji cells was higher in the presence of anti-CD47 blockade (PI = 0.47, $p < 0.0001$) and anti-CD20 antibodies (PI = 0.48, $p = 0.0143$) compared to the control **(Figure 3.3-A and 3.3-B)**. The PI of dominant negative expressing cells did not show an impact in the B cell uptake (lower) by macrophages in combination with anti-CD47 (WT = 0.18; T19N = 0.21 - $p = 0.0966$; and R5Q= 0.19 - $p = 0.2306$) or anti-CD20 antibodies (WT = 0.24; T19N = 0.19 - $p = 0.2001$; R5Q = 0.19 - $p = 0.1379$) when compared to the controls **(Figure 3.3-C and 3.3-D)**. In summary, these results show that higher activity of

RhoA is associated with better internalization with both pro-phagocytic therapies. Still, reduced functionality of RhoA through mutagenesis does affect the internalization capacity of macrophages.

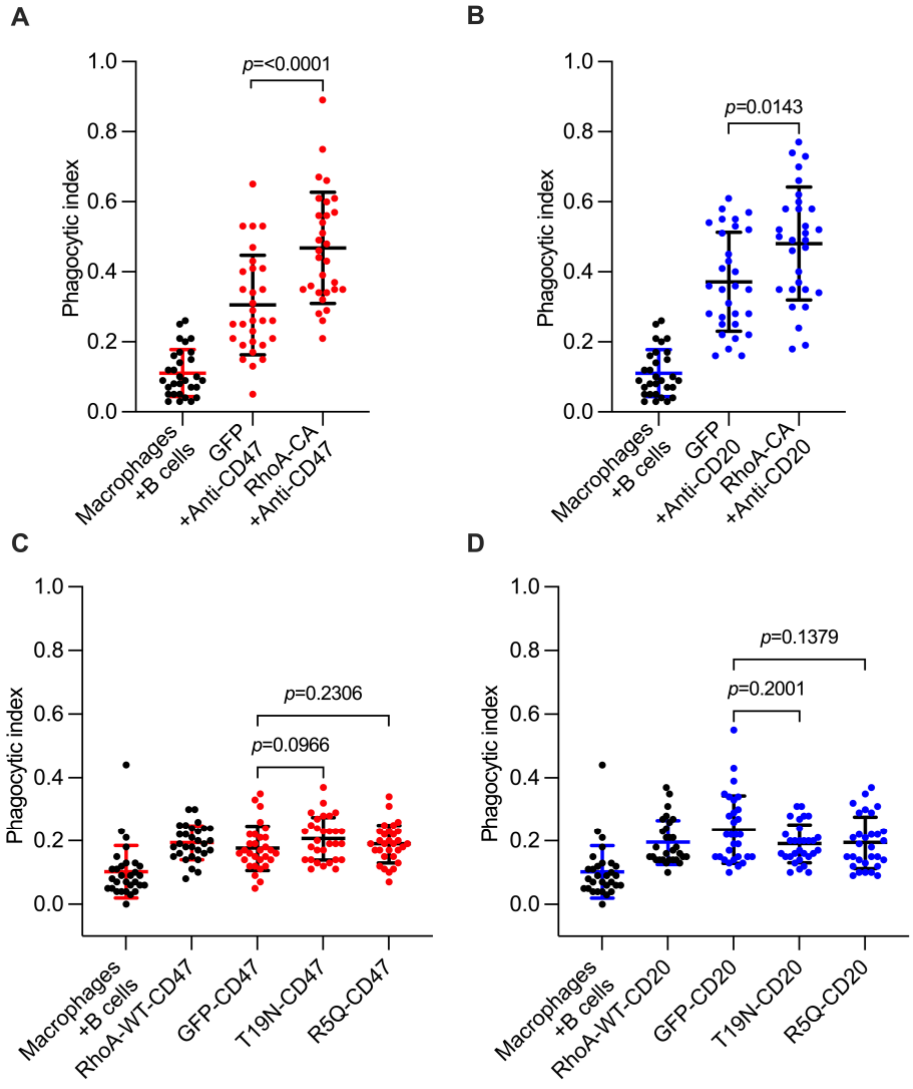

Figure 3.3. RhoA activity in the lymphoma cells affects their phagocytosis by macrophages.

Phagocytosis assay of Raji cells expressing **(A)** constitutively active and **(C)** dominant negative mutated RhoA in the presence of CD47 blockade. **(B)** Constitutively active and **(D)** dominant negative mutated Raji cells were also exposed to macrophages in the presence of Rituximab (n = 30 fields of view, three experimental replicates). RhoA-CA denotes the constitutively active mutation, while T19N and R5Q are RhoA dominant negative mutations. Bars represent means and SD. Mann Whitney tests were used for comparisons.

3.3.2. Chemical inhibition of RhoA activity

As an alternative method to modify the cell cortex, we performed phagocytosis assays of Raji cells using chemically inhibited and activated RhoA. Inhibition of RhoA with the C3 exoenzyme of *C. botulinum* showed significantly lower internalization of B cells with anti-CD47 blockade and anti-CD20 antibodies, compared to the control (anti-CD47 = 0.32 – p = < 0.0001; anti-CD20= 0.18 - p = 0.0403) **(Figure 3.4)**. Furthermore, internalization of Raji cells treated with the *E. coli* cytotoxic necrotizing factor-1 (RhoA activator) did not increase B cell internalization by macrophages in the presence of blocking antibodies (anti-CD47 = 0.32 - p = 0.0680, anti-CD20= 0.25 - p = 0.1431) **(Figure 3.4)**; these results are concordant with the actin cortex quantification using the phalloidin staining, where the RhoA activator had no significant increase on F-actin. In contrast, modifying the actin cortex by constitutively active RhoA increases F-actin levels in the cell and positively impacts B cell internalization by macrophages. Moreover, unlike the decreased uptake of B cells treated with the C3 exoenzyme of *C. botulinum* by macrophages, the internalization of dominant negative RhoA transfected Raji cells did not decrease as expected. To clearly define if lower actin levels in the cell cortex affect internalization, we must explore other targets. For instance, by using inactivating mutations in the myosin regulatory light chain or Rac1 (T17N), we can reduce myosin activity and F-actin polymerization to pinpoint other relevant regulators that contribute to mechanosensitive phagocytosis[195]. Finally, additional targets involving actin crosslinkers proteins, which are essential for connecting and stabilizing the actin cytoskeleton structure, represent suitable candidates for modifying the mechanical properties of cancer cells. We can alter the activity and conformation of proteins such us alpha actinin, filamin, and fascin, by introducing punctual mutations. If we want to use mutagenesis, we should employ and inducible system as these processes are vital for cell survival. Subsequently, we can confirm the impact on the cytoskeleton structure and cell stiffness thorough the phalloidin staining and atomic force microscopy.

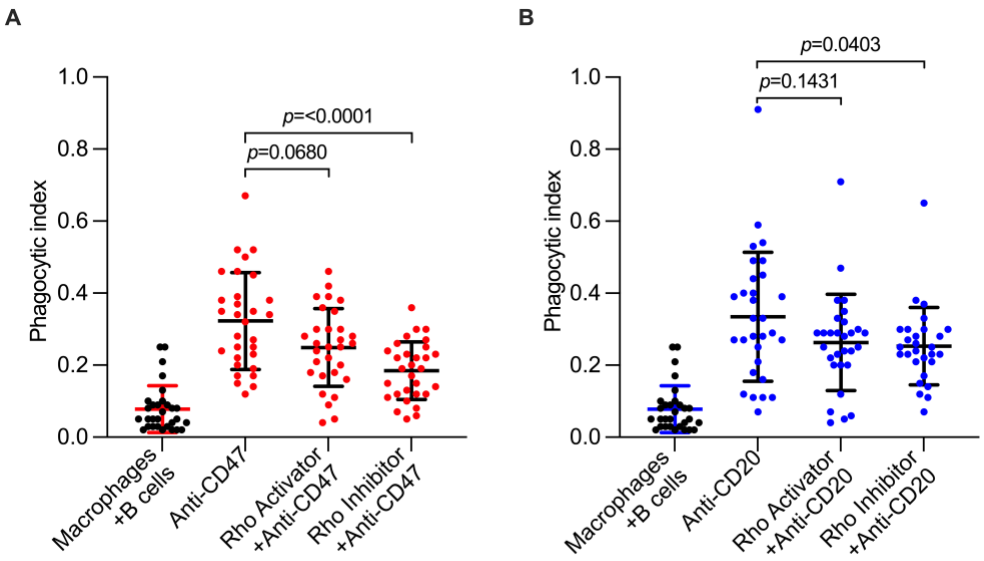

Figure 3.4. Treatment of Raji cells with the RhoA inhibitor impacts their phagocytosis by macrophages.

Phagocytosis assay of Raji cells treated with the RhoA inhibitor (C3 exoenzyme of *C. botulinum*) and activator (*E. coli* cytotoxic necrotizing factor-1) for 4 hours in the presence of **(A)** anti-CD47 and **(B)** anti-CD20 antibodies (n = 30 fields of view, three experimental replicates). Bars represent means and SD. Mann Whitney tests were used for comparisons.

As the macrophage internalization of B cells expressing constitutively active RhoA was significantly higher compared to the control, the effect of the RhoA mutations in the expression of CD47, CD20, ICAM-1, and ICAM-2 ligands on the surface of transfected Raji cells was evaluated by flow cytometry **(Figure 3.5).** There were no differences in the expression of these ligands on B cells compared to pSBtet-GFP control. This result indicates that the RhoA activity does not alter the surface expression of phagocytic ligands in lymphoma cells, demonstrating that the increased internalization of constitutively active mutated Raji cells is not associated with higher ligand availability for the Mac-1 integrin.

To assess if the increased internalization of cells with constitutively active mutated RhoA is associated with modifications in cell stiffness, the surface tension of the mutated cell lines was evaluated using atomic force microscopy by our collaborators at the National Institutes of Health. Measurements of surface tension in Raji cells expressing mutated RhoA showed that the surface tension necessary to deform cells expression constitutively active RhoA was significantly higher compared to the pSBtet-GFP control ($p < 0.0001$) **(Figure 3.6-A)**; also, a significant difference was observed for

the dominant negative RhoA expressing cells (T19N - p = 0.0291, R5Q - p = 0.0006) **(Figure 3.6-B)**. These results reveal that the RhoA activity determines the stiffness of lymphoma cells and correlates with the increased actin cortex quantification obtained in the phalloidin staining **(Figure 3.2-A and 3.2-B)**. Although dominant negative mutated Raji cells show lower cell stiffness compared to the GFP control, there were no significant differences in their phagocytosis by macrophages. Therefore, the stiffness of Raji cells treated with the RhoA inhibitor was measured as an additional control **(Figure 3.6-C)**. A significant difference in the stiffness of Raji cells treated with the RhoA inhibitor was observed, which correlates with the results obtained in the phagocytosis assay **(Figure 3.4-A and 3.4-B)**. Overall, our findings show that RhoA activation in Raji cells increases their internalization due to their increased stiffness, but does not change the level of surface ligand expression. Furthermore, the alteration of cell stiffness after RhoA mutagenesis confirms its role as a key regulator of the actin cortex.

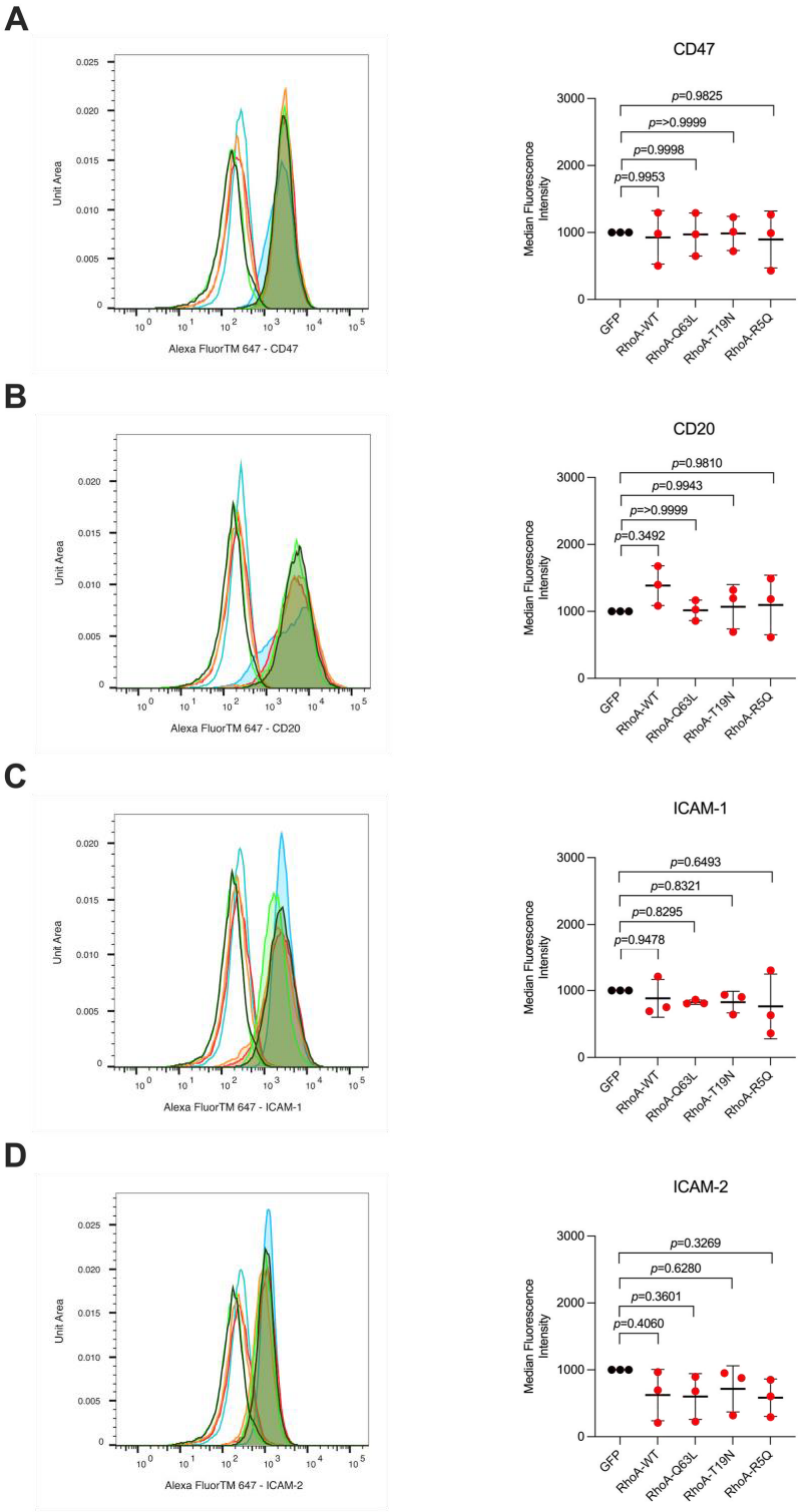

Figure 3.5. RhoA activity does not alter the surface expression of phagocytic ligands in lymphoma cells.

Representative replicate of the flow cytometry analysis of **(A)** CD47, **(B)** CD20, **(C)** ICAM-1, and **(D)** ICAM-2 ligands in RhoA dominant negative pSBtet-T19N (blue shaded curve), pSBtet-R5Q (light green shaded curve), and constitutively active pSBtet-Q63L (red shaded curve) expressing Raji cells. The pSBtet-GFP (blue shaded curve) and pSBtet-GFP-WT (orange shade curve) cell

lines are included for comparisons. Colors match the corresponding isotype control for each antibody. Bars represent means and SD. One-way ANOVA test was used for comparisons of the Median Fluorescence Intensity (n=3 experimental replicates).

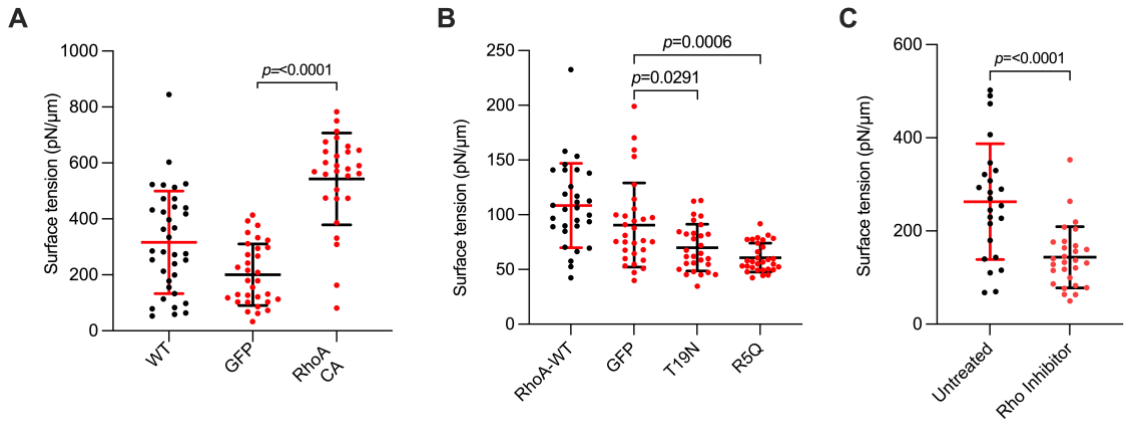

Figure 3.6. RhoA activity determines the stiffness of lymphoma cells. Measurements of surface tension by atomic force microscopy in Raji cells expressing **(A)** constitutively active, and **(B)** dominant negative mutated RhoA. **(C)** Untransfected Raji cells treated with the RhoA Inhibitor. (n = 26 – 36 cells, one experimental replicate). Bars represent means and SD. One-way ANOVA test was used for comparisons.

3.3.3. Modification of actin polymerization

To modify the mechanical properties of Raji cells independently of the RhoA protein, the constructs mCherry, De-Act, and megakaryocytic leukemia 1 (MKL1) were generated. De-Act-SpvB is an ADP-ribosyltransferase derived from *Salmonella enterica* that ADP-ribosylates actin monomers on a conserved arginine at position 177 (Arg-177), preventing the assembly of actin filaments[196]. Moreover, MKL1 is a transcriptional co-activator that can increase G-actin production, promote actin polymerization, and increase the stiffness of tumoral cells (breast cancer)[197,198]. To determine the polymerized actin levels in cells transfected with these constructs, the actin cortex brightness was assessed using the phalloidin staining. Results showed that De-Act expressing Raji cells have lower actin levels compared to the control (p = 0.0192), and cells expressing MKL1 have significantly higher F-actin levels (p = 0.0248) **(Figure 3.7)**.

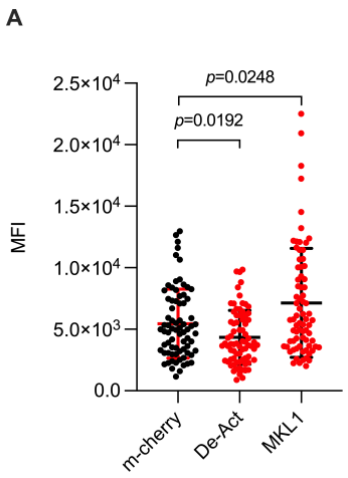

Figure 3.7. Modification of the actin cortex levels in non-mutated RhoA Raji cells.

Quantification of the actin cortex brightness (Mean Fluorescence Intensity – MFI) of mCherry, De-Act, and MKL1 expressing Raji cells using ImageJ (n = 3 experimental replicates). Bars represent means and SD. Mann Whitney tests were used for comparisons.

To evaluate the internalization of mCherry, De-Act, and MKL1 transfected Raji cells by J774 macrophages, phagocytosis assays were performed 24 hours after doxycycline addition. The phagocytosis of De-Act and MKL1 transfected Raji cells during the CD47 blockade did not show a significant difference compared to the control (PI mCherry = 0.19, De-Act = 0.19 - p = 0.7160; MKL1 = 0.21 - p = 0.3631) **(Figure 3.8-A)**; moreover, no differences were observed in the internalization of De-Act expressing Raji cells in the presence of anti-CD20 antibodies (PI mCherry = 0.20, De-Act = 0.21, p = 0.5686); however, a significant difference in the internalization of MKL1 transfected Raji cells was observed (PI mCherry = 0.20, MKL1 = 0.24, p = 0.0216) **(Figure 3.8-B)**. Then, to determine if there are significant modifications in the surface tension of De-Act and MKL1 expressing Raji cells, the stiffness was evaluated using atomic force microscopy. Measurements of surface tension in these transfected Raji cells showed a significant difference in the stiffness compared to the control for both molecules (p < 0.0001) **(Figure 3.9)**, which correlates with the lower level of polymerized actin seen in cells transfected with De-Act **(Figure 3.7).** However, despite the lower stiffness of these transfected cell lines, their internalization by macrophages was no different from the control condition **(Figure 3.8).** We effectively modified the levels of F-actin but found no direct correlation of this modulation with cell stiffness or phagocytic efficiency. Interestingly, MKL1 increased phagocytosis despite not affecting the biomechanical measurements of the cells.

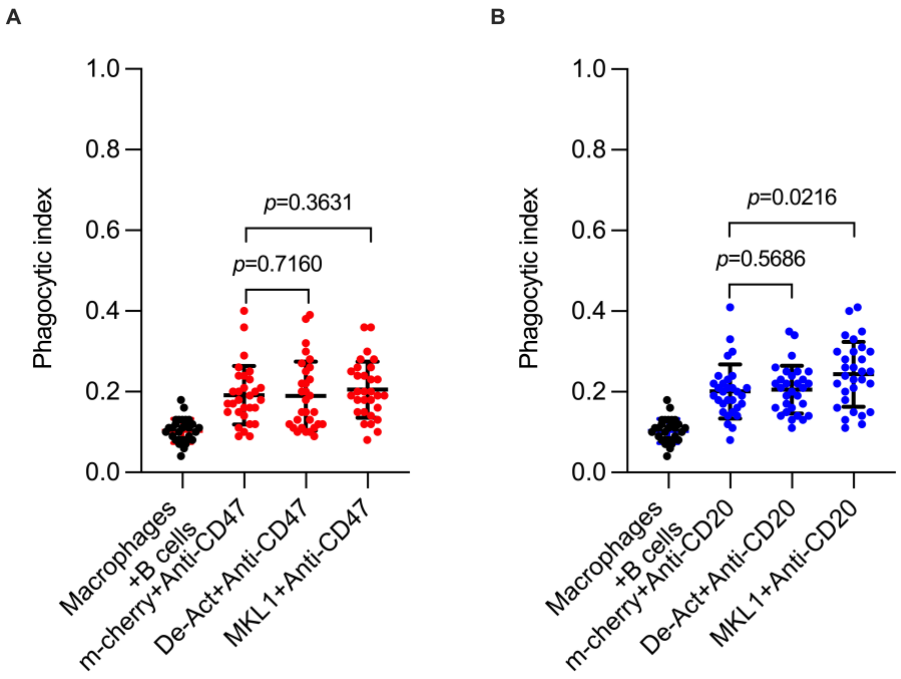

Figure 3.8. Impact of the modification of polymerized actin cortex levels on the phagocytosis by macrophages.

Phagocytosis assay of mutated Raji cells expressing mCherry, De-Act, and MKL1 constructs in the presence of **(A)** anti-CD47, and **(B)** anti-CD20 antibodies (n = 30 fields of view, three experimental replicates). Bars represent means and SD. Mann Whitney tests were used for comparisons.

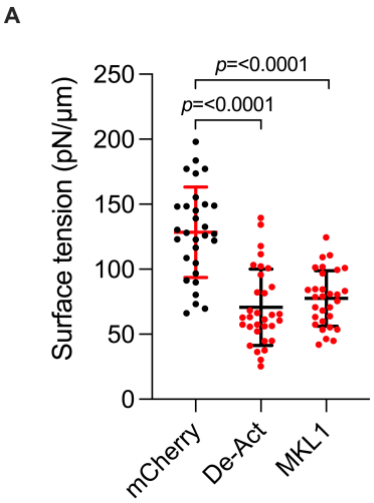

Figure 3.9. Surface tension of De-Act and MKL1 mutated Raji cells.

Measurements of surface tension by atomic force microscopy in Raji cells expressing **(A)** De-Act and **(B)** MKL1 constructs (n = 26 – 36 cells, one experimental replicate). Bars represent means and SD. One-way ANOVA test was used for comparisons.

Finally, to evaluate if the internalization of De-Act and MKL1 transfected Raji cells by macrophages is correlated with the availability of CD47, CD20, ICAM-1, and ICAM-2 ligands on the cell surface, their expression was measured by flow cytometry **(Figure 3.10)**. As expected, neither De-Act nor MKL1 had significantly different levels of CD47, CD20, ICAM-1 and ICAM-2 ligands. Therefore, despite establishing the role of RhoA in internalization, we are not certain if the MKL1 construct is effectively modulating F-actin levels to impact (increase) the phagocytosis of lymphoma cells by macrophages. Therefore, we need additional experimental replicates of atomic force microscopy to confirm this result.

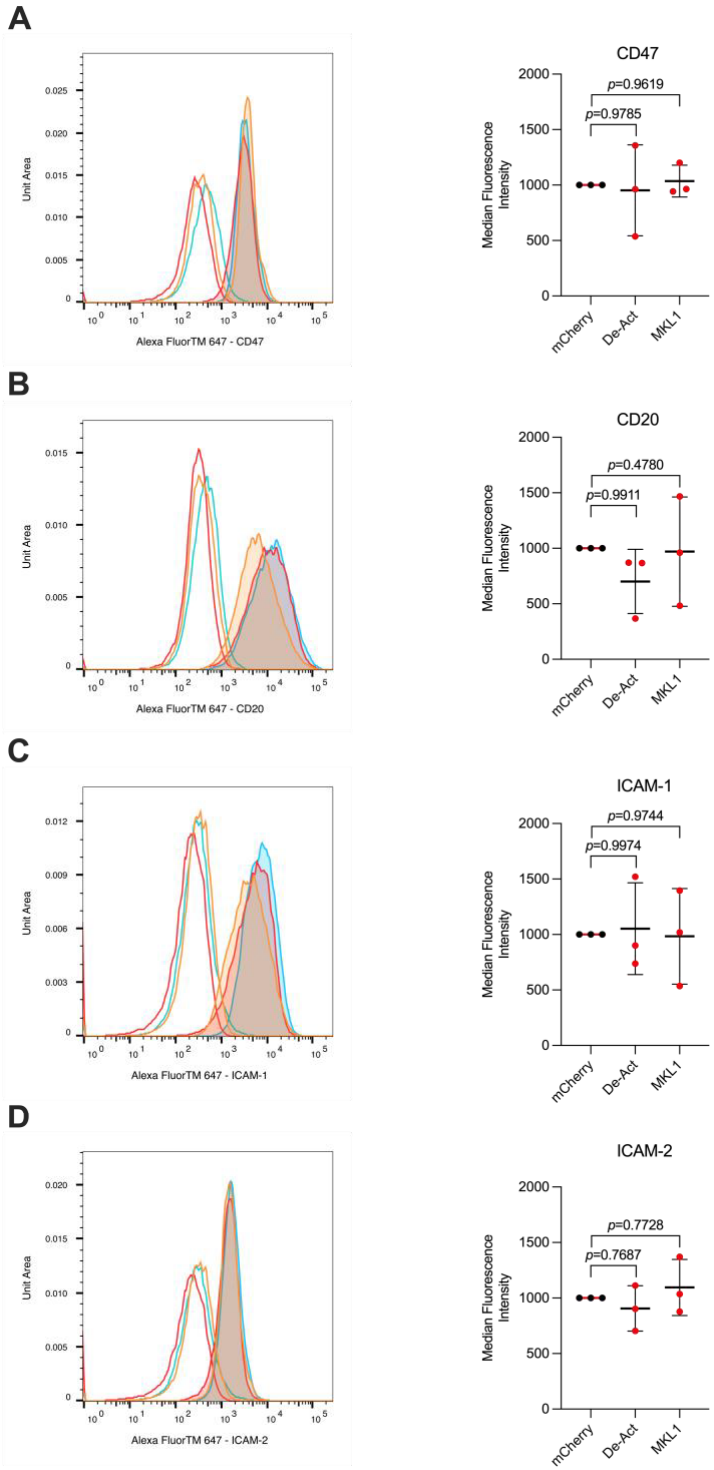

Figure 3.10. Surface expression of phagocytic ligands in De-Act and MKL1 expressing Raji cells.

Representative replicate of the flow cytometry analysis of **(A)** CD47, **(B)** CD20, **(C)** ICAM-1, and **(D)** ICAM-2 ligands in mCherry (blue shaded curve), De-Act (red shaded curve), and MKL1(orange shaded curve) cell lines. Colors match the corresponding isotype control for each antibody. Bars represent means and SD. One-way ANOVA test was used for comparisons of the Median Fluorescence Intensity (n=3 experimental replicates).

3.4. Discussion

Our experiments showcase a relationship between the activity of RhoA, the actin cytoskeleton, and the cortical tension of cells as measured by atomic force microscopy. Particularly, Burkitt lymphoma cells with overactive RhoA had higher actin levels and increased cell stiffness. In contrast, cells with inactivating RhoA mutations displayed lower F-actin levels without changes in the cell biomechanical measurements. Increasing the cell stiffness through mutations of RhoA resulted in greater internalization of Burkitt lymphoma cells by macrophages. To evaluate if the increased phagocytic rate was dependent on cell stiffness or RhoA activity, we targeted the actin cortex cytoskeleton (primary determinant of cell surface tension) through additional techniques. We established that lower stiffness (exhibited by cells with dominant negative RhoA, pharmacological inhibition of RhoA, and decreased actin by De-Act) does not reduce the internalization efficiency by phagocytes. Unfortunately, other approaches to increase the cortical tension of Raji cells via increased actin polymerization (like MKL1) did not affect the mechanical properties of cells. We also verified that our mutagenesis approach on Raji cells was not changing the abundance of ligands participating in Mac-1 (ICAM1, ICAM2, CD47) or FcγR (CD20, CD47) phagocytosis. The flow cytometry analyses showed no significant changes in these ligands, increasing our confidence that a higher phagocytic rate is mainly mediated by changes in biomechanical properties.

Changing the levels of F-actin at a cellular level is not necessarily translated into modifications of the biomechanical properties of the cell. We found variable results when we targeted other actin cytoskeleton regulators outside of RhoA. On one hand, a decrease in actin polymerization by De-Act did not change phagocytosis even after decreasing the cell stiffness. Also, the increased actin levels resulting from exposure to MKL1 did not translate into cell stiffness changes and only improved the phagocytic efficiency in the presence of anti-CD20 antibodies. There are several explanations for these results. These modulators act on actin polymerization but are not specific for the cortical actin cytoskeleton, which is the main determinant of cell surface tension. However, it is difficult to isolate the cell cortex effect on the mechanical properties with the currently available analytical methods[153]. Yet, it would be interesting to conduct an in-depth characterization of biophysical properties in our cell lines using complementary procedures to explore if other related mechanical measurements (besides stiffness) are

associated with our results[199]. Alternatively, the architecture of the actin cortex is also known to contribute to the mechanical attributes of cells. Here, we only modified the polymerization of actin filaments, but future validation efforts should measure if an increase in branching or cross-linking of filaments is more relevant for this case.

The key role of the mechanical properties of a target for Mac-1 mediated phagocytosis was only recently described, and there are no studies about this mechanosensitive internalization in lymphoma or any other cancer cells[140]. According to the literature, cancer cells have increased deformability, helping them to stretch and migrate through a solid extracellular matrix during metastasis and invasion[153–155]. This mechanical property of neoplastic cells could grant additional protection against mechanosensitive phagocytosis by macrophages. Our results align with this hypothesis as cells with reduced stiffness due to pharmacologically inhibited RhoA, displayed reduced phagocytosis by macrophages. Interestingly, previous authors have described the biomechanical changes of malignant cells during different stages of cancer progression and how these properties contribute to cancer metastasis compared to non-malignant cells[153]. However, the correlation between RhoA activity and the significance of this pathway on the cytoskeleton structure of Burkitt lymphoma cells has not been described previously. Furthermore, as expected, the artificial increase in cell stiffness of Burkitt lymphoma cells correlated with an improved uptake by macrophages in our *in vitro* model. In future experiments, we could evaluate other malignant and non-malignant cells as phagocytic targets to clarify the role of modified stiffness in cancer.

The Mac-1 integrin is the only phagocytic receptor with definitive mechanosensing capacity, although other integrins have mechanosensitive properties for tissue adhesion. Anti-CD47 antibodies block a “don’t eat me” signal on the surface of cancer cells and enhance internalization dependent on the Mac-1 integrin[137]. Thus, even if other integrins have mechanosensing capacity, it is unlikely they have an active role in our phagocytic model. Interestingly, some authors attribute mechanosensing properties to the Fc-receptor, the key molecule in antibody-dependent internalization[200]. Our experiments employed anti-CD47 and anti-CD20 antibodies to maximize the *in-vitro* internalization of Raji cells. Rituximab is an anti-CD20 antibody that increases internalization through FcγR phagocytosis[201]. If FcγR does have mechanosensitive capacity, it could mediate the changes observed in phagocytic efficiency. For instance, MKL1 increased F-actin levels and internalization without affecting cell stiffness by AFM.

This pro-phagocytic role of F-actin was evident only in the presence of anti-CD20, which requires functional FcγR for internalization [124,126]. To explore this potential role of FcγR, we could repeat our phagocytosis experiments using cells with altered biomechanical properties while blocking the activity of this internalization pathway.

Tumor cell phagocytosis occurs in a complex tumor microenvironment that may influence the results from our *in vitro* model. The model we developed allows accurate quantification of live cells internalized by macrophages. In addition, we used an inducible system of transfection that minimizes unwanted effects of RhoA modulation in other relevant cellular processes like cell proliferation. Furthermore, we verified that our mutagenesis approach was not inducing unwanted and confounding effects on phagocytic ligand expression (ICAM1, ICAM2, CD20, or CD47). We also employed different techniques to modify the function of RhoA and the actin levels of the cells, finding consistency among the results. However, in some cases, we could not translate the effects seen on actin polymerization into effective changes in the cell's biomechanical properties. We suspect that altering the dynamics of actin polymerization is not enough, so further efforts should also alter the architecture of the cell cortex by disrupting the balance between formins and Arp2/3 activity[148]. In addition, we can better define the role of mechanosensing by Mac-1 integrin if we knockdown talin and vinculin, two proteins that mediate its interaction with the cytoskeleton. Talin and vinculin anchor Mac-1 to the cytoskeleton and their dysfunction would help isolate the role of the Mac-1 integrin in these processes[140]. Finally, to better approximate the *in vivo* role of mechanical properties in B cell lymphoma phagocytosis, we need to mimic the *in vivo* tumor microenvironment. In patients, the extracellular matrix actively interacts with integrins affecting their conformation and affinity for ligands. Also, the *in vivo* abundance of soluble factors with agonistic or antagonistic roles for macrophages can influence phagocytosis in unexpected ways. Thus, animal xenograft models, *ex vivo* culture systems, or organoids are the ideal next step to evaluate the overall effect of the mechanical properties in macrophage activity against B cell lymphomas[202].

In summary, we provide evidence about the role of the biomechanical properties of Burkitt lymphoma cells on the phagocytic efficiency of macrophages. Also, we established RhoA GTPase as a modulator of actin polymerization and cell stiffness in Burkitt lymphoma, and the driving variable for mechanosensitive internalization of cancer cells. The role of phagocytosis in anti-tumoral responses is widely accepted, particularly

in B cell malignancies. Rituximab, a monoclonal antibody that targets CD20 on B cells, has demonstrated significant improvement in survival for non-Hodgkin lymphomas and is the first line of therapy for aggressive variants such as Burkitt lymphoma and DLBCL. Furthermore, more modulators of phagocytosis in the tumor site are in early clinical development[203]. This study advances our understanding of immune escape from phagocytes in Burkitt lymphoma. Although we focused on this non-Hodgkin lymphoma due to its aggressiveness and challenging response to Rituximab, the biomechanical properties of malignant B cells are likely to play a role in many other lymphomas, particularly those where anti-CD20 therapy is effective (like DLBCL). It would also be interesting to explore if similar results are found in other cancers given the differences in tumor microenvironments according to the affected body site. Finally, understanding the role of the mechanical forces in different pathways of phagocytosis can pave the way for novel or optimized therapies for Burkitt lymphoma and other non-Hodgkin lymphomas.

Chapter 4. Concluding remarks and future perspectives

Macrophages are an important player in the tumor microenvironment that can have beneficial or harmful effects on the host during cancer. In this thesis, I designed a novel *in vitro* model to quantify the phagocytic rate of macrophages using confocal microscopy. Then, we employed this model to study the effect of altered mechanical properties of Burkitt lymphoma cells on phagocytosis by macrophages.

Phagocytosis is a complex mechanism that requires receptor-ligand interactions, activation of intracellular pathways, priming of phagocytic cells, and dynamic modifications of the actin cytoskeleton. *In vivo*, phagocytic cells have additional roles in tissue homeostasis including efferocytosis (removal of apoptotic bodies). Our initial literature review demonstrated that current microscopy-based phagocytosis assays had inherent limitations that could bias our interpretation of results. Thus, I improved upon available alternatives and designed a robust protocol that minimizes error due to misleading quantification of non-internalized cells and efferocytosis. We believe this protocol can be leveraged for many cells amenable to fluorescent labeling, making it applicable to many infectious and autoimmune diseases too. Furthermore, we believe that instead of immortalized cell lines, our assay can also use primary human or mouse cells, making it helpful for research groups studying potential therapies that promote macrophage phagocytosis. Moreover, the use of BMDM could help us confirm the results obtained in our *in vitro* assays with the benefit of having an increased phagocytic activity, a property that characterizes mouse macrophages. We anticipate that BMDM have a heightened uptake of malignant B cells coupled with an efficient proinflammatory profile, which can be confirmed by measuring cytokine production. Moreover, the use of primary macrophages from patients or healthy volunteers would enable us to mimic the in vivo uptake of malignant cells by macrophages. Finally, our phagocytosis model can be applied to drug susceptibility assays, allowing us to evaluate the response to drugs against intracellular microorganisms that infect macrophages, such as *Leishmania* spp., *Mycobacterium*, and others.

The initial validation of the model proved to have reliable and consistent results maintaining a coefficient of variation below an acceptable threshold of 20%. Also, we

evaluated the functionality of one of the primary pathways for macrophage phagocytosis, Mac-1 mediated phagocytosis, which is the overarching topic of our work. We did not test the competency of FcγR mediated phagocytosis directly, although it is probably functional given the increased internalization seen with anti-CD20 antibodies, a therapy associated with FcγR[204]. Future steps include additional validation of other phagocytic pathways by knocking out or using blocking antibodies against key receptors (FcγR, Dectin-1) and evaluating the model's performance after changing the target and effector cells.

With our robust phagocytosis assay, I studied how modifying the cortical actin cytoskeleton and the cell stiffness of lymphoma cells could impact the phagocytic efficiency of macrophages. The mechanical properties of cells are mainly dependent on the cytoskeleton; however, many intracellular pathways convene and interact to drive dynamic changes in the cytoskeleton architecture. Thus, we employed different approaches (mutagenesis and pharmacological) to modify the biomechanical attributes of our target: Raji cells derived from a human Burkitt lymphoma patient. In some cases, the altered levels of F-actin did not impact the biomechanical properties of the cell. However, we found a correlation between increased stiffness of the target and higher phagocytic rate in our model. This primary conclusion was consistent over several replicates and independent of the mechanism that altered the cell stiffness.

Our results represent the phagocytic rate stimulated with known pro-phagocytic antibodies (Rituximab and anti-CD47). Further validation is necessary to identify other conditions that facilitate the internalization based on mechanosensing. In the future, we would like to validate if the same effect holds in the absence of monoclonal antibodies or with alternative cytokine stimuli. We found conflicting results in cells with decreased cell stiffness. Reduced cell stiffness due to dominant negative RhoA or De-Act had no impact on macrophage activity, while cells with decreased stiffness through pharmacological inhibition (C3 exoenzyme of *C. botulinum*) had lower internalization rates. Curiously, the effect of the latter over F-actin was stronger according to our phalloidin analysis; as Burkitt lymphoma cells already have a decreased stiffness, we would like to explore if there are thresholds that determine a poorer internalization. The lack of effect on phagocytosis by dominant negative mutations of RhoA could also be explained by the characteristically deficient expression of these constructs. Finally, we plan to ascertain if other pathways besides the RhoA cascade play a role in the

internalization of these softer cells by repeating our phagocytosis assays while blocking key molecules in Mac-1 mediated phagocytosis (like talin and vinculin).

Overall, we designed an assay that facilitates accurate and unbiased quantification of macrophage phagocytosis. This protocol is reproducible and ideal for preliminary evaluation of compounds targeting phagocytosis. Also, we defined the link between cancer biomechanical properties and internalization by macrophages, showing that artificial increases in cell stiffness, which restores the inhibition of RhoA in cancer, led to higher uptake by macrophages. Furthermore, the modification of the mechanical properties of cancer cells represents a potential therapeutic strategy that could be implemented in future drug development projects. While this preliminary evidence is promising, validation in more complex models that mimic the tumor microenvironment is essential. Nevertheless, we offer significant evidence for cancer researchers, providing insights to better understand the dynamics of phagocytosis evasion at the tumor site.

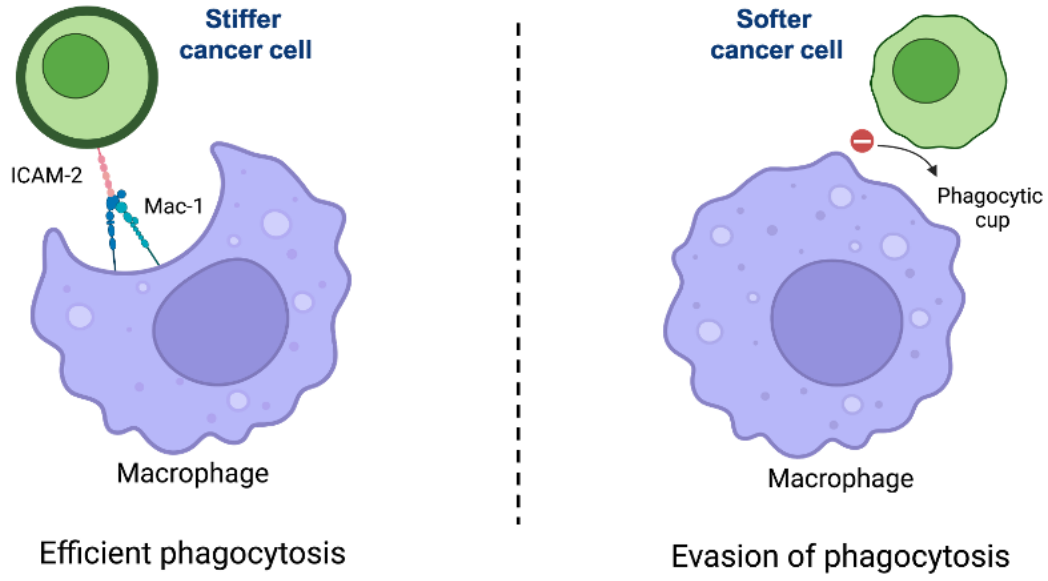

Figure 4.1 The cell stiffness could represent a mechanism for immune evasion. In the presence of the CD47 blockade, the Mac-1 integrin mediates the internalization of cancer cells through ICAM-1 and increases the phagocytosis efficiency by macrophages. During Rituximab mediated phagocytosis, the Mac-1 integrin binds to ICAM-1 and ICAM-2 ligands to increase malignant B cell uptake. On the other hand, softer cancer cells with lower surface tension are less internalized by the mechanosensitive Mac-1 integrin in the presence of the CD47 blockade and Rituximab, which prevents their phagocytosis by macrophages and could represent a mechanism for immune evasion. Created with BioRender.com.

References

1. Meng, X., Min, Q. & Wang, J.-Y. B Cell Lymphoma. in *B Cells in Immunity and Tolerance* (ed. Wang, J.-Y.) 161–181 (Springer, 2020). doi:10.1007/978-981-15-3532-1_12.

2. de Leval, L. & Jaffe, E. S. Lymphoma Classification. *Cancer J. Sudbury Mass* **26**, 176–185 (2020).

3. Swerdlow, S. H. *et al.* The 2016 revision of the World Health Organization classification of lymphoid neoplasms. *Blood* **127**, 2375–2390 (2016).

4. Aggarwal, P. & Limaiem, F. Reed Sternberg Cells. in *StatPearls* (StatPearls Publishing, 2023).

5. Thandra, K. C. *et al.* Epidemiology of Non-Hodgkin's Lymphoma. *Med. Sci.* **9**, 5 (2021).

6. Bowzyk Al-Naeeb, A., Ajithkumar, T., Behan, S. & Hodson, D. J. Non-Hodgkin lymphoma. *BMJ* **362**, k3204 (2018).

7. Canadian Cancer Statistics Advisory Committee in collaboration with the Canadian Cancer Society, Statistics Canada and the Public Health Agency of Canada. *Canadian Cancer Statistics 2021*. https://cancer.ca/en/ (2021).

8. Kalisz, K. *et al.* An update on Burkitt lymphoma: a review of pathogenesis and multimodality imaging assessment of disease presentation, treatment response, and recurrence. *Insights Imaging* **10**, 56 (2019).

9. Della Rocca, A. M. *et al.* Chemotherapy Treatments for Burkitt Lymphoma: Systematic Review of Interventional Studies. *Clin. Lymphoma Myeloma Leuk.* **21**, 514–525 (2021).

10. Graham, B. S. & Lynch, D. T. Burkitt Lymphoma. in *StatPearls* (StatPearls Publishing, 2023).

11. Canadian Cancer Survivor Network. Burkitt Lymphoma [Internet]. https://survivornet.ca/cancer-type/rare-cancers/rare-blood-bone-marrow-cancers/non-hodgkins-lymphoma/burkitt-lymphoma/ (2023).

12. Roschewski, M., Staudt, L. M. & Wilson, W. H. Burkitt's Lymphoma. *N. Engl. J. Med.* **387**, 1111–1122 (2022).

13. Mbulaiteye, S. M. *et al.* Pediatric, elderly, and emerging adult-onset peaks in Burkitt's lymphoma incidence diagnosed in four continents, excluding Africa. *Am. J. Hematol.* **87**, 573–578 (2012).

14. Roy, S. F. *et al.* Epidemiology of adult and pediatric Burkitt lymphoma in Canada: sequelae of the HIV epidemic. *Curr. Oncol.* **27**, 83–89 (2020).

15. López, C. *et al.* Burkitt lymphoma. *Nat. Rev. Dis. Primer* **8**, 1–26 (2022).

16. Translocation. *Genome.gov* https://www.genome.gov/genetics-glossary/Translocation.

17. Haluska, F. G., Finver, S., Tsujimoto, Y. & Croce, C. M. The t(8; 14) chromosomal translocation occurring in B-cell malignancies results from mistakes in V-D-J joining. *Nature* **324**, 158–161 (1986).

18. Radkiewicz, C. *et al.* Sex differences in lymphoma incidence and mortality by subtype: A population-based study. *Am. J. Hematol.* **98**, 23–30 (2023).

19. Molyneux, E. M. *et al.* Burkitt's lymphoma. *Lancet Br. Ed.* **379**, 1234–1244 (2012).

20. Quintana, M. del P., Smith-Togobo, C., Moormann, A. & Hviid, L. Endemic Burkitt lymphoma – an aggressive childhood cancer linked to Plasmodium falciparum exposure, but not to exposure to other malaria parasites. *APMIS* **128**, 129–135 (2020).

21. Rochford, R., Cannon, M. J. & Moormann, A. M. Endemic Burkitt's lymphoma: a polymicrobial disease? *Nat. Rev. Microbiol.* **3**, 182–187 (2005).

22. Donati, D. *et al.* Identification of a Polyclonal B-Cell Activator in Plasmodium falciparum. *Infect. Immun.* **72**, 5412–5418 (2004).

23. Moormann, A. M. *et al.* Exposure to holoendemic malaria results in elevated Epstein-Barr virus loads in children. *J. Infect. Dis.* **191**, 1233–1238 (2005).

24. Atallah-Yunes, S. A., Murphy, D. J. & Noy, A. HIV-associated Burkitt lymphoma. *Lancet Haematol.* **7**, e594–e600 (2020).

25. Sall, F. B. *et al.* HIV-1 Tat protein induces aberrant activation of AICDA in human B-lymphocytes from peripheral blood. *J. Cell. Physiol.* **234**, 15678–15685 (2019).

26. Martin, G. *et al.* Human Immunodeficiency Virus Type 1-Associated CD40 Ligand Transactivates B Lymphocytes and Promotes Infection of CD4+ T Cells. *J. Virol.* **81**, 5872–5881 (2007).

27. Imbeault, M. *et al.* Acquisition of host-derived CD40L by HIV-1 in vivo and its functional consequences in the B-cell compartment. *J. Virol.* **85**, 2189–2200 (2011).

28. Giagulli, C. *et al.* Opposite Effects of HIV-1 p17 Variants on PTEN Activation and Cell Growth in B Cells. *PLoS ONE* **6**, e17831 (2011).

29. Dolcetti, R., Gloghini, A., Caruso, A. & Carbone, A. A lymphomagenic role for HIV beyond immune suppression? *Blood* **127**, 1403–1409 (2016).

30. Gloghini, A., Dolcetti, R. & Carbone, A. Lymphomas occurring specifically in HIV-infected patients: from pathogenesis to pathology. *Semin. Cancer Biol.* **23**, 457–467 (2013).

31. Thirlwell, C., Sarker, D., Stebbing, J. & Bower, M. Acquired immunodeficiency syndrome-related lymphoma in the era of highly active antiretroviral therapy. *Clin. Lymphoma* **4**, 86–92 (2003).

32. Grande, B. M. *et al.* Genome-wide discovery of somatic coding and noncoding mutations in pediatric endemic and sporadic Burkitt lymphoma. *Blood* **133**, 1313–1324 (2019).

33. Soyland, D. J., Thanel, P. F., Sievers, M. E., Wagner, K. & Vuong, S. M. Primary epidural sporadic Burkitt lymphoma in a 3-year-old: Case report and literature review. *Surg. Neurol. Int.* **13**, 106 (2022).

34. Murphy, S. B. & Magrath, I. T. Workshop on pediatric lymphomas: current results and prospects. *Ann. Oncol. Off. J. Eur. Soc. Med. Oncol.* **2 Suppl 2**, 219–223 (1991).

35. Childhood Non-Hodgkin's Lymphoma Survival Rates | American Cancer Society [Internet]. https://www.cancer.org/cancer/types/childhood-non-hodgkin-lymphoma/detection-diagnosis-staging/survival-rates.html (2023).

36. Kim, H. *et al.* Clinical Outcome of Relapsed or Refractory Burkitt Lymphoma and Mature B-Cell Lymphoblastic Leukemia in Children and Adolescents. *Cancer Res. Treat. Off. J. Korean Cancer Assoc.* **46**, 358–365 (2014).

37. De Silva, N. S. & Klein, U. Dynamics of B cells in germinal centres. *Nat. Rev. Immunol.* **15**, 137–148 (2015).

38. Mayberry, C. L., Logan, N. A., Wilson, J. J. & Chang, C.-H. Providing a Helping Hand: Metabolic Regulation of T Follicular Helper Cells and Their Association With Disease. *Front. Immunol.* **13**, (2022).

39. Basso, K. & Dalla-Favera, R. Germinal centres and B cell lymphomagenesis. *Nat. Rev. Immunol.* **15**, 172–184 (2015).

40. Martin, A., Chahwan, R., Parsa, J. Y. & Scharff, M. D. Somatic Hypermutation. in *Molecular Biology of B Cells* 363–388 (Elsevier, 2015). doi:10.1016/B978-0-12-397933-9.00020-5.

41. Küppers, R. Mechanisms of B-cell lymphoma pathogenesis. *Nat. Rev. Cancer* **5**, 251–262 (2005).

42. Allen, C. D. C. *et al.* Germinal center dark and light zone organization is mediated by CXCR4 and CXCR5. *Nat. Immunol.* **5**, 943–952 (2004).

43. Victora, G. D. *et al.* Identification of human germinal center light and dark zone cells and their relationship to human B-cell lymphomas. *Blood* **120**, 2240–2248 (2012).

44. Pasqualucci, L. *et al.* Hypermutation of multiple proto-oncogenes in B-cell diffuse large-cell lymphomas. *Nature* **412**, 341–346 (2001).

45. Ahmadi, S. E., Rahimi, S., Zarandi, B., Chegeni, R. & Safa, M. MYC: a multipurpose oncogene with prognostic and therapeutic implications in blood malignancies. *J. Hematol. Oncol.J Hematol Oncol* **14**, 121 (2021).

46. Dang, C. V. MYC on the Path to Cancer. *Cell* **149**, 22–35 (2012).

47. Dave, S. S. *et al.* Molecular Diagnosis of Burkitt's Lymphoma. *N. Engl. J. Med.* **354**, 2431–2442 (2006).

48. Steininger, A. *et al.* Genomic loss of the putative tumor suppressor gene E2A in human lymphoma. *J. Exp. Med.* **208**, 1585–1593 (2011).

49. Guan, H., Xie, L., Wirth, T. & Ushmorov, A. Repression of TCF3/E2A contributes to Hodgkin lymphomagenesis. *Oncotarget* **7**, 36854–36864 (2016).

50. Kitada, S., Pedersen, I. M., Schimmer, A. D. & Reed, J. C. Dysregulation of apoptosis genes in hematopoietic malignancies. *Oncogene* **21**, 3459–3474 (2002).

51. Schmitz, R., Ceribelli, M., Pittaluga, S., Wright, G. & Staudt, L. M. Oncogenic Mechanisms in Burkitt Lymphoma. *Cold Spring Harb. Perspect. Med.* **4**, a014282 (2014).

52. O'Hayre, M. *et al.* Inactivating Mutations in GNA13 and RHOA in Burkitt's Lymphoma and Diffuse Large B cell Lymphoma: A Tumor Suppressor Function for the Gα13/RhoA Axis in B Cells. *Oncogene* **35**, 3771–3780 (2016).

53. Pasqualucci, L. & Dalla-Favera, R. Genetics of diffuse large B-cell lymphoma. *Blood* **131**, 2307–2319 (2018).

54. Voena, C. & Chiarle, R. RHO Family GTPases in the Biology of Lymphoma. *Cells* doi:10.3390/cells8070646.

55. Anderson, N. M. & Simon, M. C. The tumor microenvironment. *Curr. Biol.* **30**, R921–R925 (2020).

56. Visser, K. E. de & Joyce, J. A. The evolving tumor microenvironment: From cancer initiation to metastatic outgrowth. *Cancer Cell* **41**, 374–403 (2023).

57. Xiao, Y. & Yu, D. Tumor microenvironment as a therapeutic target in cancer. *Pharmacol. Ther.* **221**, 107753 (2021).

58. Hanahan, D. & Weinberg, R. A. Hallmarks of Cancer: The Next Generation. *Cell* **144**, 646–674 (2011).

59. Baghban, R. *et al.* Tumor microenvironment complexity and therapeutic implications at a glance. *Cell Commun. Signal.* **18**, 59 (2020).

60. Wang, X. *et al.* TIMEDB: tumor immune micro-environment cell composition database with automatic analysis and interactive visualization. *Nucleic Acids Res.* **51**, D1417–D1424 (2023).

61. Arneth, B. Tumor Microenvironment. *Medicina (Mex.)* **56**, 15 (2020).

62. Popova, N. V. & Jücker, M. The Functional Role of Extracellular Matrix Proteins in Cancer. *Cancers* **14**, 238 (2022).

63. Henke, E., Nandigama, R. & Ergün, S. Extracellular Matrix in the Tumor Microenvironment and Its Impact on Cancer Therapy. *Front. Mol. Biosci.* **6**, (2020).

64. Mao, X. *et al.* Crosstalk between cancer-associated fibroblasts and immune cells in the tumor microenvironment: new findings and future perspectives. *Mol. Cancer* **20**, 131 (2021).

65. Kalluri, R. The biology and function of fibroblasts in cancer. *Nat. Rev. Cancer* **16**, 582–598 (2016).

66. Wang, M. *et al.* Role of tumor microenvironment in tumorigenesis. *J. Cancer* **8**, 761–773 (2017).

67. Sahai, E. *et al.* A framework for advancing our understanding of cancer-associated fibroblasts. *Nat. Rev. Cancer* **20**, 174–186 (2020).

68. Pallegar, N. K. & Christian, S. L. Adipocytes in the Tumour Microenvironment. in *Tumor Microenvironment: Non-Hematopoietic Cells* (ed. Birbrair, A.) 1–13 (Springer International Publishing, 2020). doi:10.1007/978-3-030-37184-5_1.

69. De Palma, M., Biziato, D. & Petrova, T. V. Microenvironmental regulation of tumour angiogenesis. *Nat. Rev. Cancer* **17**, 457–474 (2017).

70. Sobierajska, K., Ciszewski, W. M., Sacewicz-Hofman, I. & Niewiarowska, J. Endothelial Cells in the Tumor Microenvironment. in *Tumor Microenvironment: Non-Hematopoietic Cells* (ed. Birbrair, A.) 71–86 (Springer International Publishing, 2020). doi:10.1007/978-3-030-37184-5_6.

71. Shang, A. *et al.* Exosomal KRAS mutation promotes the formation of tumor-associated neutrophil extracellular traps and causes deterioration of colorectal cancer by inducing IL-8 expression. *Cell Commun. Signal.* **18**, (2020).

72. Baranwal, S. & Alahari, S. K. miRNA control of tumor cell invasion and metastasis. *Int. J. Cancer* **126**, 1283–1290 (2010).

73. Bhan, A., Soleimani, M. & Mandal, S. S. Long Noncoding RNA and Cancer: A New Paradigm. *Cancer Res.* **77**, 3965–3981 (2017).

74. Lei, X. *et al.* Immune cells within the tumor microenvironment: Biological functions and roles in cancer immunotherapy. *Cancer Lett.* **470**, 126–133 (2020).

75. Greten, F. R. & Grivennikov, S. I. Inflammation and Cancer: Triggers, Mechanisms, and Consequences. *Immunity* **51**, 27–41 (2019).

76. Gajewski, T. F., Schreiber, H. & Fu, Y.-X. Innate and adaptive immune cells in the tumor microenvironment. *Nat. Immunol.* **14**, 1014–1022 (2013).

77. Lu, C., Liu, Y., Ali, N. M., Zhang, B. & Cui, X. The role of innate immune cells in the tumor microenvironment and research progress in anti-tumor therapy. *Front. Immunol.* **13**, 1039260 (2023).

78. Granot, Z. & Jablonska, J. Distinct Functions of Neutrophil in Cancer and Its Regulation. *Mediators Inflamm.* **2015**, (2015).

79. Cedervall, J., Zhang, Y. & Olsson, A. K. Tumor-induced NETosis as a risk factor for metastasis and organ failure. *Cancer Res.* **76**, 4311–4315 (2016).

80. Ireland, A. S. & Oliver, T. G. Neutrophils Create an ImpeNETrable Shield between Tumor and Cytotoxic Immune Cells. (2020) doi:10.1016/j.immuni.2020.04.009.

81. Teijeira, Á. *et al.* CXCR1 and CXCR2 Chemokine Receptor Agonists Produced by Tumors Induce Neutrophil Extracellular Traps that Interfere with Immune Cytotoxicity. *Immunity* **52**, 856-871.e8 (2020).

82. Perera Molligoda Arachchige, A. S. Human NK cells: From development to effector functions. *Innate Immun.* **27**, 212–229 (2021).

83. Guillerey, C. NK Cells in the Tumor Microenvironment. in *Tumor Microenvironment: Hematopoietic Cells – Part B* (ed. Birbrair, A.) 69–90 (Springer International Publishing, 2020). doi:10.1007/978-3-030-49270-0_4.

84. Morvan, M. G. & Lanier, L. L. NK cells and cancer: you can teach innate cells new tricks. *Nat. Rev. Cancer* **16**, 7–19 (2016).

85. Hinshaw, D. C. & Shevde, L. A. The Tumor Microenvironment Innately Modulates Cancer Progression. *Cancer Res.* **79**, 4557–4566 (2019).

86. Gardner, A., de Mingo Pulido, Á. & Ruffell, B. Dendritic Cells and Their Role in Immunotherapy. *Front. Immunol.* **11**, (2020).

87. Marciscano, A. E. & Anandasabapathy, N. The role of dendritic cells in cancer and anti-tumor immunity. *Semin. Immunol.* **52**, 101481 (2021).

88. Gabrilovich, D. I. Myeloid-Derived Suppressor Cells. *Cancer Immunol. Res.* **5**, 3–8 (2017).

89. Veglia, F., Sanseviero, E. & Gabrilovich, D. I. Myeloid-derived suppressor cells in the era of increasing myeloid cell diversity. *Nat. Rev. Immunol.* **21**, 485–498 (2021).

90. Ostrand-Rosenberg, S. & Sinha, P. Myeloid-Derived Suppressor Cells: Linking Inflammation and Cancer 1. *J. Immunol.* **182**, 4499–4506 (2009).

91. Chen, D. S. & Mellman, I. Oncology Meets Immunology: The Cancer-Immunity Cycle. *Immunity* **39**, 1–10 (2013).

92. Laumont, C. M., Banville, A. C., Gilardi, M., Hollern, D. P. & Nelson, B. H. Tumour-infiltrating B cells: immunological mechanisms, clinical impact and therapeutic opportunities. *Nat. Rev. Cancer* **22**, 414–430 (2022).

93. Yuen, G. J., Demissie, E. & Pillai, S. B Lymphocytes and Cancer: A Love–Hate Relationship. *Trends Cancer* **2**, 747–757 (2016).

94. Mehta, A. K., Kadel, S., Townsend, M. G., Oliwa, M. & Guerriero, J. L. Macrophage Biology and Mechanisms of Immune Suppression in Breast Cancer. *Front. Immunol.* **0**, 626–626 (2021).

95. Zhang, C., Yang, M. & Ericsson, A. C. Function of Macrophages in Disease: Current Understanding on Molecular Mechanisms. *Front. Immunol.* **0**, 635–635 (2021).

96. Noy, R. & Pollard, J. W. Tumor-Associated Macrophages: From Mechanisms to Therapy. *Immunity* **41**, 49–61 (2014).

97. Jahchan, N. S. *et al.* Tuning the Tumor Myeloid Microenvironment to Fight Cancer. *Front. Immunol.* **10**, 1611–1611 (2019).

98. Mehla, K. & Singh, P. K. Metabolic Regulation of Macrophage Polarization in Cancer. *Trends Cancer* **5**, 822–822 (2019).

99. Xiang, X., Wang, J., Lu, D. & Xu, X. Targeting tumor-associated macrophages to synergize tumor immunotherapy. *Signal Transduct. Target. Ther. 2021 61* **6**, 1–12 (2021).

100. Khalaf, K. *et al.* Aspects of the Tumor Microenvironment Involved in Immune Resistance and Drug Resistance. *Front. Immunol.* **0**, 1764–1764 (2021).

101. Christofides, A. *et al.* The complex role of tumor-infiltrating macrophages. *Nat. Immunol.* **23**, 1148–1156 (2022).

102. Zhu, Y. *et al.* Tissue-Resident Macrophages in Pancreatic Ductal Adenocarcinoma Originate from Embryonic Hematopoiesis and Promote Tumor Progression. *Immunity* **47**, 323-338.e6 (2017).

103. Loyher, P.-L. *et al.* Macrophages of distinct origins contribute to tumor development in the lung. *J. Exp. Med.* **215**, 2536–2553 (2018).

104. Geeraerts, X. *et al.* Macrophages are metabolically heterogeneous within the tumor microenvironment. *Cell Rep.* **37**, 110171 (2021).

105. Ma, R.-Y., Black, A. & Qian, B.-Z. Macrophage diversity in cancer revisited in the era of single-cell omics. *Trends Immunol.* **43**, 546–563 (2022).

106. Zheng, J. *et al.* Chemokine receptor CX3CR1 contributes to macrophage survival in tumor metastasis. *Mol. Cancer* **12**, 141 (2013).

107. Harney, A. S. *et al.* Real-time imaging reveals local, transient vascular permeability, and tumor cell intravasation stimulated by TIE2hi macrophage–derived VEGFA. *Cancer Discov.* **5**, 932–943 (2015).

108. Di Conza, G. *et al.* Tumor-induced reshuffling of lipid composition on the endoplasmic reticulum membrane sustains macrophage survival and pro-tumorigenic activity. *Nat. Immunol.* **22**, 1403–1415 (2021).

109. Casanova-Acebes, M. *et al.* Tissue-resident macrophages provide a pro-tumorigenic niche to early NSCLC cells. *Nature* **595**, 578–584 (2021).

110. Yuan, S., Liu, Z., Xu, Z., Liu, J. & Zhang, J. High mobility group box 1 (HMGB1): a pivotal regulator of hematopoietic malignancies. *J. Hematol. Oncol.J Hematol Oncol* **13**, 91 (2020).

111. Scott, D. W. & Gascoyne, R. D. The tumour microenvironment in B cell lymphomas. *Nat. Rev. Cancer* **14**, 517–534 (2014).

112. Kline, J., Godfrey, J. & Ansell, S. M. The immune landscape and response to immune checkpoint blockade therapy in lymphoma. *Blood* **135**, 523–533 (2020).

113. Xiong, X., Xie, X., Wang, Z., Zhang, Y. & Wang, L. Tumor-associated macrophages in lymphoma: From mechanisms to therapy. *Int. Immunopharmacol.* **112**, 109235 (2022).

114. Zhang, J. *et al.* Amphotericin B suppresses M2 phenotypes and B7-H1 expression in macrophages to prevent Raji cell proliferation. *BMC Cancer* **18**, 467 (2018).

115. Murata, Y. *et al.* Anti-human SIRPα antibody is a new tool for cancer immunotherapy. *Cancer Sci.* **109**, 1300–1308 (2018).

116. Willingham, S. B. *et al.* The CD47-signal regulatory protein alpha (SIRPa) interaction is a therapeutic target for human solid tumors. *Proc. Natl. Acad. Sci.* **109**, 6662–6667 (2012).

117. Morrissey, M. A., Kern, N. & Vale, R. D. CD47 Ligation Repositions the Inhibitory Receptor SIRPA to Suppress Integrin Activation and Phagocytosis. *Immunity* **53**, 290-302.e6 (2020).

118. Armitage, J. O., Gascoyne, R. D., Lunning, M. A. & Cavalli, F. Non-Hodgkin lymphoma. *The Lancet* **390**, 298–310 (2017).

119. National Guideline Alliance (UK). *Non-Hodgkin's Lymphoma: Diagnosis and Management*. (National Institute for Health and Care Excellence (NICE), 2016).

120. Sehn, L. H. *et al.* Introduction of Combined CHOP Plus Rituximab Therapy Dramatically Improved Outcome of Diffuse Large B-Cell Lymphoma in British Columbia. *J. Clin. Oncol.* **23**, 5027–5033 (2005).

121. Surveillance Research Program, National Cancer Institute. SEER*Explorer: An interactive website for SEER cancer statistics [Internet]. https://seer.cancer.gov/index.html (2023).

122. Evens, A. M. *et al.* Burkitt lymphoma in the modern era: real-world outcomes and prognostication across 30 US cancer centers. *Blood* **137**, 374–386 (2021).

123. Crombie, J. & LaCasce, A. The treatment of Burkitt lymphoma in adults. *Blood* **137**, 743–750 (2021).

124. Weiskopf, K. & Weissman, I. L. Macrophages are critical effectors of antibody therapies for cancer. *mAbs* **7**, 303–310 (2015).

125. Grandjean, C. L. *et al.* Intravital imaging reveals improved Kupffer cell-mediated phagocytosis as a mode of action of glycoengineered anti-CD20 antibodies. *Sci. Rep.* **6**, 34382 (2016).

126. Pierpont, T. M., Limper, C. B. & Richards, K. L. Past, Present, and Future of Rituximab—The World's First Oncology Monoclonal Antibody Therapy. *Front. Oncol.* **8**, 163 (2018).

127. Cerny, T., Borisch, B., Introna, M., Johnson, P. & Rose, A. L. Mechanism of action of rituximab. *Anticancer. Drugs* **13 Suppl 2**, S3-10 (2002).

128. Seyfizadeh, N., Seyfizadeh, N., Hasenkamp, J. & Huerta-Yepez, S. A molecular perspective on rituximab: A monoclonal antibody for B cell non Hodgkin lymphoma and other affections. *Crit. Rev. Oncol. Hematol.* **97**, 275–290 (2016).

129. Coiffier, B. Rituximab therapy in malignant lymphoma. *Oncogene* **26**, 3603–3613 (2007).

130. Klein, C., Jamois, C. & Nielsen, T. Anti-CD20 treatment for B-cell malignancies: current status and future directions. *Expert Opin. Biol. Ther.* **21**, 161–181 (2021).

131. Chao, M. P., Weissman, I. L. & Majeti, R. The CD47–SIRPα pathway in cancer immune evasion and potential therapeutic implications. *Curr. Opin. Immunol.* **24**, 225–232 (2012).

132. Feng, M. *et al.* Phagocytosis checkpoints as new targets for cancer immunotherapy. *Nat. Rev. Cancer* **19**, 568–586 (2019).

133. Rosales, C. & Uribe-Querol, E. Phagocytosis: A Fundamental Process in Immunity. *BioMed Res. Int.* **2017**, e9042851 (2017).

134. Uribe-Querol, E. & Rosales, C. Phagocytosis: Our Current Understanding of a Universal Biological Process. *Front. Immunol.* **11**, (2020).

135. Rosales, C. Fc receptor and integrin signaling in phagocytes. *Signal Transduct.* **7**, 386–401 (2007).

136. Flannagan, R. S., Jaumouillé, V. & Grinstein, S. The cell biology of phagocytosis. *Annu. Rev. Pathol.* **7**, 61–98 (2012).

137. Chen, J. *et al.* SLAMF7 is critical for phagocytosis of haematopoietic tumour cells via Mac-1 integrin. *Nature* **544**, 493–497 (2017).

138. Torres-Gomez, A., Cabañas, C. & Lafuente, E. M. Phagocytic Integrins: Activation and Signaling. *Front. Immunol.* **11**, (2020).

139. Jaumouillé, V. & Waterman, C. M. Physical Constraints and Forces Involved in Phagocytosis. *Front. Immunol.* **11**, 1097–1097 (2020).

140. Jaumouillé, V., Cartagena-Rivera, A. X. & Waterman, C. M. Coupling of β2 integrins to actin by a mechanosensitive molecular clutch drives complement receptor-mediated phagocytosis. *Nat. Cell Biol.* **21**, 1357–1369 (2019).

141. Izard, T. & Brown, D. T. Mechanisms and Functions of Vinculin Interactions with Phospholipids at Cell Adhesion Sites *. *J. Biol. Chem.* **291**, 2548–2555 (2016).

142. Lamers, C., Plüss, C. J. & Ricklin, D. The Promiscuous Profile of Complement Receptor 3 in Ligand Binding, Immune Modulation, and Pathophysiology. *Front. Immunol.* **12**, (2021).

143. Mylvaganam, S., Freeman, S. A. & Grinstein, S. The cytoskeleton in phagocytosis and macropinocytosis. *Curr. Biol.* **31**, R619–R632 (2021).

144. Svitkina, T. M. Actin Cell Cortex: Structure and Molecular Organization. *Trends Cell Biol.* **30**, 556–565 (2020).

145. Chugh, P. & Paluch, E. K. The actin cortex at a glance. *J. Cell Sci.* **131**, jcs186254 (2018).

146. Kelkar, M., Bohec, P. & Charras, G. Mechanics of the cellular actin cortex: From signalling to shape change. *Curr. Opin. Cell Biol.* **66**, 69–78 (2020).

147. Haase, K. & Pelling, A. E. Investigating cell mechanics with atomic force microscopy. *J. R. Soc. Interface* **12**, 20140970 (2015).

148. Breitsprecher, D. & Goode, B. L. Formins at a glance. *J. Cell Sci.* **126**, 1–7 (2013).

149. Firat-Karalar, E. N. & Welch, M. D. New mechanisms and functions of actin nucleation. *Curr. Opin. Cell Biol.* **23**, 4–13 (2011).

150. Bros, M., Haas, K., Moll, L. & Grabbe, S. RhoA as a Key Regulator of Innate and Adaptive Immunity. *Cells* **8**, 733 (2019).

151. Bagci, H. *et al.* Mapping the proximity interaction network of the Rho-family GTPases reveals signalling pathways and regulatory mechanisms. *Nat. Cell Biol.* **22**, 120–134 (2020).

152. Lessey, E. C., Guilluy, C. & Burridge, K. From Mechanical Force to RhoA Activation. *Biochemistry* **51**, 7420–7432 (2012).

153. Alibert, C., Goud, B. & Manneville, J. B. Are cancer cells really softer than normal cells? *Biol. Cell* **109**, 167–189 (2017).

154. Nagelkerke, A., Bussink, J., Rowan, A. E. & Span, P. N. The mechanical microenvironment in cancer: How physics affects tumours. *Semin. Cancer Biol.* **35**, 62–70 (2015).

155. Yu, W. *et al.* Cancer cell mechanobiology: a new frontier for cancer research. *J. Natl. Cancer Cent.* **2**, 10–17 (2022).

156. Li, M. *et al.* Atomic force microscopy imaging and mechanical properties measurement of red blood cells and aggressive cancer cells. *Sci. China Life Sci.* **55**, 968–973 (2012).

157. Freeman, S. A. & Grinstein, S. Phagocytosis: receptors, signal integration, and the cytoskeleton. *Immunol. Rev.* **262**, 193–215 (2014).

158. Ostrowski, P. P., Grinstein, S. & Freeman, S. A. Diffusion Barriers, Mechanical Forces, and the Biophysics of Phagocytosis. *Dev. Cell* **38**, 135–146 (2016).

159. Schneider, C. A., Rasband, W. S. & Eliceiri, K. W. NIH Image to ImageJ: 25 years of image analysis. *Nat. Methods 2012 97* **9**, 671–675 (2012).

160. Lv, D., Zhang, Y., Kim, H.-J., Zhang, L. & Ma, X. CCL5 as a potential immunotherapeutic target in triple-negative breast cancer. *Cell. Mol. Immunol.* **10**, 303–310 (2013).

161. Kang, T. G., Park, H. J., Moon, J., Lee, J. H. & Ha, S.-J. Enriching CCL3 in the Tumor Microenvironment Facilitates T cell Responses and Improves the Efficacy of Anti-PD-1 Therapy. *Immune Netw.* **21**, e23 (2021).

162. Rabin, R. L. CC, C, and CX3C Chemokines. in *Encyclopedia of Hormones* (eds. Henry, H. L. & Norman, A. W.) 255–263 (Academic Press, 2003). doi:10.1016/B0-12-341103-3/00044-9.

163. Fujihara, M. *et al.* Molecular mechanisms of macrophage activation and deactivation by lipopolysaccharide: roles of the receptor complex. *Pharmacol. Ther.* **100**, 171–194 (2003).

164. Castro, F., Cardoso, A. P., Gonçalves, R. M., Serre, K. & Oliveira, M. J. Interferon-Gamma at the Crossroads of Tumor Immune Surveillance or Evasion. *Front. Immunol.* **9**, 847 (2018).

165. Voorzanger, N. & Blay, J.-Y. Interleukin 10 and non Hodgkin's lymphomas. in *Cancer in Transplantation: Prevention and Treatment: Proceedings of the 27th Conference on Transplantation and Clinical Immunology, 22–24 May 1995* (eds. Touraine, J. L. et al.) 229–241 (Springer Netherlands, 1996). doi:10.1007/978-94-009-0175-9_26.

166. Pham, L. V., Pogue, E. & Ford, R. J. The Role of Macrophage/B-Cell Interactions in the Pathophysiology of B-Cell Lymphomas. *Front. Oncol.* **8**, (2018).

167. Podolnikova, N. P., Kushchayeva, Y. S., Wu, Y., Faust, J. & Ugarova, T. P. The Role of Integrins αMβ2 (Mac-1, CD11b/CD18) and αDβ2 (CD11d/CD18) in Macrophage Fusion. *Am. J. Pathol.* **186**, 2105–2116 (2016).

168. Bednarczyk, M., Stege, H., Grabbe, S. & Bros, M. β2 Integrins—Multi-Functional Leukocyte Receptors in Health and Disease. *Int. J. Mol. Sci. 2020 Vol 21 Page 1402* **21**, 1402–1402 (2020).

169. Liu, Y. *et al.* Emerging phagocytosis checkpoints in cancer immunotherapy. *Signal Transduct. Target. Ther.* **8**, 1–42 (2023).

170. Russ, A. *et al.* Blocking “don’t eat me” signal of CD47-SIRPα in hematological malignancies, an in-depth review. *Blood Rev.* **32**, 480–489 (2018).

171. Gilead Sciences. *ENHANCE: A Randomized, Double-blind, Multicenter Study Comparing Magrolimab in Combination With Azacitidine Versus Azacitidine Plus Placebo in Treatment-naïve Patients With Higher Risk Myelodysplastic Syndrome*. https://clinicaltrials.gov/study/NCT04313881 (2023).

172. Bule, P., Aguiar, S. I., Aires-Da-Silva, F. & Dias, J. N. R. Chemokine-Directed Tumor Microenvironment Modulation in Cancer Immunotherapy. *Int. J. Mol. Sci.* **22**, 9804 (2021).

173. Cendrowicz, E., Sas, Z., Bremer, E. & Rygiel, T. P. The Role of Macrophages in Cancer Development and Therapy. *Cancers* **13**, 1946 (2021).

174. Ciesielska, A., Matyjek, M. & Kwiatkowska, K. TLR4 and CD14 trafficking and its influence on LPS-induced pro-inflammatory signaling. *Cell. Mol. Life Sci.* **78**, 1233–1261 (2021).

175. Faridi, M. H. *et al.* Small molecule agonists of integrin CD11b/CD18 do not induce global conformational changes and are significantly better than activating antibodies in reducing vascular injury. *Biochim. Biophys. Acta BBA - Gen. Subj.* **1830**, 3696–3710 (2013).

176. Maiguel, D. *et al.* Small Molecule–Mediated Activation of the Integrin CD11b/CD18 Reduces Inflammatory Disease. *Sci. Signal.* **4**, ra57–ra57 (2011).

177. Ortiz-Stern, A. & Rosales, C. Cross-talk between Fc receptors and integrins. *Immunol. Lett.* **90**, 137–143 (2003).

178. Majeti, R. *et al.* CD47 Is an Adverse Prognostic Factor and Therapeutic Antibody Target on Human Acute Myeloid Leukemia Stem Cells. *Cell* **138**, 286–299 (2009).

179. Chao, M. P. *et al.* Anti-CD47 Antibody Synergizes with Rituximab to Promote Phagocytosis and Eradicate Non-Hodgkin Lymphoma. *Cell* **142**, 699–713 (2010).

180. Tseng, D. *et al.* Anti-CD47 antibody-mediated phagocytosis of cancer by macrophages primes an effective antitumor T-cell response. *Proc. Natl. Acad. Sci. U. S. A.* **110**, 11103–11108 (2013).

181. Barkal, A. A. *et al.* CD24 signalling through macrophage Siglec-10 is a target for cancer immunotherapy. *Nature* **572**, 392–396 (2019).

182. Nam, G.-H. *et al.* An optimized protocol to determine the engulfment of cancer cells by phagocytes using flow cytometry and fluorescence microscopy. *J. Immunol. Methods* **470**, 27–32 (2019).

183. Nie, M. *et al.* Effect of rituximab on adult Burkitt's lymphoma: a systematic review and meta-analysis. *Ann. Hematol.* **95**, 19–26 (2016).

184. O'Connor, K. & Chen, M. Dynamic functions of RhoA in tumor cell migration and invasion. *Small GTPases* **4**, 141–147 (2013).

185. Longenecker, K. *et al.* Structure of a constitutively activated RhoA mutant (Q63L) at 1.55 Å resolution. *Acta Crystallogr. D Biol. Crystallogr.* **59**, 876–880 (2003).

186. Strassheim, D., Porter, R. A., Phelps, S. H. & Williams, C. L. Unique in Vivo Associations with SmgGDS and RhoGDI and Different Guanine Nucleotide Exchange Activities Exhibited by RhoA, Dominant Negative RhoAAsn-19, and Activated RhoAVal-14*. *J. Biol. Chem.* **275**, 6699–6702 (2000).

187. Kowarz, E., Löscher, D. & Marschalek, R. Optimized Sleeping Beauty transposons rapidly generate stable transgenic cell lines. *Biotechnol. J.* **10**, 647–653 (2015).

188. Mátés, L. *et al.* Molecular evolution of a novel hyperactive Sleeping Beauty transposase enables robust stable gene transfer in vertebrates. *Nat. Genet.* **41**, 753–761 (2009).

189. Cartagena-Rivera, A. X., Logue, J. S., Waterman, C. M. & Chadwick, R. S. Actomyosin Cortical Mechanical Properties in Nonadherent Cells Determined by Atomic Force Microscopy. *Biophys. J.* **110**, 2528–2539 (2016).

190. Park, J. H. & Strittmatter, S. M. Promoting the Regeneration of Axons within the Central Nervous System. in *From Neuroscience To Neurology* 433–xviii (Elsevier, 2005). doi:10.1016/B978-012738903-5/50027-8.

191. Williamson, K. C., Smith, L. A., Moss, J. & Vaughan, M. Guanine nucleotide-dependent ADP-ribosylation of soluble rho catalyzed by Clostridium botulinum C3 ADP-ribosyltransferase. Isolation and characterization of a newly recognized form of rhoA. *J. Biol. Chem.* **265**, 20807–20812 (1990).

192. Flatau, G. *et al.* Toxin-induced activation of the G protein p21 Rho by deamidation of glutamine. *Nature* **387**, 729–733 (1997).

193. Mundhara, N., Majumder, A. & Panda, D. Methyl-β-cyclodextrin, an actin depolymerizer augments the antiproliferative potential of microtubule-targeting agents. *Sci. Rep.* **9**, 7638 (2019).

194. Cooper, J. A. Effects of cytochalasin and phalloidin on actin. *J. Cell Biol.* **105**, 1473–1478 (1987).

195. Chen, X., Pavlish, K. & Benoit, J. N. Myosin phosphorylation triggers actin polymerization in vascular smooth muscle. *Am. J. Physiol. - Heart Circ. Physiol.* **295**, H2172–H2177 (2008).

196. Harterink, M. *et al.* DeActs: genetically encoded tools for perturbing the actin cytoskeleton in single cells. *Nat. Methods* **14**, 479–482 (2017).

197. Hu, X. *et al.* MKL1-actin pathway restricts chromatin accessibility and prevents mature pluripotency activation. *Nat. Commun.* **10**, 1695 (2019).

198. Tello-Lafoz, M. *et al.* Cytotoxic lymphocytes target characteristic biophysical vulnerabilities in cancer. *Immunity* **54**, 1037-1054.e7 (2021).

199. Pegoraro, A. F., Janmey, P. & Weitz, D. A. Mechanical Properties of the Cytoskeleton and Cells. *Cold Spring Harb. Perspect. Biol.* **9**, a022038 (2017).

200. Beningo, K. A. & Wang, Y. Fc-receptor-mediated phagocytosis is regulated by mechanical properties of the target. *J. Cell Sci.* **115**, 849–856 (2002).

201. Glennie, M. J., French, R. R., Cragg, M. S. & Taylor, R. P. Mechanisms of killing by anti-CD20 monoclonal antibodies. *Mol. Immunol.* **44**, 3823–3837 (2007).

202. Foxall, R. *et al.* Developing a 3D B Cell Lymphoma Culture System to Model Antibody Therapy. *Front. Immunol.* **11**, (2021).

203. Advani, R. *et al.* CD47 Blockade by Hu5F9-G4 and Rituximab in Non-Hodgkin's Lymphoma. *N. Engl. J. Med.* **379**, 1711–1721 (2018).

204. Díaz de león, J. S. A., Aguilar, I. & Barb, A. W. Macrophage N-glycan processing inhibits antibody-dependent cellular phagocytosis. *Glycobiology* cwad078 (2023) doi:10.1093/glycob/cwad078.

Appendix A.
Supplementary information for standardization of phagocytosis model

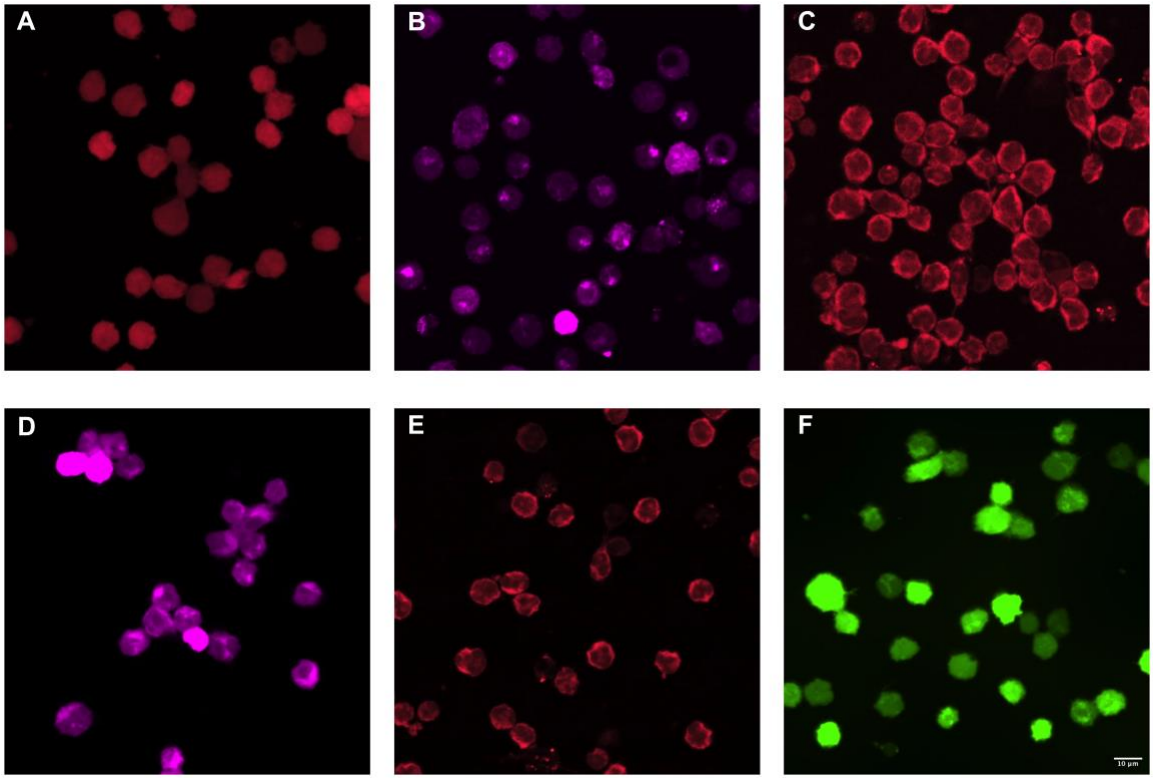

Figure A.1. Standardization of Raji cell viability staining.
Various viability dyes were used to stain Raji cells. Images **(A)** and **(F)** show Raji cells stained with Calcein red-orange and Calcein green. These staining reagents homogeneously distribute in the cytoplasm of the cell and allow us to clearly identify viable cells; images **(B), (C), (D),** and **(E)** show Raji cells stained with cell trace, Calcein deep red, proliferation dye and propidium iodide, respectively. The fluorescence emission and distribution of these dyes was not uniform among cells and fields, and difficulted the visualization of fragmented B cells that were internalized by macrophages. Objective 40X.

Therapeutic antibodies	Primary antibody	Secondary antibody	Concentration
Anti-CD20	Anti-CD47 Anti-F4/80	1:400 IgG anti-mouse and IgG anti-rat	F4/80: 10 ug/mL CD19: 10 ug/mL CD20: 5 ug/mL CD47: 5 ug/mL Anti-CD47 and anti-CD20 as primary antibodies in the inside-out staining: 10 ug/mL
Anti-CD20	Anti-CD19 Anti-F4/80	1:400 IgG anti-mouse and IgG anti-rat	
Anti-CD47	Anti-CD20 Anti-F4/80	1:400 IgG anti-human and IgG anti-rat	
Anti-CD47	Anti-CD19 Anti-F4/80	1:400 IgG anti-mouse and IgG anti-rat	
Anti-CD47	Anti-CD20 Anti-F4/80	1:400 IgG anti-human and IgG anti-rat	
Anti-CD20	Anti-CD47 Anti-F4/80	1:400 IgG anti-mouse and IgG anti-rat	

Figure A.2. Summary of primary and secondary antibodies evaluated during the standardization process to develop the inside-out staining of Raji cells.

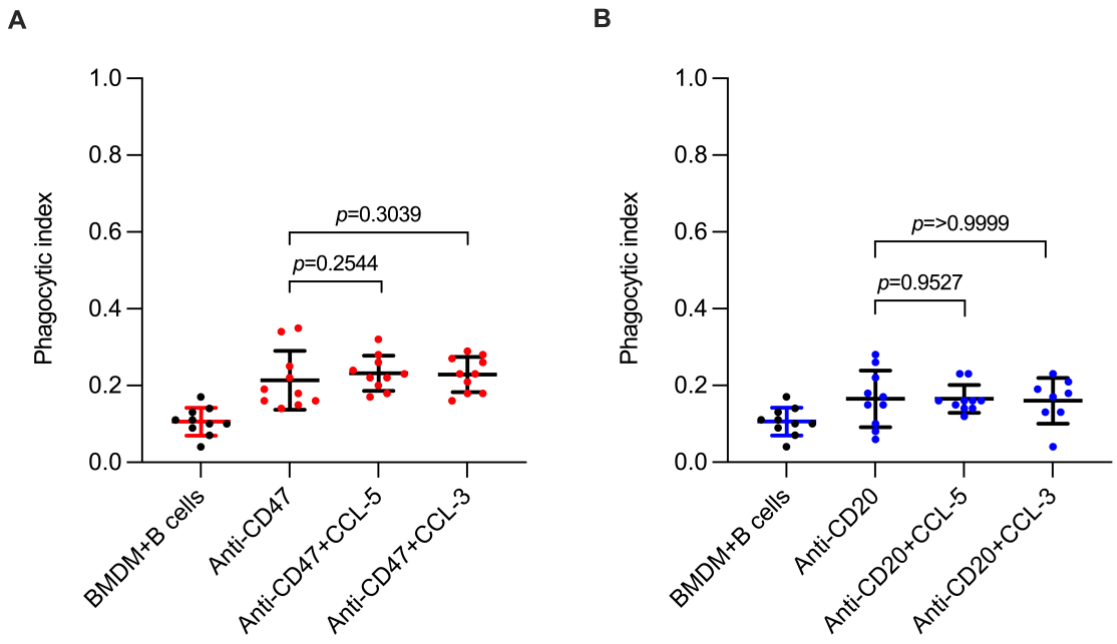

Figure A.3. Stimulation of bone marrow derived macrophages with CCL-5 and CCL-3 chemokines.

Internalization of Raji cells after 2 hours of incubation with bone marrow derived macrophages and anti-CD47 **(A)** or anti-CD20 antibodies **(B)**. Macrophages were stimulated for 24 hours before the assay (n = 10 fields of view). Bars represent means and SD. Mann-Whitney test was used for comparisons.

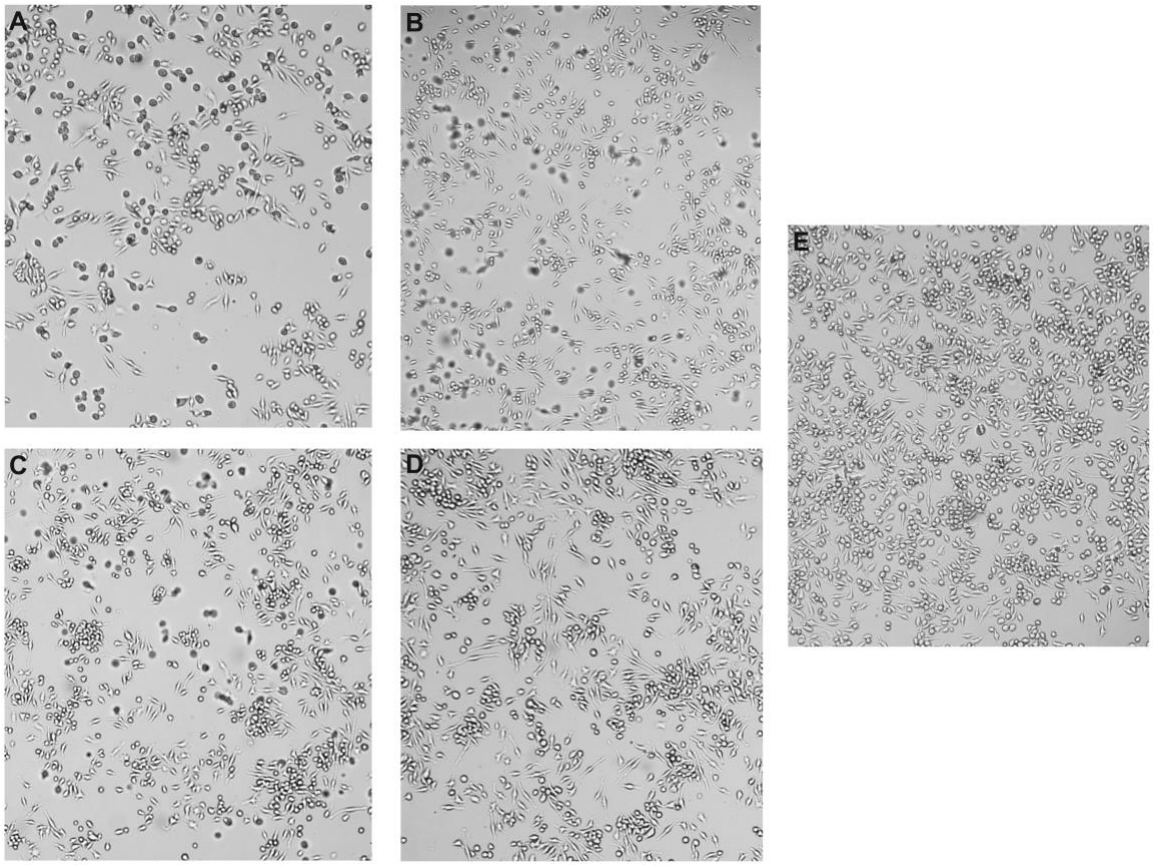

Figure A.4. Standardization of J774A.1 macrophage adherence for phagocytosis assays.

(**E)** 50 x 10^3 macrophages adhered per well. The cell confluency of this condition shows consistency among fields. This cell concentration allows formation of a monolayer that maintains cells attached during the phagocytosis assays, **(B)** 30 x 10^3 and **(C)** 35 x 10^3, **(D)** 40 x 10^3, and **(A)** 45 x 10^3 macrophages adhered per well, 40x.

Appendix B.
Supplementary information for evaluation of RhoA in cancer phagocytosis

Table B.1. Sequence of primers used in the mutagenesis approach of Raji cells

Primer name	Primer sequence
pSBtet-GFP-C1-F	CTCGAAAggcctctgGATCCGCTAGCGCTACCGG
pSBtet-GFP-C1-R	GAAGCTTggcctgacCAAGTAAAACCTCTACAAATGTGGTATGGC
FP-C18-RhoA-R5Q-F	cggtaccgcgatggctgccatccagaagaaactgg
pSBtet-RhoA-20-R	TATCGATGGAAGCTTGGCCTtcacaagacaaggcacccagatttttttcttc
pSBtet-FB-2-F2-F	ACCCTCGAAAGGCCTgccACCATGGTGAGCAAGGGCGAGG
pSBtet-RhoA-15-R	ATGGAAGCTTGGCCTtcacaagacaaggcacccagatttttttcttc
FD-C18-RhoA-WT-F	cggtaccgcgatggctgccatccggaagaaactgg

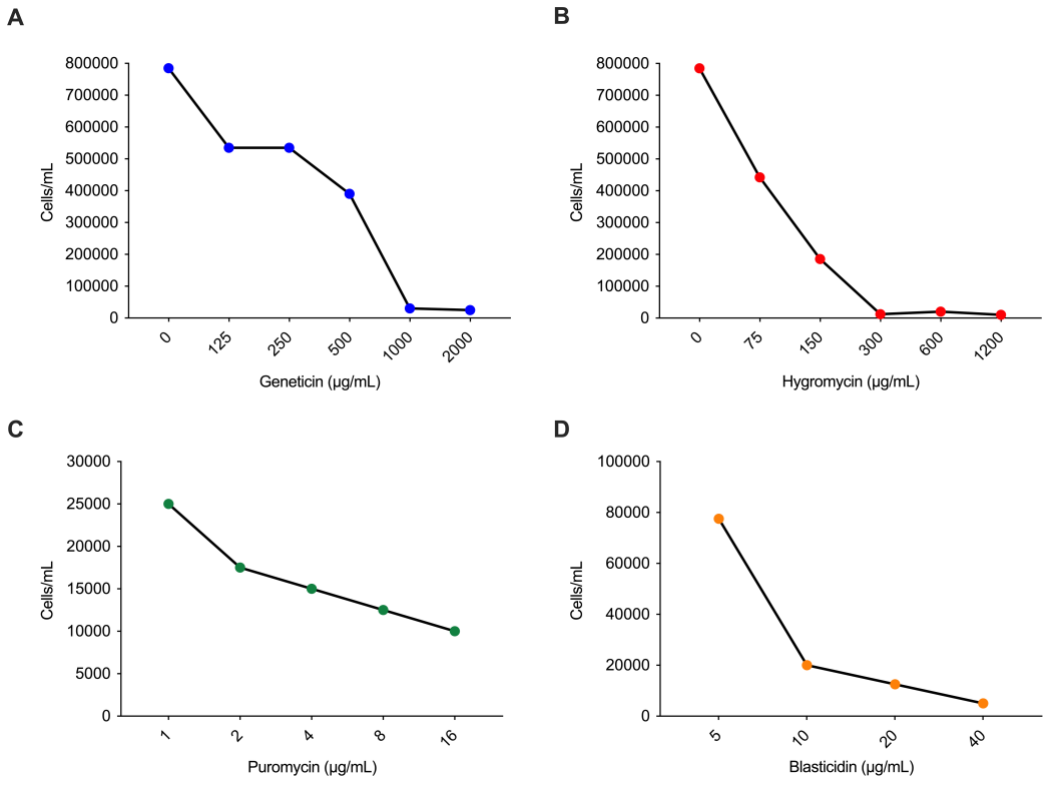

Figure B.2. EC50 assays of Raji cells exposed to different concentrations of (A) Geneticin, (B) Hygromycin, (C) Puromycin, and (D) Blasticidin.

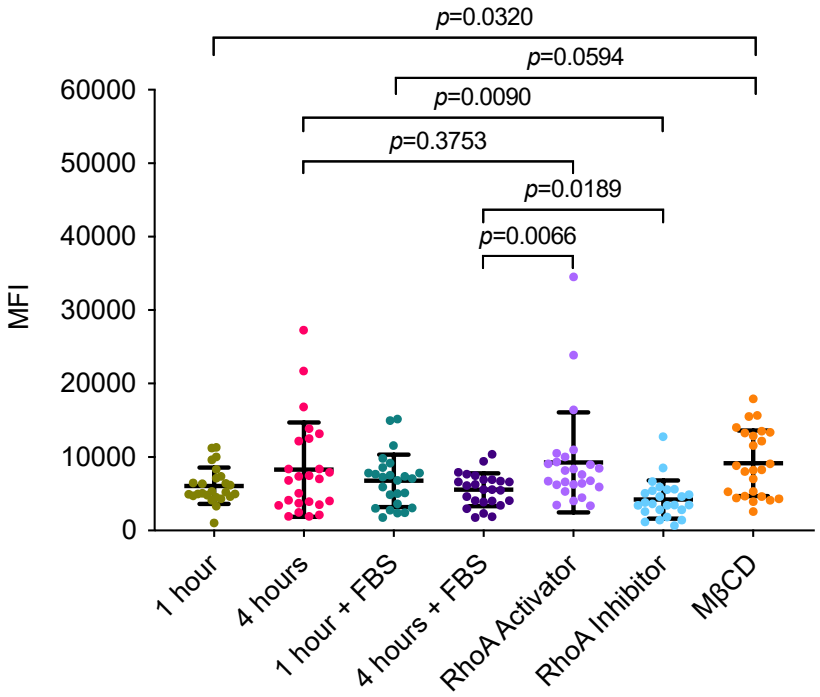

Figure B.3. Pharmacological approach to modify the actin cortex of Raji cells. Raji cells were incubated with and without FBS for 1 and 4 hours at 37℃, 5% CO2. Also, cells were treated with methyl-beta-cyclodextrin (MβCD) for 1 hour, and with the RhoA activator (*Escherichia coli* cytotoxic necrotizing factor-1) and inhibitor (C3 exoenzyme of *Clostridium botulinum*) for 4 hours (n = 30). Bars represent means and SD. Mann-Whitney test was used for comparisons.